HYDROLOGY DOCUMENT NUMBER 429

1378
ROUGH DRAFT

LA-10532-MS

8-16-85

J. Younker
SAIC

TWO-DIMENSIONAL NUMERICAL SIMULATION OF GEOCHEMICAL TRANSPORT IN YUCCA MOUNTAIN

by

B. J. Travis and H. E. Nuttall

ABSTRACT

Several physical and chemical processes can affect transport of radionuclides in Yucca Mountain. Geometric spreading and lateral flow will reduce the concentration of contaminated water reaching the accessible environment. Travel times to the water table are calculated to be at least several tens of thousands of years. Colloid transport can also enhance transport, but will be important only if fracture flow is. Finally, the heat load from repository waste can alter the distribution of naturally occurring dissolved minerals. In particular, dissolution and precipitation of SiO_2 should lead to a region of reduced permeability around waste canisters.

I. INTRODUCTION

The Nevada Nuclear Waste Storage Investigations (NNWSI) program of the US Department of Energy is studying the suitability of an area in southern Nevada as a potential repository for high-level radioactive waste. The investigations include site and regional studies of the Nevada Test Site (NTS) area to determine whether the site is technically acceptable. Los Alamos researchers are contributing to these investigations through studies of the geochemistry, mineralogy, and petrology of Yucca Mountain and its environs and through engineering design for the exploratory test shaft. Our goal is to ascertain whether the site will retard the transport of radionuclides to the accessible environment over the lifetime of the waste package.

Figure 1 presents a cross section of Yucca Mountain. The potential site lies in the Topopah Spring Member, some 300 m below the surface, and about 200 m above the water table. The stratigraphy is detailed in a recent report.[1] At the respository location Yucca Mountain has five stratigraphic units: (1) Surficial units are alluvium and densely to moderately welded, fractured Tiva Canyon tuff. (2) Below this lies the upper clastic unit, which has bedded and nonwelded tuffs of the Yucca Mountain and Pah Canyon

ROUGH DRAFT

Paintbrush tuffs. This unit is highly porous and relatively (matrix) permeable. (3) The next unit down is densely welded with a thin upper and lower vitrophyre and a thick central zone of densely welded ashflow. The matrix permeability of this central zone of the Topopah Spring member is very low, but the rock is highly fractured. (4) Below this lies the lower clastic unit, which contains nonwelded ashflow, ashfall, and reworked tuffs (the lowest part of the Topopah Spring tuff and the Calico Hills tuff). This unit is highly porous and relatively permeable. (5) The bottom unit consists of several nonwelded to moderately welded tuffs with some thinner layers of densely welded ashflow and bedded ashfall tuffs. These rocks appear to be moderately fractured. Much of this unit is below the water table.

In a previous report,[2] we estimated the effects of lithology and fractures on water flow and radionuclide transport in Yucca Mountain. We presented a sensitivity analysis of transport along a one-dimensional vertical pathway to the water table. The effect of waste heat on near field water saturation was also estimated.

In this report, we address several questions not treated in that last report.

1) How will geometric spreading and lateral flow affect transport?
2) Will waste-heat-induced hydrologic transients significantly alter distribution of salts in pore water near waste canisters?
3) Under what conditions will colloidal transport be important?

A. Geometric Effects

In a previous study,[2] we estimated water flow and radionuclide transport through fractured Yucca mountain tuffs. Travel times to the water table without fracture flow are very large because of the low-recharge rate and because of sorption retardation. With fracture flow, travel times are less, but are still on the order of 10,000 years for nonsorbing ions such as Technetium-99 because of diffusion from fractures into the porous tuff matrix. In those studies, we assumed a source of infinite horizontal extent. A more realistic calculation of travel time would account for the finite extent of the source--namely, the placing and spacing of individual canisters. In addition, concentrations of nuclides at the canisters was not known, so that only relative concentrations could be calculated.

ROUGH DRAFT

Two calculations, using the TRACR3D code,[3] are described here that compute radionuclide transport from discrete sources for two flow scenarios. Processes included in these calculations are steady advection, molecular diffusion, hydrodynamic dispersion, radioactive decay and equilibrium adsorption. In the first situation, flow is assumed vertical from the respository to the water table and then horizontal in the saturated zone. The canisters are assumed to be in long regularly spaced rows as shown in Fig. 2. Because of symmetry, we need only calculate transport between a vertical line through a canister and a vertical line midway between that canister and the next row. An average vertical recharge of 4.5 mm/yr[4] is assumed. The radionuclides included in the calculation are listed in Table A-1 with some of their transport properties. In the highly fractured Topopah Spring tuff, transport is assumed to be primarily in fractures. For 100 μm fractures with a 5 cm spacing,[1] fracture flow rate is approximately 2.3 m/yr.

$$(V_c \cdot A_c = V \cdot A \rightarrow V_c = \frac{VA}{A_c} = 4.5 \text{ mm/yr} \times \frac{5 \text{ cm}}{10^{-2} \text{cm}} = 225 \text{ cm/yr})$$

In the Topopah Spring layer, we use equivalent fracture water flow rates V_c, for conservatism. Because of diffusion into the matrix, the effective flow rate for radionuclides must be modified. Sudicky and Frind[5] have worked out an expression for this. The effective fracture transport velocity V_E in a medium with regular fracture spacing is

$$V_E = V/\{\frac{\gamma}{2}[-1 + (1 + \frac{4}{\gamma}(1 + \beta))^{1/2}]\}$$

where

$$\gamma = \frac{v^2}{\lambda D R}, \quad \beta = \frac{\theta \sqrt{R' D'}}{bR\sqrt{\lambda}} \tanh(\sigma\sqrt{\lambda}), \quad \lambda = \frac{\ln 2}{t_{1/2}},$$

$$D = \alpha_L V + D^*, \quad D' = \tau D^*, \quad \sigma = \sqrt{\frac{R'}{D'}}(B-b),$$

ROUGH DRAFT

TABLE A-1

PROPERTIES OF TRANSPORTED RADIONUCLIDES

Radionuclide	Half-Life (yrs)	Diffusivity (10^{-2} m^2/yr)
^{141}Ce	90	3.15
^{135}Cs	3×10^6	6.30
^{90}Sr	28	2.44
^{89}Tc	2×10^5	3.15
^{238}U	4.5×10^9	3.15
^{237}Np	2×10^6	3.15
^{239}Pu	2.4×10^4	3.15
^{243}Am	8×10^3	3.15
^{152}Eu	90	3.15
^{133}Ba	1.6×10^3	3.15

^{152}Eu and ^{133}Ba are analogues for ^{151}Sm and ^{226}Ra.

$t_{1/2}$ = half-life, θ = matrix porosity, b = fracture half-width, R' = matrix retardation coefficient, R = crack face retardation coefficient, V = steady fracture water velocity, D^* = molecular diffusivity, α_L = longitudinal dispersivity, τ = matrix tortuosity, B = half of the fracture spacing. For this study, we used R=1, θ=.11 for Topopah, θ = .20 for Prow Pass, $b=5\times10^{-3}$ cm, B=2.5 cm, τ=0.1, α_L=10, V=225 cm/yr. This modification is like a retardation factor due to matrix diffusion from fractures, and is reflected in the retardation values given in Table A-2.

In the bedded tuff layer at the bottom of the Topopah Spring layer and in the Calico Hills formation, steady porous flow is assumed, with a flux of 4.5 mm/yr.

For our calculations, we include the bottom 50 m of the Topopah Spring unit, a 15 m thick bedded tuff layer, 135 m of Calico Hills tuff, and the top 50 m of the Prow Pass unit.

Concentration of radionuclides in the water[6] passing through canisters has the time histories shown in Table A-3. Linear interpolation is used for times between table entries. Concentrations are determined from a saturation-limited dissolution model,[6] assuming high-level waste storage. Radioactive decay of the source is reflected in Table A-3. This gives the largest release for several possible waste conditions.

The results of the numerical simulation are shown in Figs. 3 through 22. Contour plots of concentration for several radionuclides are shown at selected times.

ROUGH DRAFT

TABLE A-2

RETARDATION FACTORS FOR RADIONUCLIDES

	Stratigraphic Unit			
Element	Topopah Spring*	Bedded Tuff	Calico Hills	Prow Pass
^{141}Ce	2000/1.11x10^4	3 x 10^4	7000	5000/3.03x10^4
^{135}Cs	6000/3.29x10^5	7 x 10^4	4 x 10^4	1200/1.2x10^5
^{90}Sr	1100/3865	8 x 10^4	2 x 10^4	140/3.7x10^3
^{99}Tc	7/389	12	2	2/201
^{238}U	40/2176	40	33	16/1530
^{237}Np	150/8288	100	50	40/4001
^{239}Pu	1300/6.50x10^4	540	630	480/4.632x10^4
^{243}Am	2.5x10^4/5.13x10^6	820	2 x 10^4	3000/2.12x10^5
^{152}Eu	10^4/ 1.78x10^4	3 x 10^4	2 x 10^4	10^4/3.67x10^4
^{133}Ba	2x10^4/1.61x10^5	2 x 10^5	7 x 10^5	4000/1.51x10^5

*For Topopah Spring and Prow Pass, the first number is matrix retardation coefficient, the second is the effective retardation coefficient for fracture flow with diffusion from fractures.

In the fault, retardation values for fractured Prow Pass are used.

TABLE A-3

SOURCE CONDITIONS: CALCULATED CONCENTRATIONS IN WATER PASSING THROUGH canister (moles/ℓ)

Element	Solubility Limit	Time (Years) After Emplacement 10^2	10^3	10^4	10^5
^{243}Am	10^{-8}	6.16×10^{-9}	8.59×10^{-9}	9.96×10^{-9}	3.22×10^{-12}
^{14}C	1.	3.14×10^{-9}	2.82×10^{-9}	9.52×10^{-10}	1.77×10^{-14}
^{135}Cs	1.	2.44×10^{-7}	2.44×10^{-7}	2.43×10^{-7}	2.37×10^{-7}
^{237}Np	3×10^{-3}	2.09×10^{-7}	2.28×10^{-7}	2.32×10^{-7}	2.26×10^{-7}
^{239}Pu	1.8×10^{-6}	1.2×10^{-8}	1.48×10^{-8}	2.88×10^{-8}	3.78×10^{-9}
^{226}Ra	10^{-7}	7.2×10^{-16}	3.65×10^{-14}	1.54×10^{-12}	1.20×10^{-11}
^{90}Sr	9.4×10^{-4}	6.06×10^{-8}	3.02×10^{-17}	0	0
^{99}Tc	1.	8.56×10^{-7}	8.54×10^{-7}	8.28×10^{-7}	6.18×10^{-7}
^{126}Sn	10^{-9}	2.99×10^{-10}	2.98×10^{-10}	2.85×10^{-10}	1.77×10^{-10}
^{238}U	2.1×10^{-4}	2.18×10^{-6}	2.18×10^{-6}	2.18×10^{-6}	2.18×10^{-6}

ROUGH DRAFT

Transport time to the water table are considerably greater than in the previous study[2], in part due to the more reasonable fracture flow rate used here for the Topopah Spring unit. The fastest moving specie ^{99}Tc takes 1.5×10^4 years to reach the water table. However, the concentration at the water table is six orders of magnitude smaller than in the source. By 2×10^4 years, concentration of ^{99}Tc at the bottom of the Calico Hills is about 50 times lower than in the source. In addition, the chromatographic effect of the tuff is evident. Because of the varying retardation factors, the migrating radionuclides are segregated from the initial mixture at the canister. In addition, we can estimate the absolute concentrations reaching the water table. These values are considerably less than at the canisters, due to retardation and decay and lateral spreading. Not all the radionuclides were calculated. ^{99}Tc is the fastest traveling, then ^{238}U and ^{237}Np, then ^{239}Pu. ^{243}Am migrates very little because of the very high retardation onto Topopah Spring tuff. The remaining nuclides were not calculated. They would lie between the results for ^{239}Pu and ^{243}Am. Other than ^{99}Tc, none of the radionuclides will reach the water table in less than 100,000 years.

Transport through the Topopah Spring unit is seen to follow a narrow path because of the fracture flow assumption. In the remaining units (below 50 m depth), porous flow is assumed. Lateral spreading is much stronger because of the diffusive darcy flow.

In the second calculation, lateral flow is included. The horizontal scale is considerably greater, encompassing one end of the repository and some distance beyond, as shown in Fig. 23. In the calculation, a vertical section 250 m thick is considered (the bottom 50 m of Topopah Spring tuff, a 15 m thick bedded tuff layer, 135 m thick Calico Hills unit, and the top 50 m of the Prow Pass. The horizontal extent is 250 m. We assume 32 m spacing between waste canister rows. The last five rows of a hypothetical repository are included. Then a fault has been included 100 m horizontal distance from the last row of canisters. An additional 20 m horizontal distance beyond the fault brings us to the edge of the computed region. The conceptual hydrologic model discussed in Ref. 4 includes the possibility of lateral flow at the interface between the Calico Hills and the Topopah Spring units, and within the Calico Hills, and vertical flow down structural pathways (faults). The spacing used here between the end of the

ROUGH DRAFT

repository and a fault is arbitrary. The ratio of vertical to lateral flow rates and the rate of flow down faults is difficult to determine at this time. We are forced to use what we hope are reasonable estimates, and expect the transport behavior that results to be qualitatively correct. Table A-4 lists vertical and horizontal flow rates used for each unit. In the fault region, we used retardation values calculated in Table A-2 for fractured Prow Pass tuff. Results of the second calculation are included in Figs. 24 to 37 . Arrival times at the water table are essentially the same as in the previous calculation. Concentrations show some increase downstream in the lateral flow region between the Topopah Spring and Calico Hills units. The lateral flow causes an overall shift of the concentration patterns but not to a large extent. In addition, in this calculation, lateral flow is not strong enough to transport radionuclides 100 m downstream to the fault. Retardation and diffusion and vertical flow move species down into the Calico Hills before they can travel laterally to the fault through the bedded tuff layer. Eventually, however, species will get into the fault due to lateral movement in the Calico Hills unit. For the parameters of this calculation, the fault actually has little impact on transport to the water table. Absolute concentrations at the water table are quite small, due to lateral spreading and to retardation. Travel time to the water table for the fastest moving specie, ^{99}Tc, is still about 1.5×10^4 years.

It is important to remember that we are assuming a recharge rate of 4.5 mm/yr, which may be high. The results shown should scale roughly linearly with the recharge rate. Only two nuclides (^{99}Tc and ^{238}U) are considered. None of the others will even reach Calico Hills layer within 10^5 years; it would be meaningless to calculate those.

TABLE A-4

FLOW RATES USED IN SIMULATION (mm/yr)

Unit	Vertical	Horizontal
Topopah Spring*	2250	0
Bedded Tuff	3.5	3.0
Calico Hills	3.5	1.0
Fault*	3000	0
Prow Pass*	0	5000

*Fracture flow assumed

B. Salt Deposition

In our previous study,[2] we examined numerically the effects of waste heat on near-field hydrology. We found that a dry region developed around individual canisters, surrounded by a shell of elevated saturation. This condition persisted for several decades. There were major uncertainties, however, in material and hydrologic properties at that time. This heat load effect is being re-examined because we now have a more accurate picture of the hydrologic properties of Yucca Mountain tuffs and of the waste decay curve.

We are participating in a computer code benchmarking exercise coordinated by Sandia National Labs in which the heat load effect is the target problem. We present some results from that benchmarking exercise here because we are considering an additional process--the variation in mineral concentration and deposition patterns due to heat-induced hydrologic changes.

ROUGH DRAFT

Water from well J-13 has the composition listed in Table B-1. One of the main constituents is SiO_2. SiO_2 can exist in several forms--quartz and cristobalite are two examples. In a sample of Topopah Spring tuff used in a heat alteration study,[9] the mineral content was found to be 80-90% glass, 5-10% alkali feldspar, and 5-10% SiO_2 (cristobalite). The solubility of SiO_2 is strongly temperature dependent[8] (about 10^{-3} M at 23°C and about 10^{-2} M at 150°C). In the heat alteration study described in Ref. 7, a great amount of SiO_2 had dissolved at elevated temperature (152°C) and then precipitated upon cool down. In addition, a great amount of clay was deposited. Placement of waste canisters will lead to the development of a temperature gradient in the surrounding Topopah Spring rock. This will induce a solubility gradient. If water also flows, SiO_2 will be redistributed. Depending on the magnitude and duration of the heat induced flow, SiO_2 may accumulate in some region. Deposition will result in reduced pore size which will lower permeability. At late times, a region of reduced permeability around a canister will tend to isolate the canister from infiltrating water, a beneficial effect.

Whether this will happen in Yucca Mountain, however, is not clear. We have made a numerical study of this scenario using the WAFE code.[9] Figure 38 shows the problem geometry.

First, a simplified analysis is made using a numerical solution for 1-D radial flow from a heat source (canister). Material properties for the calculation are given in Tables B-2 and B-3. We assume a uniform initial saturation of 87% and temperature of 23°C and air pressure of 1.0 bar. We also assume a uniform concentration of SiO_2 in the pore water of 10^{-3} M. The heat source has a radius of 63.6 cm and is centered at radius = 0. A no-flow boundary is imposed at radius = 16 m, the assumed midpoint between waste canisters. In addition to SiO_2, a relatively simple ion, Cl^-, has been included. It will not adsorb and is not to any significant extent, present in the tuff minerals. Its source is from the surface.

We are making a number of assumptions here and no interactions between the various water components is perhaps the most important. Solubility is assumed to vary according to

$$\ln \frac{S}{S_o} = \frac{A}{T_o}\left(1 - \frac{T_o}{T}\right) \text{ where } T_o = 23^\circ C\ (296^\circ K) \text{ and } A = \frac{\ln 10}{\left(\frac{1}{296} - \frac{1}{423}\right)} .$$

 ROUGH DRAFT

Figures 39-44 show the calculated transient pressure, temperature, and saturation, and concentration distributions. The total SiO_2 (SiO_2 in solution plus precipitated) is also shown.

Pressure and temperature go through an initial buildup. A narrow elevated saturation region develops. After several decades, the pressure and temperature fields decay and the saturation returns to ambient. SiO_2 dissolves in a region near the canister and moves outward where it condenses when it reaches a cooler environment. There is some return of SiO_2 to the initially hot region, but a net outward flux of SiO_2 has occurred.

Chlorine concentration increases initially in the hottest region because of decreasing water saturation due to boiling. Concentration in the elevated saturation region decreases, however, due to the addition of distilled water as the steam condenses. At late time as the saturation returns to ambient, so too does the chlorine concentration profile.

Significant changes in the amount of SiO_2 dissolved or precipitated can lead to large permeability changes. If we assume that permeability is related to the pore diameters and that SiO_2 precipitate will pore walls uniformly, we can write an expression for permeability change as a function of porosity change. One possible relation is

$$\frac{K_2}{K_0} = \left(\frac{r_2}{r_o}\right)^2$$

where K_0 is ambient saturated permeability, K_2 is permeability after precipitation or dissolution, r_0 is initial pore radius and r_2 is pore radius after precipitation or dissolution. The value of r_2 is determined from $\Omega(SiO_2) = \varepsilon_0 \frac{\Delta\Omega}{r_0^3} (r_0^3 - r_2^3)$, where $\Delta\Omega$ is a volume of rock, ε_0 is the ambient porosity, and $\Omega(SiO_2)$ is the volume of SiO_2 dissolved or precipitated in that volume of rock.

Figure 45 shows the permeability change we would expect based on our WAFE calculation by the end of the heat decay period. The SiO_2 precipitate distribution leads to an elevated permeability region in close to the canister with a reduced permeability region immediately outside the elevated permeability region. These regions are fairly thin, only a few cm. The presence of these regions can have a significant effect on late time near-field hydrology. A reduced permeability shell around the canisters

will tend to deflect downward flowing water around instead of through the canister region. In addition, the high permeability ring inside will tend to channel water that penetrates the low permeability shell around the canister rather than through it. The exact quantitative magnitude of this effect depends of course on the details of the hydrologic behavior of Topopah Springs, in particular on the presence or absence of fractures.

Our numerical simulation cannot treat the full complexity of the water composition and reactions. Instead, we greatly simplify by considering only SiO_2 dissolution, transport, and precipitation and neglect chemical reactions. Other details of the benchmarking exercise referred to can be found in Ref. 10.

TABLE B.1

COMPOSITION OF J-13 WATER[7]

Species	Concentration (mg/ℓ)
Na	45.2
K	5.47
Ca	11.5
Mg	1.73
Al	0.026
SiO_2	64.2
Sr	0.04
Ba	0.0023
Mn	0.0011
Fe	0.044
V	0.0425
Cl^-	6.4
SO_4^{2-}	18.1
F^-	2.1
NO_3^-	10.1
HPO_4^{2-}	0.10
HCO_3^-	143.

ROUGH DRAFT

TABLE B.2

MATERIAL PROPERTIES

Property	Value
tuff permeability, sat. (cm^2)	1.925×10^{-14}
tuff porosity	0.11
tuff grain density (g/cc)	2.58
tuff specific heat (erg/g•°c)	0.84×10^7
tuff thermal conductivity (erg/cm•°C•s)	$(1.75 + 0.60 \times \text{Sat.}) \times 10^5$
canister density (g/cc)	2.535
canister specific heat (erg/g•°C)	0.325×10^7
canister heat production history (ergs/s/cm)[9]	$10^7 \times (31.7e^{-2.82\times10^{-5}\ t} + 48.6\ e^{-1.29\times10^{-4}\ t} + 443.3e^{-1.76\times10^{-3}t} + 2123\ e^{-.02\ t} + 431.5e^{-.0635\ t} + 321.9e^{-.44\ t})/505.$, t in years.

ROUGH DRAFT

TABLE B.3

HYDROLOGIC PROPERTIES

Property	Expression
Water Rel. Permeability	$\sqrt{S_e}\,(1. - (1. - S_e^{1/\lambda})^{\lambda})^2$
Air Rel. Permeability	min (1., max (0., 1.-100. x (S-0.99))
Matric Potential	$P_c = P_b\,[S_e^{-1/\lambda} - 1]^{(1-\lambda)}$ $P_b = 17.24$ bars $S_e = (S - S_o)/(1 - S_o)$, $S_o = .0801$ $\lambda = .4438$

C. Colloids

Radionuclides released from waste canisters can travel in a variety of forms--as simple rows, as complexes, either with other elements or a polymers (colloids), or embedded in or adsorped on inert particles (pseudo-colloids). Ionic transport has been studied much more than the other forms. In ionic form, most of the radionuclides of interest strongly adsorb to the tuffs of Yucca Mountain. In colloid form or attached to particulates, sorptive properties may be considerably different.

Colloids are a class of extremely small particles which were first studied early in the nineteenth century by Michael Faraday and other scientists.[11] They are characterized as particles continuing several hundred to several thousand atoms, ions, or molecules and having diameters ranging from ten to one thousand angstroms.

Matter in the colloidal state has a large surface area (300 square meters per gram), thus it is not surprising that the most important properties of colloids are those which are dependent on surface interactions such as adsorption. Drever[12] discusses the nature and geochemistry of colloids with emphasis on the charge surrounding colloids and its effect on suspension stability.

Olofsson et al.[13-15] classify radiocolloids as true colloids and pseudocolloids depending on their formation process. True colloids are formed by condensation of molecules or ions as a result of hydrolytic or precipitation processes. They consist mostly of hydroxides or polymers formed by hydrolysis. They have a very rapid formation rate and are favored at high pH values. Pseudocolloids, on the other hand, are formed as a result of adsorption on impurities in the solution and tend to be much larger than true colloids (up to 5000 angstroms). Pseudocolloids can be of two types, reversible and irreversible. The formation rate of pseudocolloids is basically determined by the sorption rate on colloidal impurities.[13]

Radiocolloids are colloids containing radionuclides. They possess all the properties of normal colloids but in addition are radioactive. They may migrate in the ground matrix by virtue of groundwater and may also be captured by existing colloids. Radiocolloids are believed to be a significant vector for the transport of radionuclides from failed waste repositories, and might actually accelerate this transport.[16,17] Radiocolloids may arise from a variety of sources. Leaching of the waste form with groundwater may

39. Calculated pressure distribution at selected times.
40. Calculated temperature distribution at selected times.
41. Calculated saturation distribution at selected times.
42. Calculated chlorine distribution at selected times.
43. Calculated SiO_2 distribution at selected times.
44. Calculated total SiO_2 (dissolved and precipitated) at selected times.
45. Calculated permeability assuming relationship between pore volume and permeability.
46. Distribution of pore sizes by % volume for a sample of Topopah Spring tuff.
47. Distribution of pore sizes by % volume for a sample of Calico Hills tuff.

ROUGH DRAFT

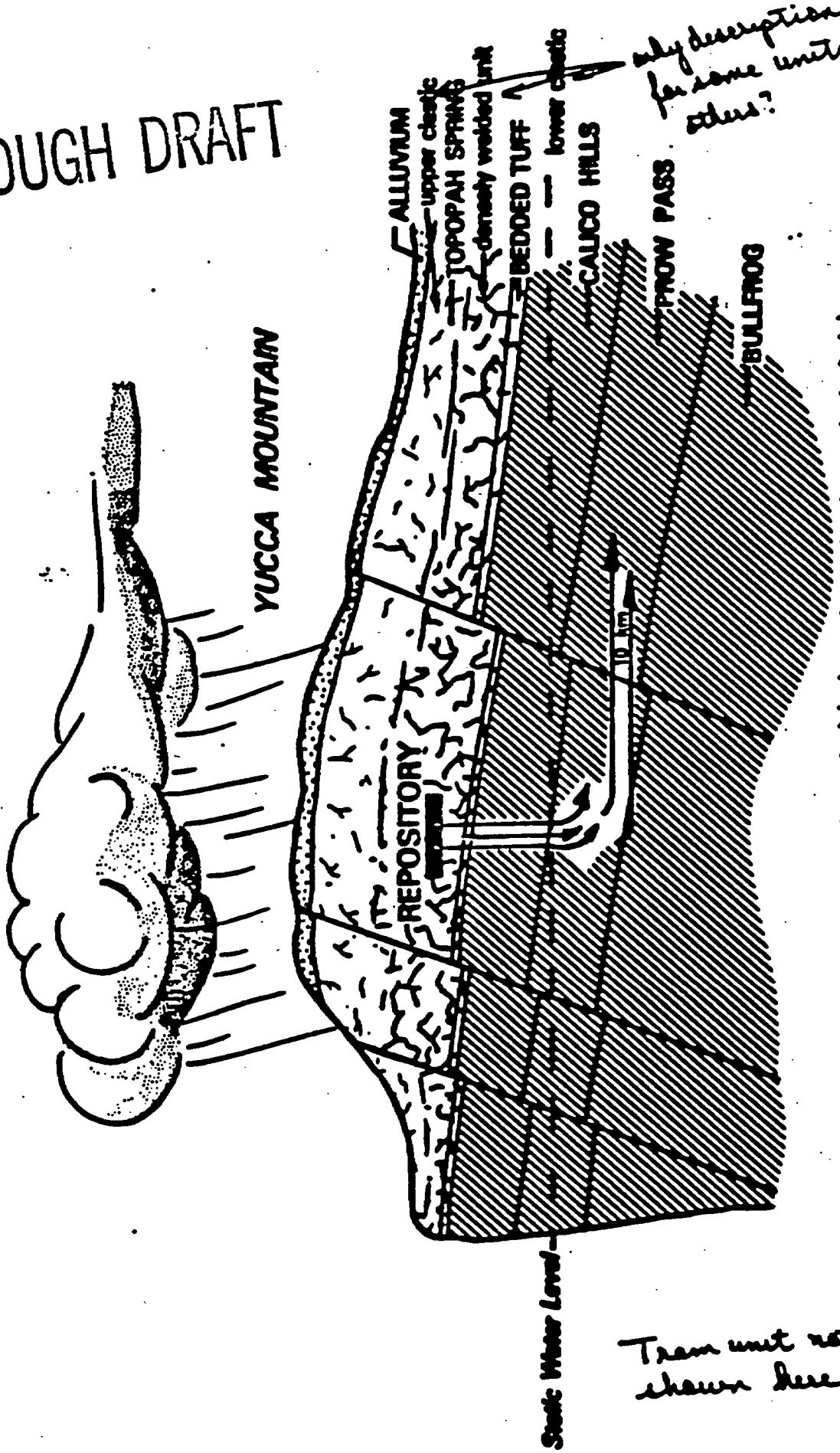

FIG. 1. CONCEPTUAL RADIONUCLIDE TRANSPORT PATH.

Fig. 1

ROUGH DRAFT

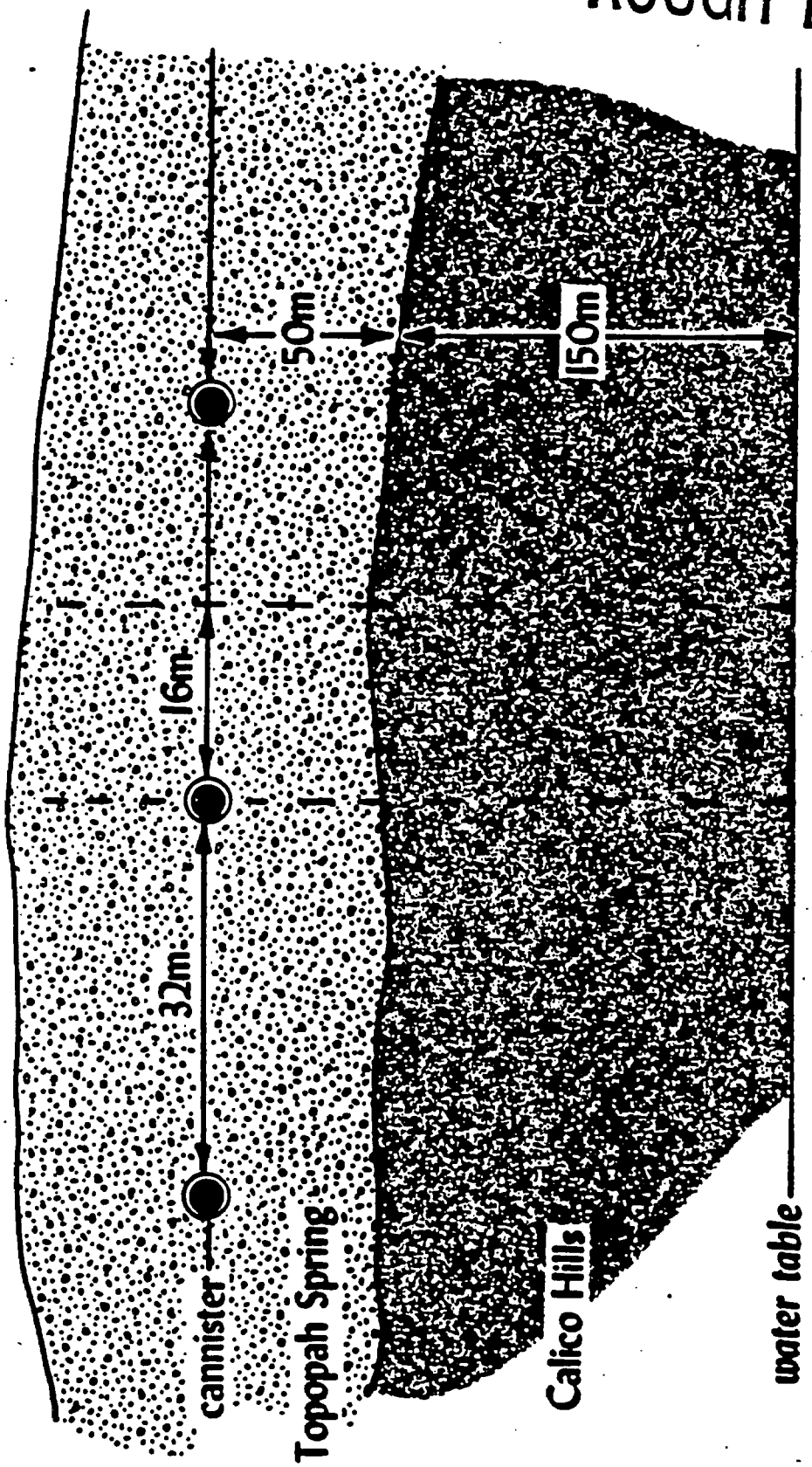

Fig. 2

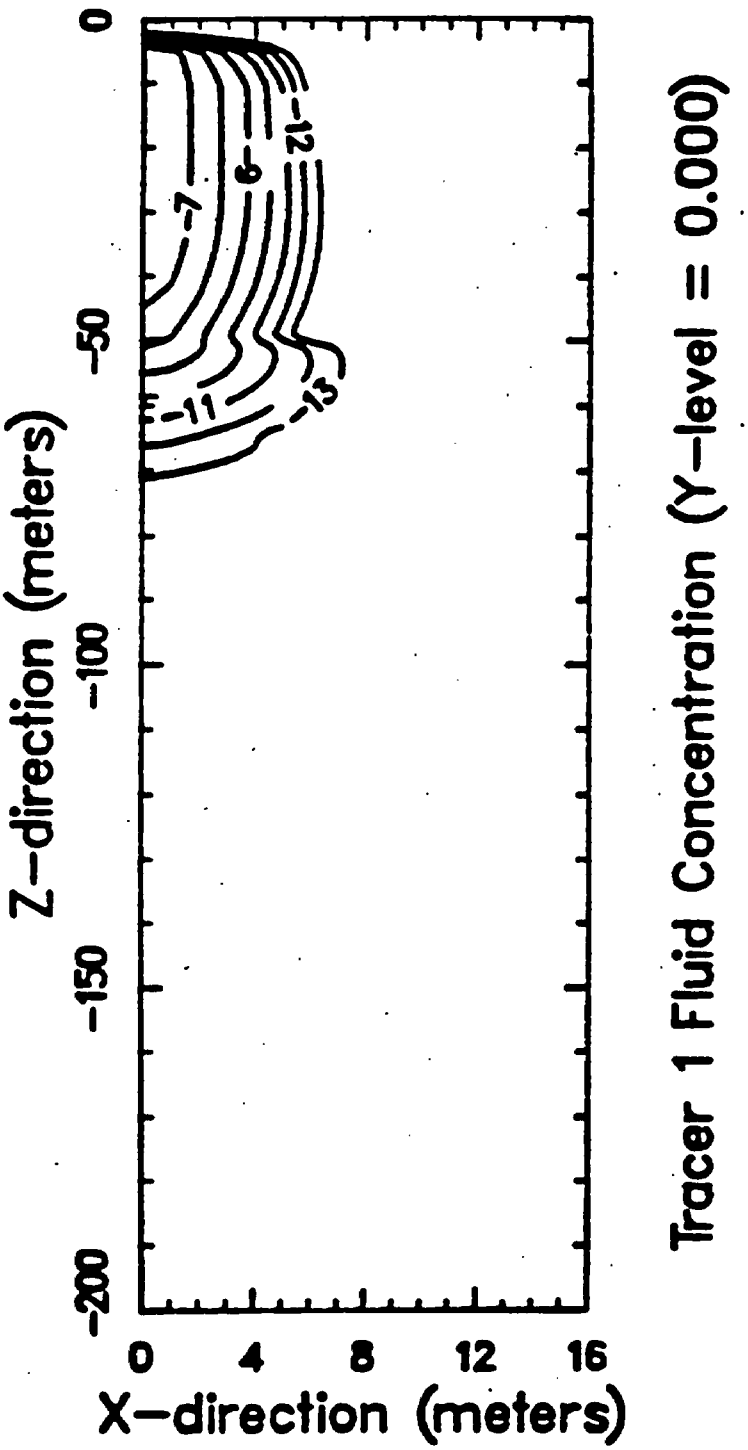

Fig.3

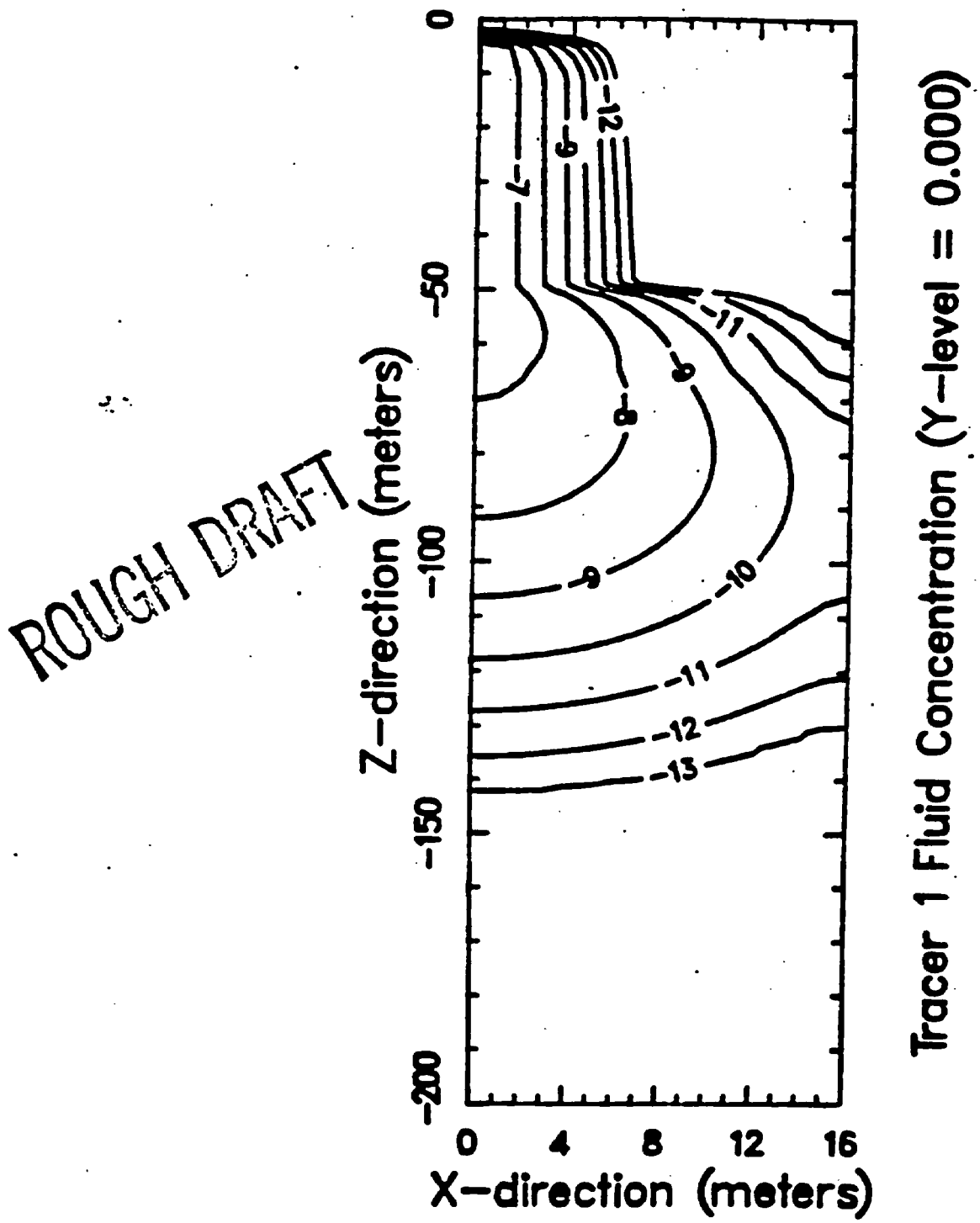
2-d yucca mountain, tc-99 10050.0 years
ROUGH DRAFT
Z-direction (meters)
0
-50
-100
-150
-200
X-direction (meters)
0
4
8
12
16
-7
-9
-12
-11
-8
-9
-10
-11
-12
-13
Tracer 1 Fluid Concentration (Y-level = 0.000)

Fig. 4

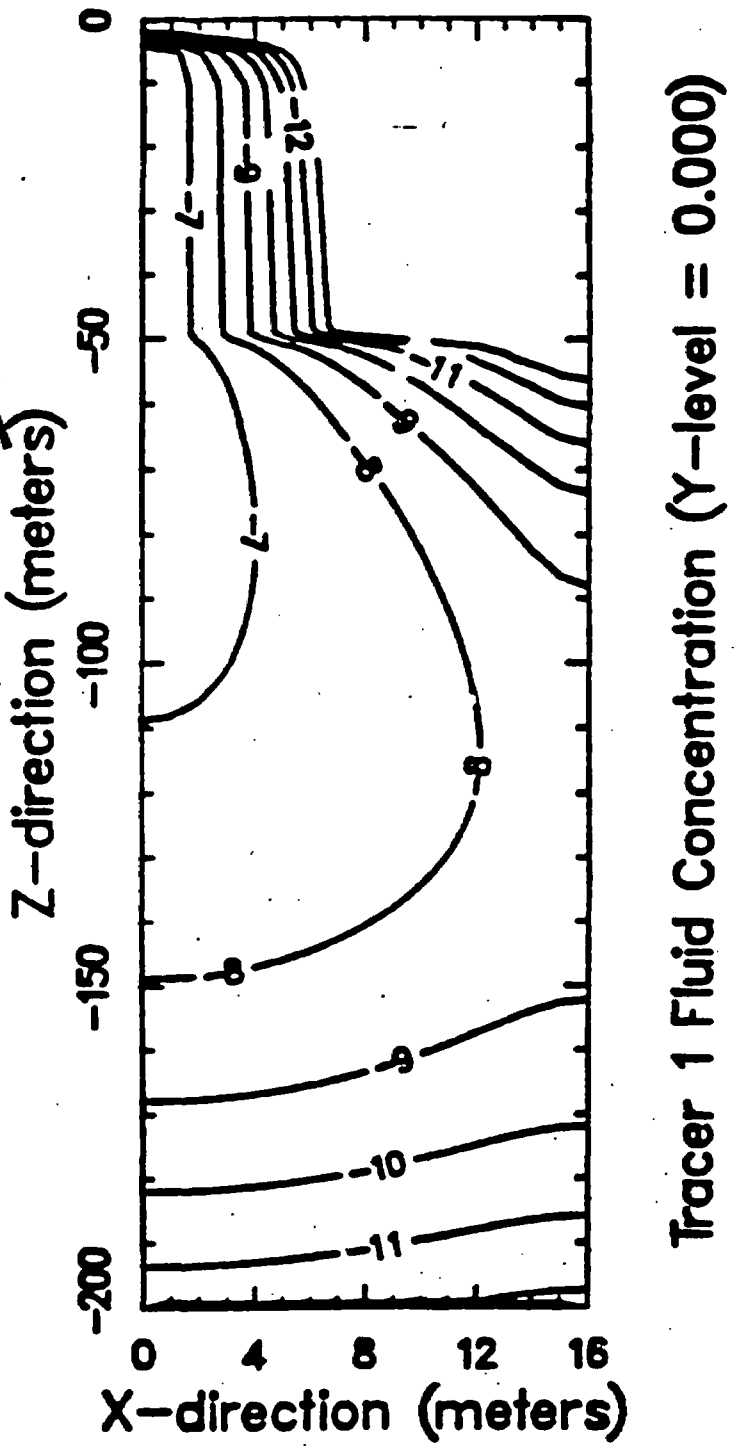

Fig. 5

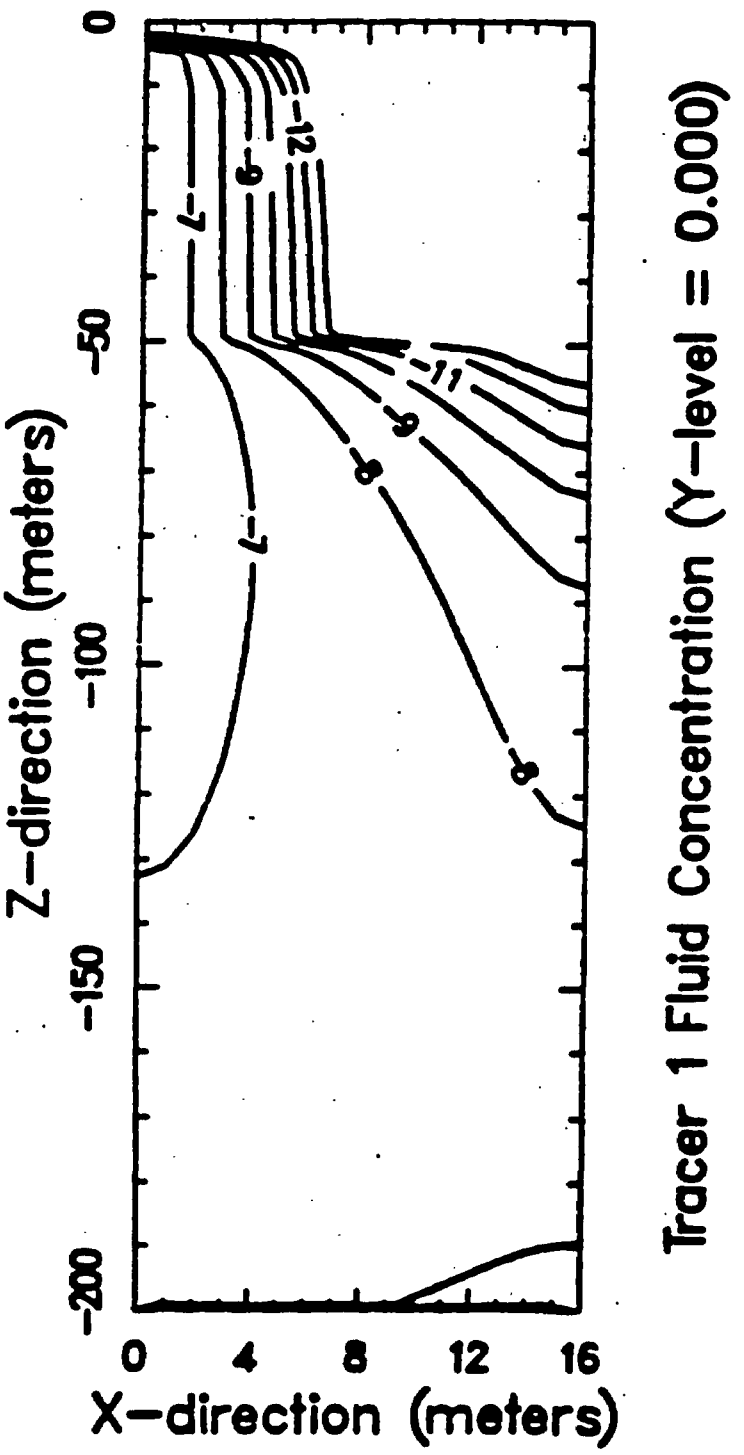

Fig. 6

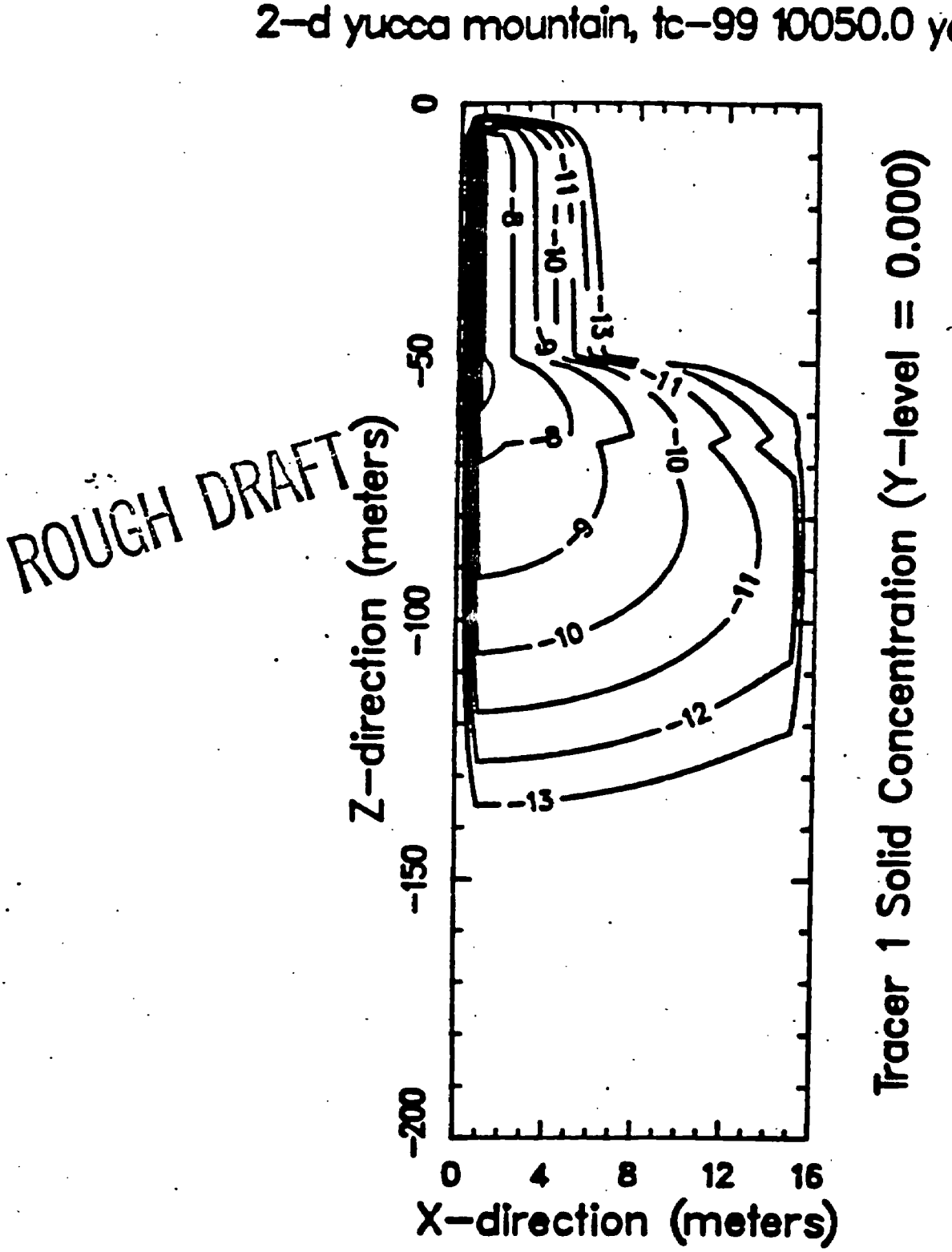
2-d yucca mountain, tc-99 10050.0 years
ROUGH DRAFT
Z-direction (meters)
X-direction (meters)
Tracer 1 Solid Concentration (Y-level = 0.000)
0
-50
-100
-150
-200
0
4
8
12
16
-8
-9
-10
-11
-12
-13

Fig. 7

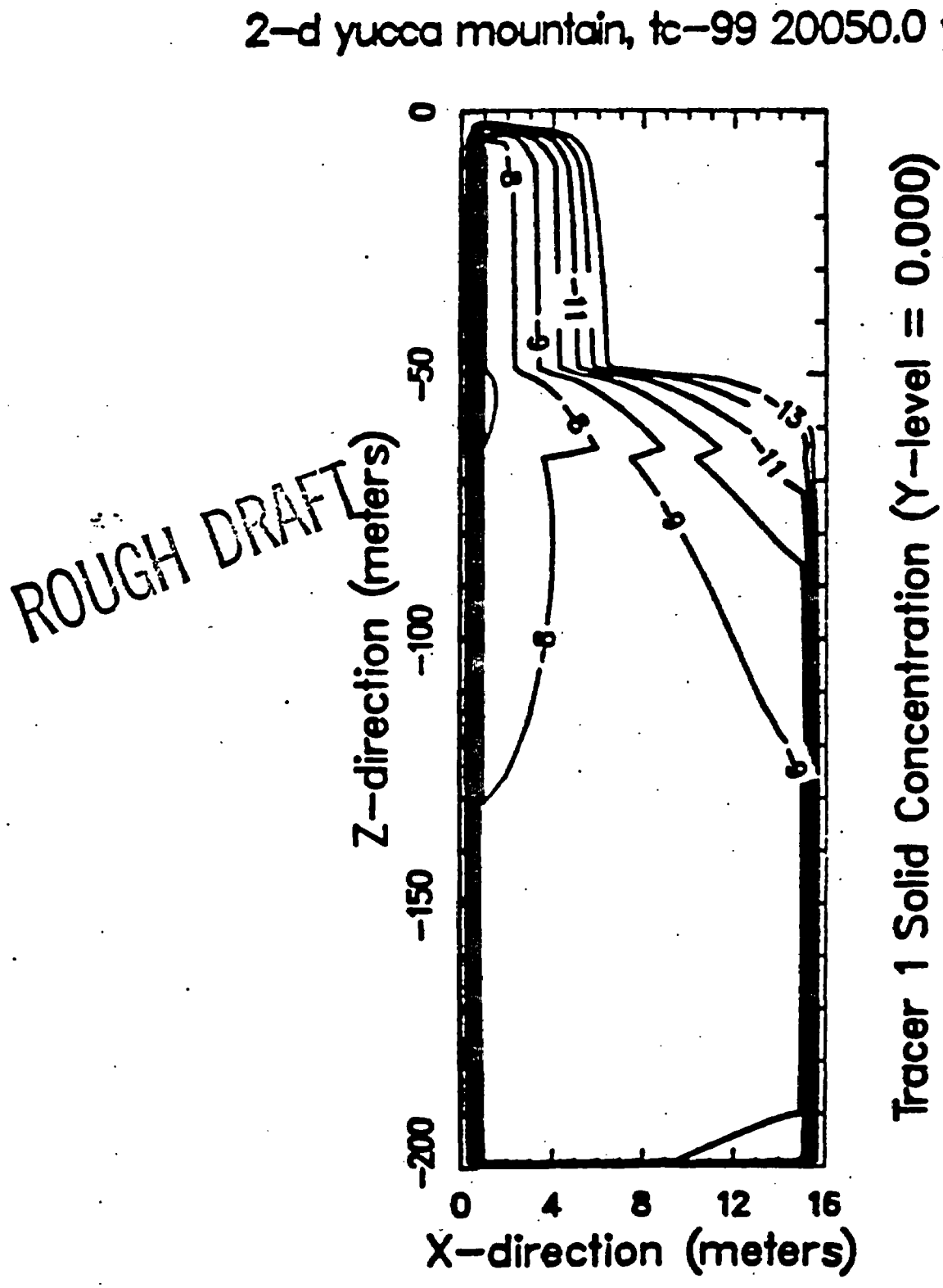
2-d yucca mountain, tc-99 20050.0 years
ROUGH DRAFT
Z-direction (meters)
0
-50
-100
-150
-200
0
4
8
12
16
X-direction (meters)
Tracer 1 Solid Concentration (Y-level = 0.000)
9
6
11
8
13
11
9
8
6

Fig. 8

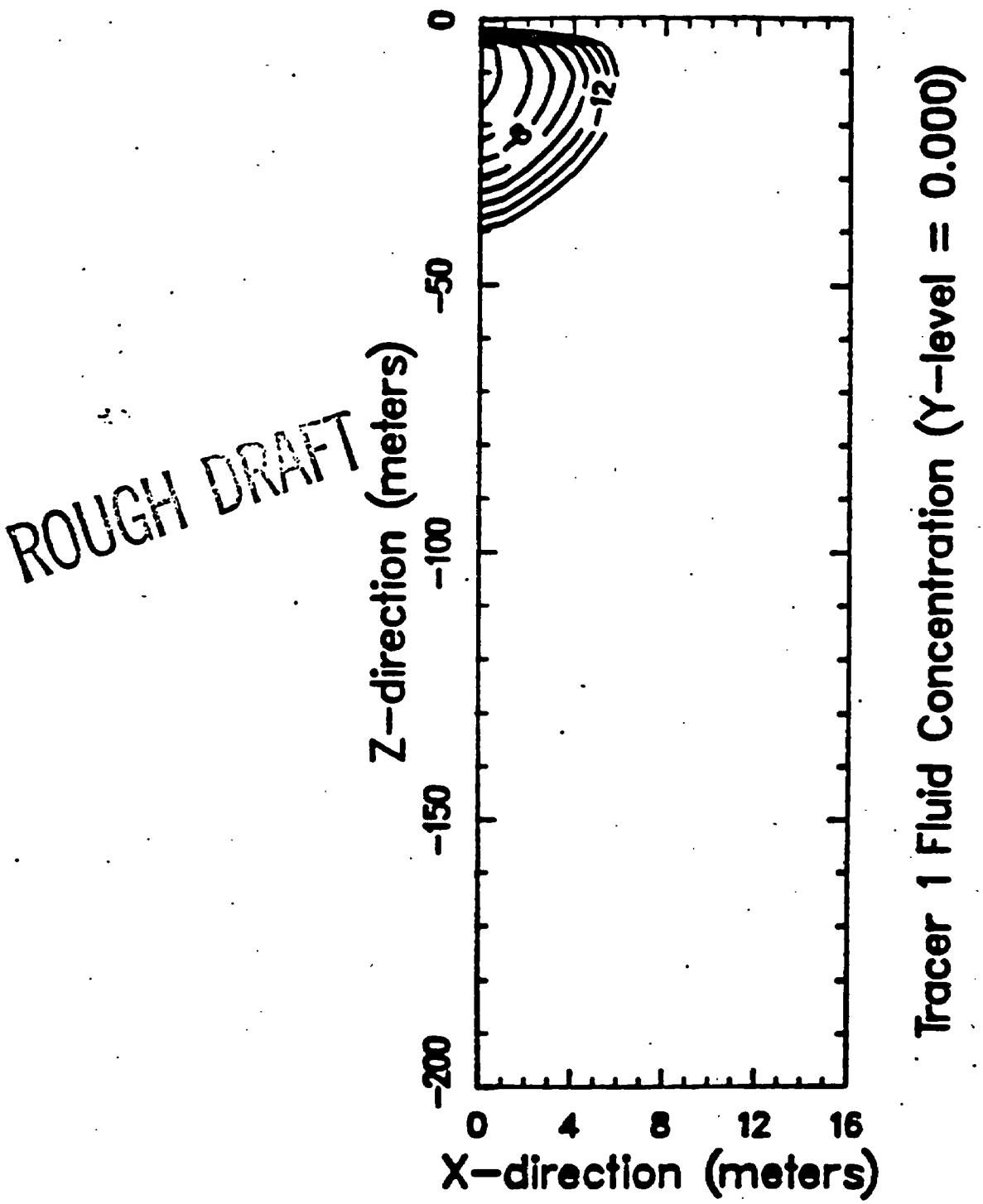

Fig. 9

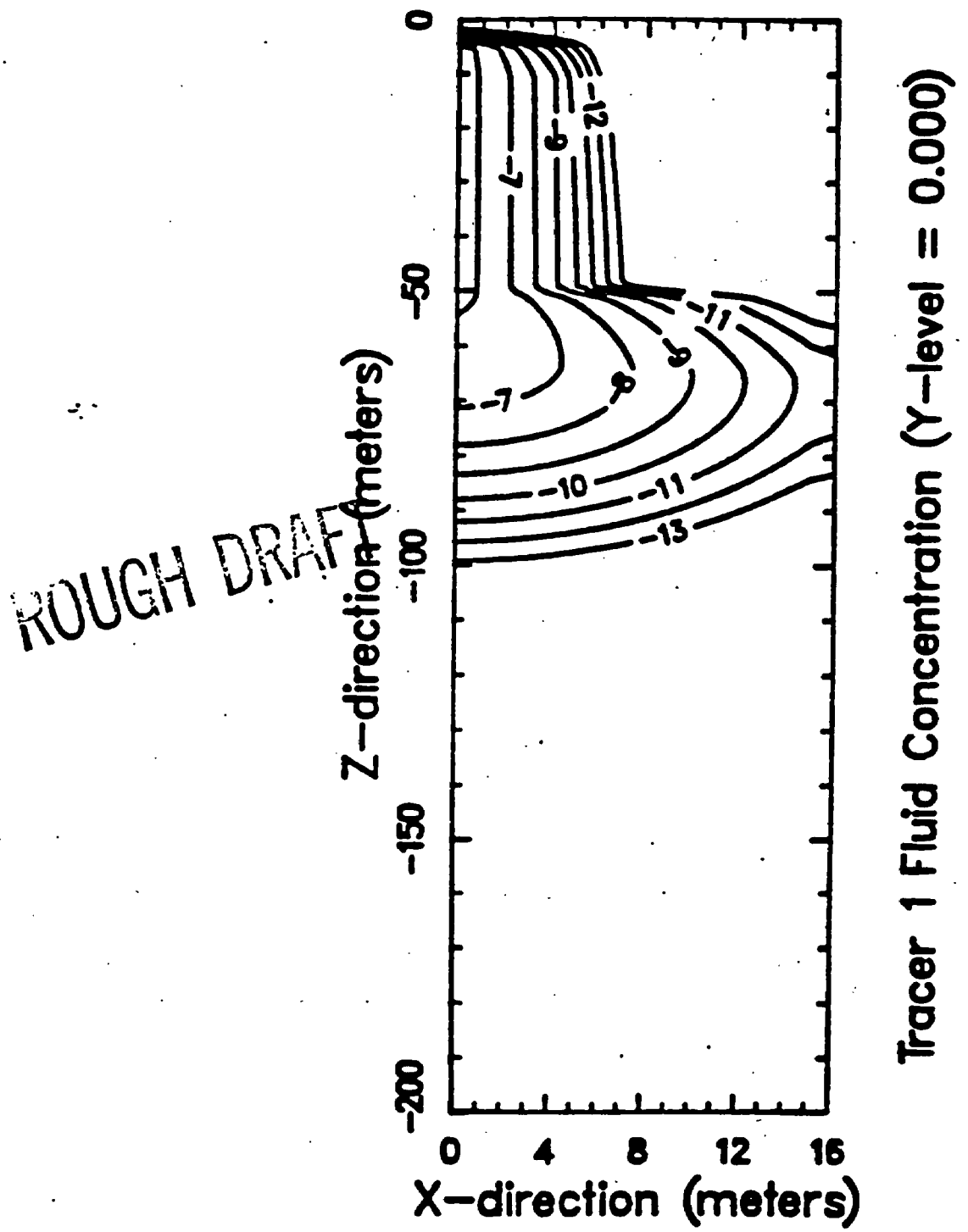

Fig. 10

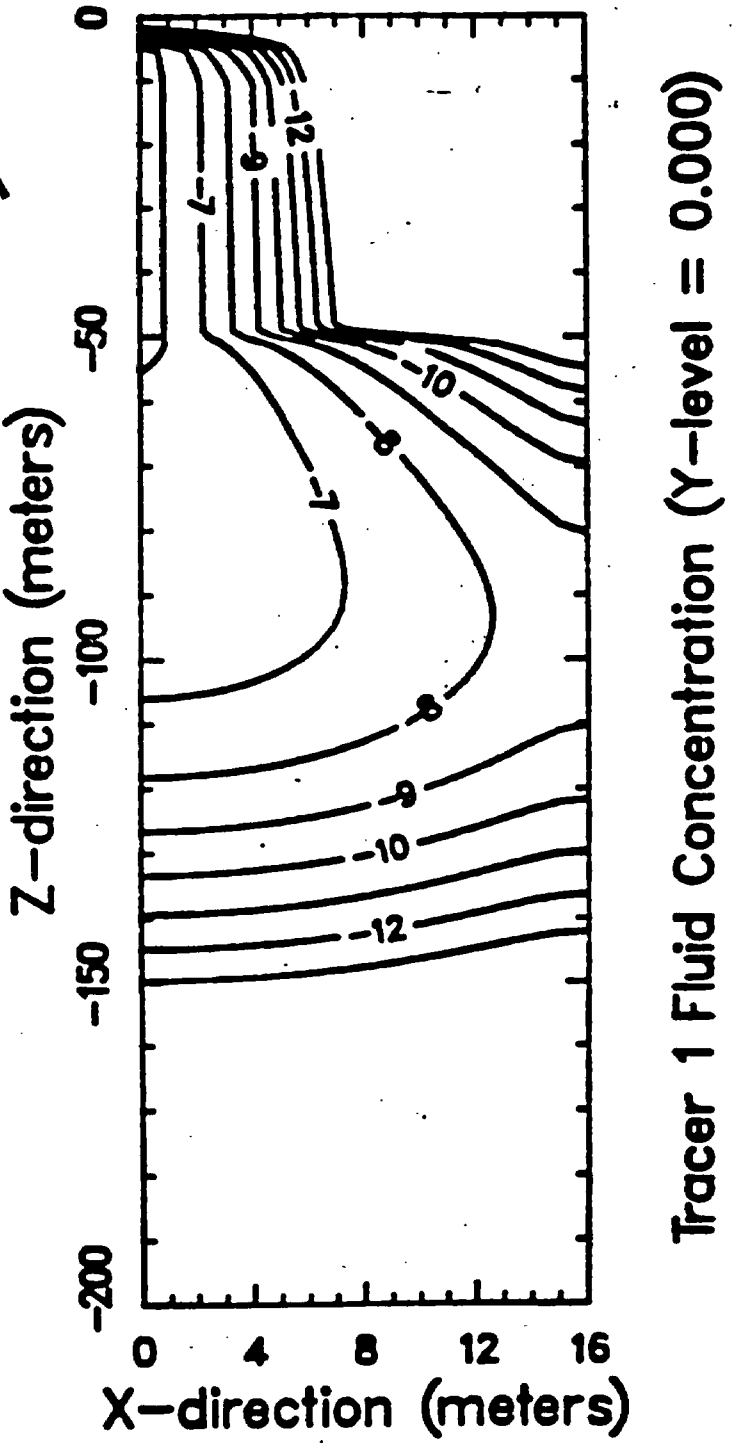

Fig. 11

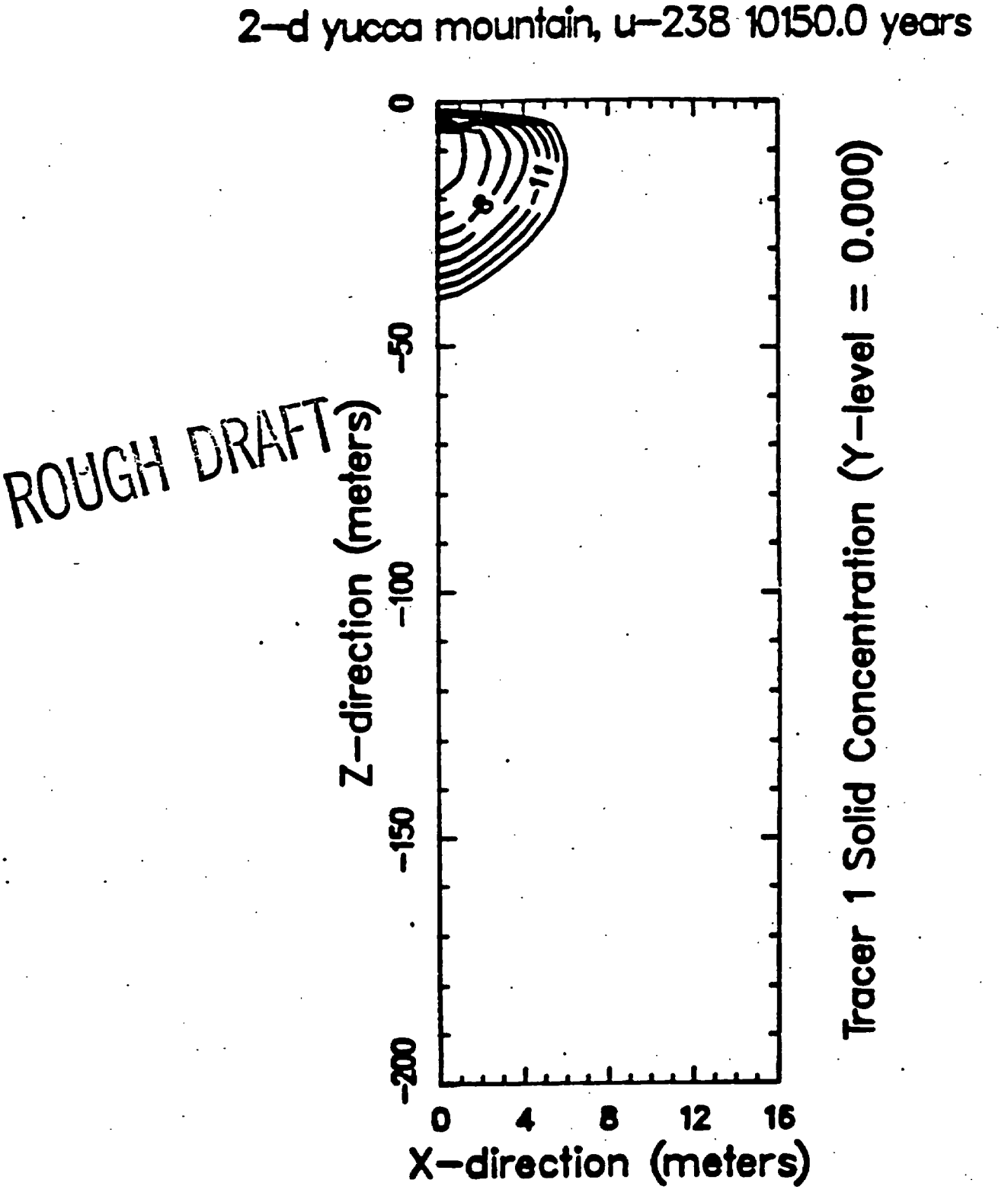
2-d yucca mountain, u-238 10150.0 years
ROUGH DRAFT
0
-50
-100
-150
-200
Z-direction (meters)
0
4
8
12
16
X-direction (meters)
Tracer 1 Solid Concentration (Y-level = 0.000)

Fig. 12

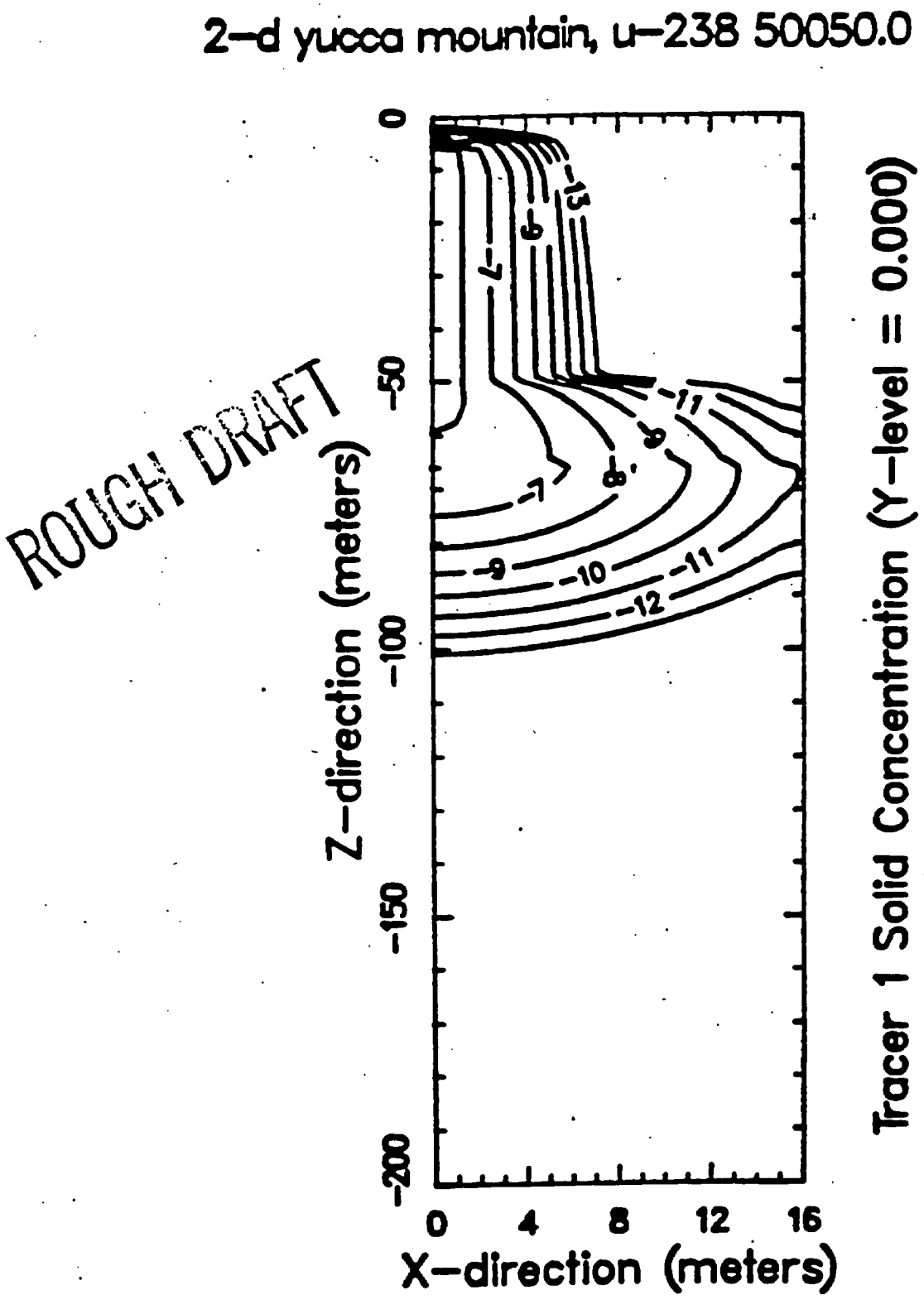
2-d yucca mountain, u-238 50050.0 years
ROUGH DRAFT
Z-direction (meters)
0
-50
-100
-150
-200
0
4
8
12
16
X-direction (meters)
-13
-9
-7
-11
-8
-7
-9
-10
-11
-12
Tracer 1 Solid Concentration (Y-level = 0.000)

Fig. 13

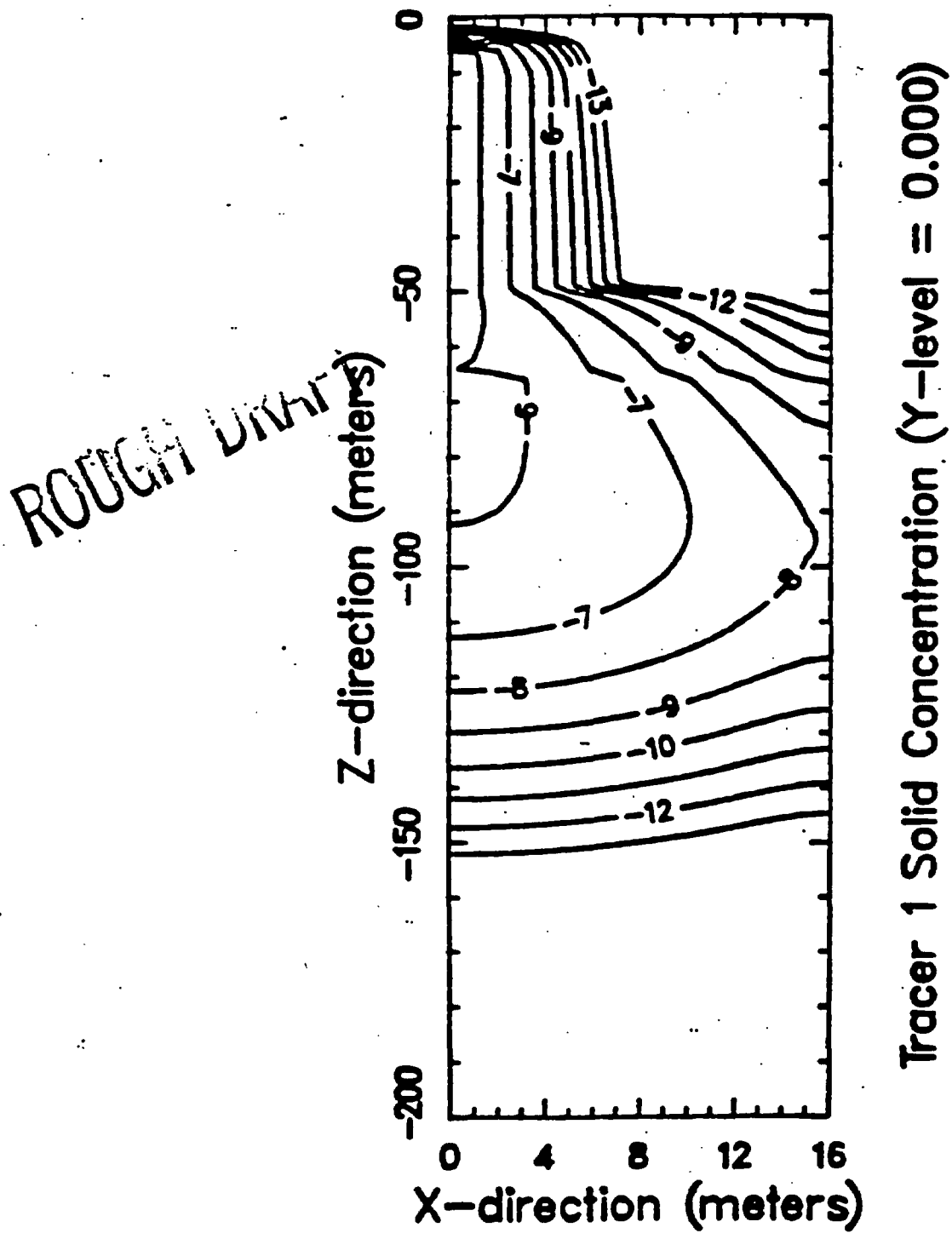
2-d yucca mountain, u-238 98175.0 years
ROUGH DRAFT
Z-direction (meters)
0
-50
-100
-150
-200
0
4
8
12
16
X-direction (meters)
-15
-6
-7
-12
-9
-7
-6
-7
-8
-9
-10
-12
Tracer 1 Solid Concentration (Y-level = 0.000)

Fig. 14

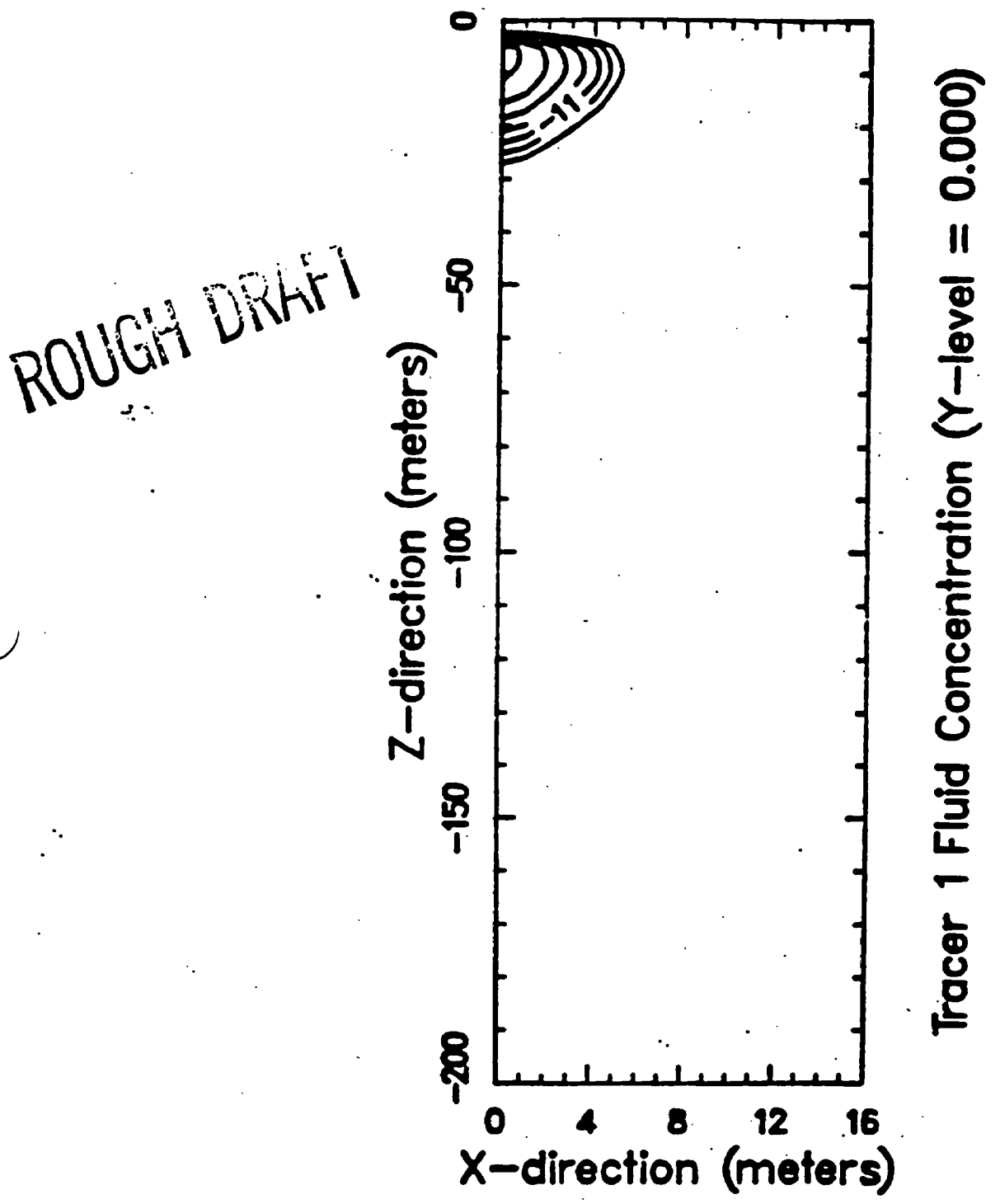
2-d yucca mountain, np-237 20250.0 years
ROUGH DRAFT
0
-50
-100
-150
-200
Z-direction (meters)
-11
0
4
8
12
16
X-direction (meters)
Tracer 1 Fluid Concentration (Y-level = 0.000)

Fig. 15

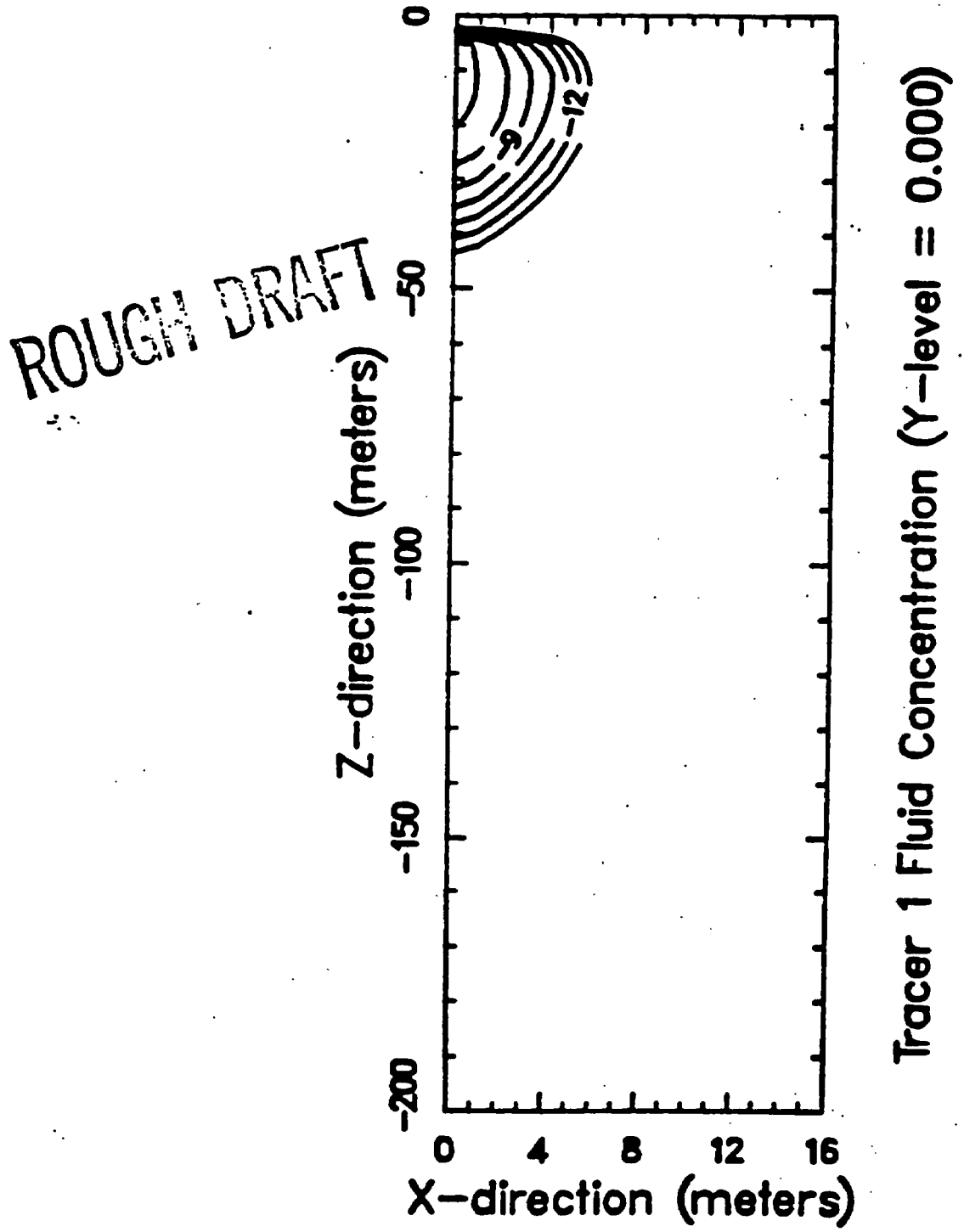
2-d yucca mountain, np-237 50250.0 years
ROUGH DRAFT
0
-50
-100
-150
-200
Z-direction (meters)
0
4
8
12
16
X-direction (meters)
-12
-9
Tracer 1 Fluid Concentration (Y-level = 0.000)

Fig. 16

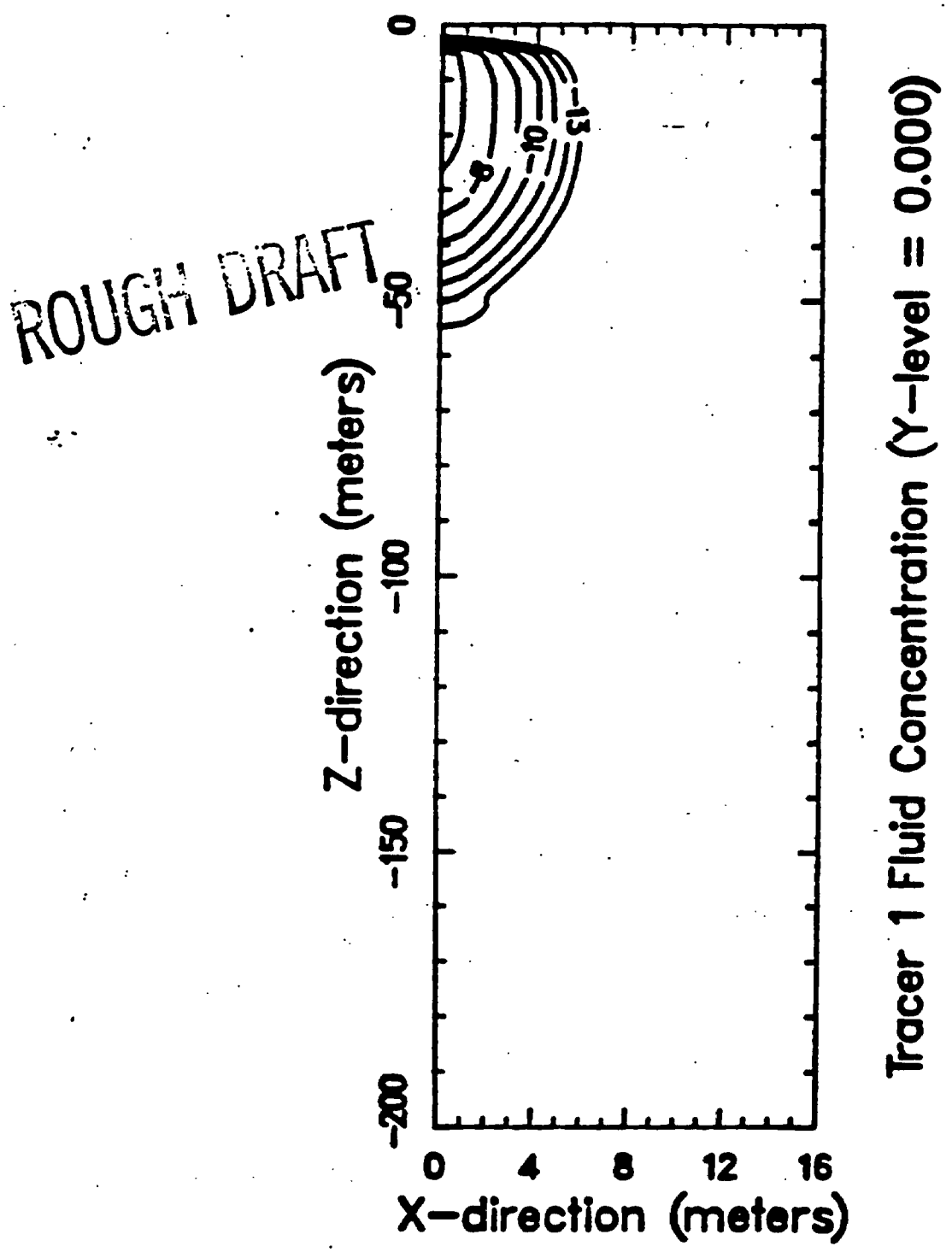
2-d yucca mountain, np-237 70250.0 years
ROUGH DRAFT
Z-direction (meters)
0
-50
-100
-150
-200
X-direction (meters)
0
4
8
12
16
Tracer 1 Fluid Concentration (Y-level = 0.000)

Fig. 17

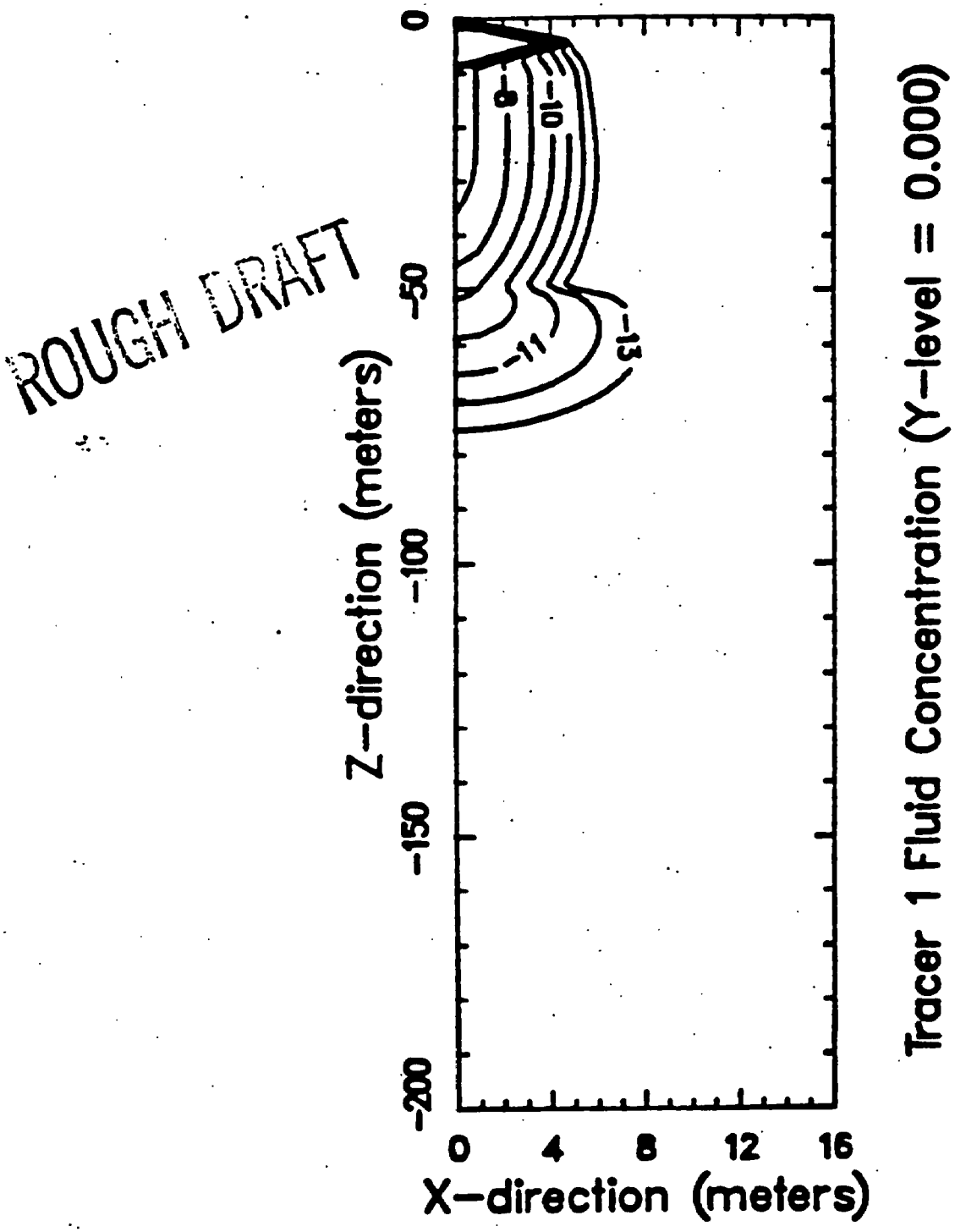
2-d yucca mountain, np-237 100250.0 years
ROUGH DRAFT
0
-50
-100
-150
-200
Z-direction (meters)
0
4
8
12
16
X-direction (meters)
-9
-10
-11
-13
Tracer 1 Fluid Concentration (Y-level = 0.000)

Fig. 18

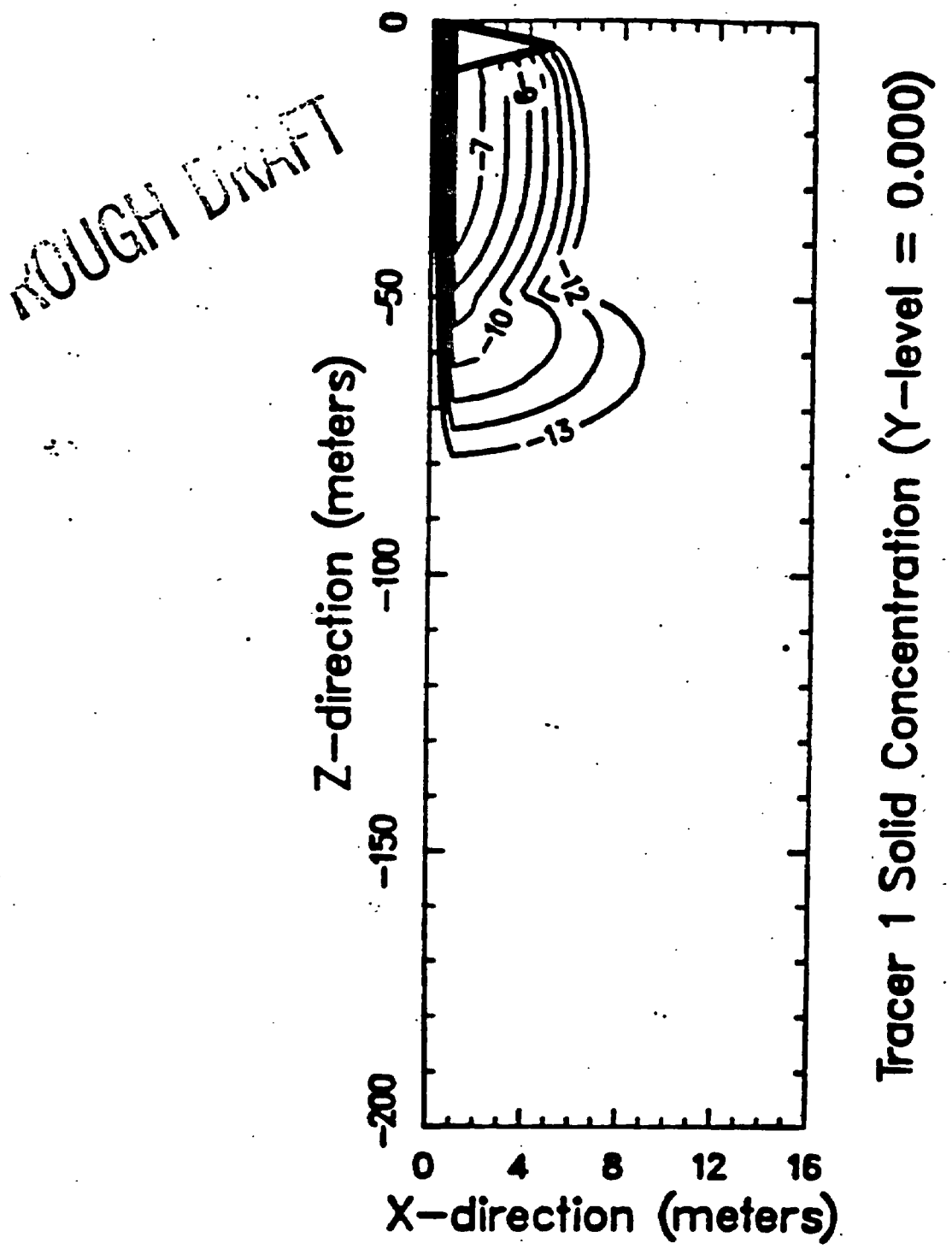
2-d yucca mountain, np-237 100250.0 years
ROUGH DRAFT
0
-50
-100
-150
-200
Z-direction (meters)
-6
-7
-10
-12
-13
0
4
8
12
16
X-direction (meters)
Tracer 1 Solid Concentration (Y-level = 0.000)

Fig. 19

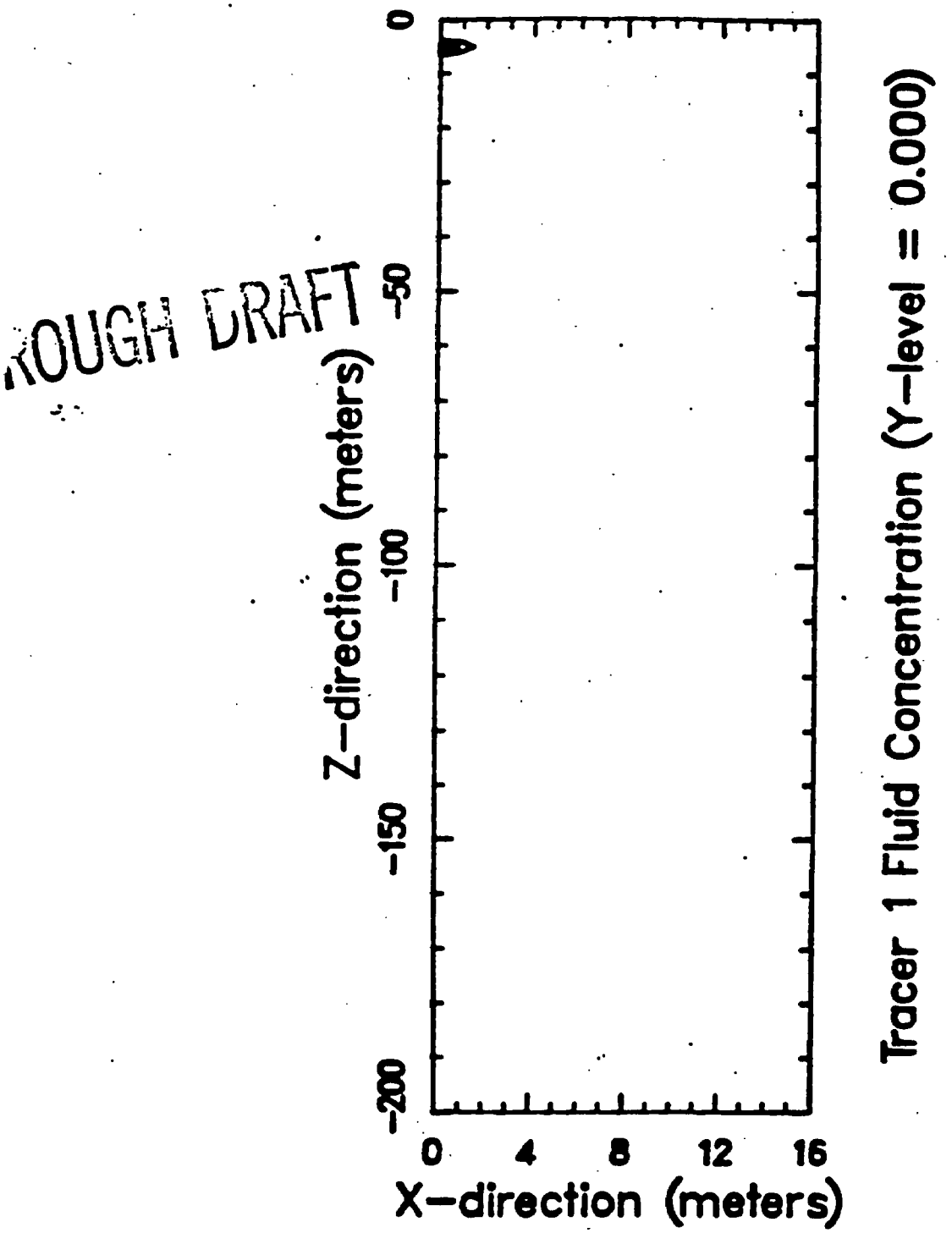
2-d yucca mountain, am-243 100500.0 years
ROUGH DRAFT
0
-50
-100
-150
-200
Z-direction (meters)
0
4
8
12
16
X-direction (meters)
Tracer 1 Fluid Concentration (Y-level = 0.000)

Fig. 20

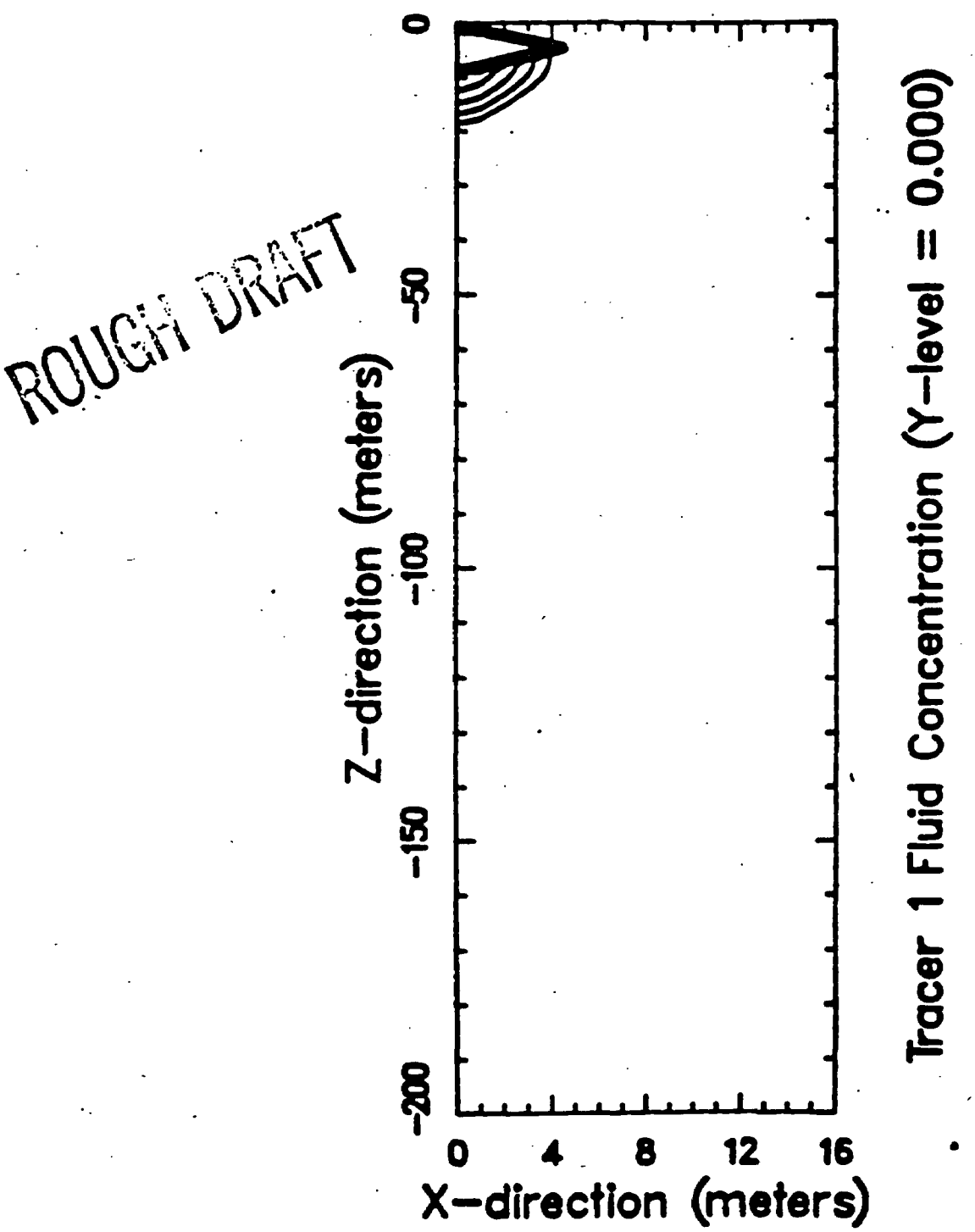
2-d yucca mountain, pu-239 102500.0 years
ROUGH DRAFT
Z-direction (meters)
0
-50
-100
-150
-200
0
4
8
12
16
X-direction (meters)
Tracer 1 Fluid Concentration (Y-level = 0.000)

Fig. 21

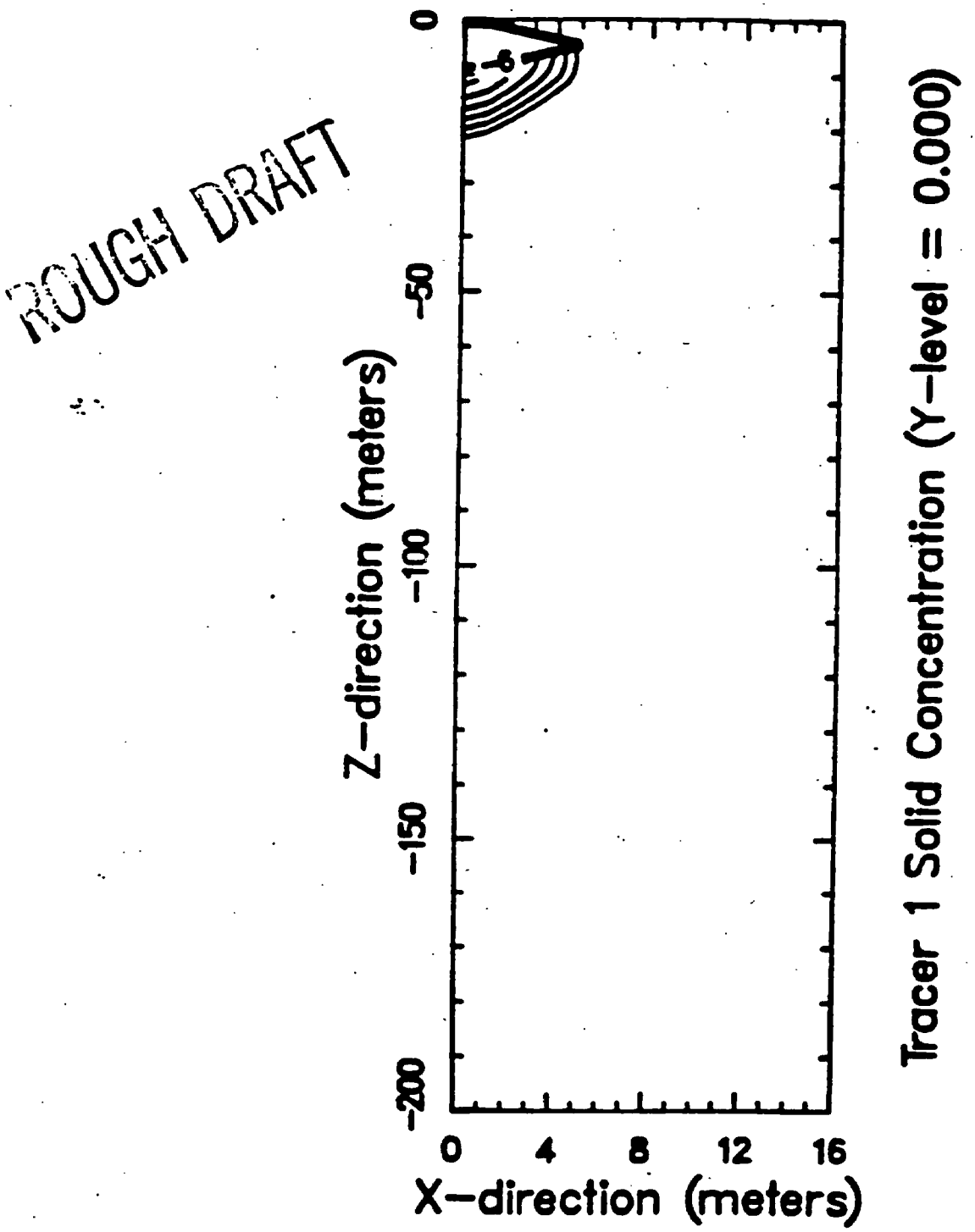

Fig 22

ROUGH DRAFT

Yucca Mountain

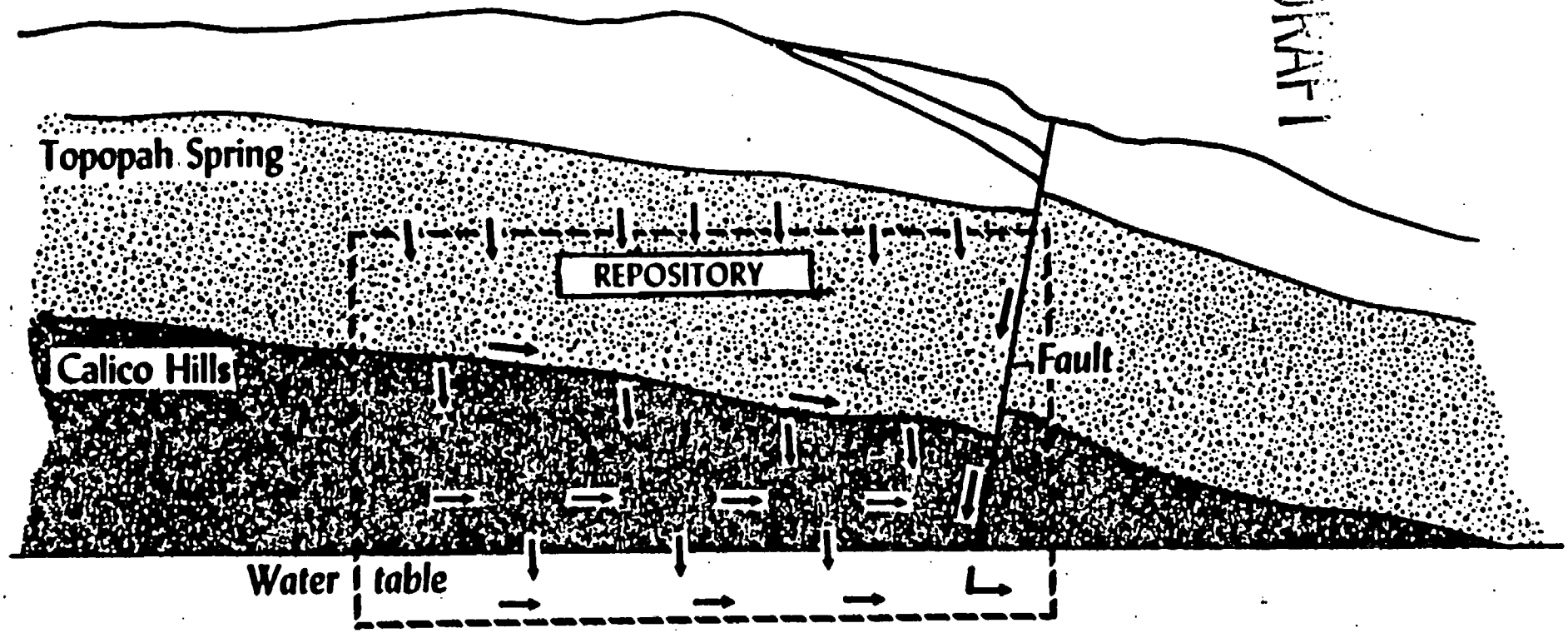

F-9-23

TRACER 1 FLUID CONCENTRATION X-Z PLANE AT Y-LEVEL = 0.500 'M TIME = 5100.00 YEARS

0= 1.000E-15 1= 1.000E-14 2= 1.000E-13 3= 1.000E-12 4= 1.000E-11 5= 1.000E-10 6= 1.000E-09 7= 1.000E-08 8= 1.000E-07 9= 1.000E-06

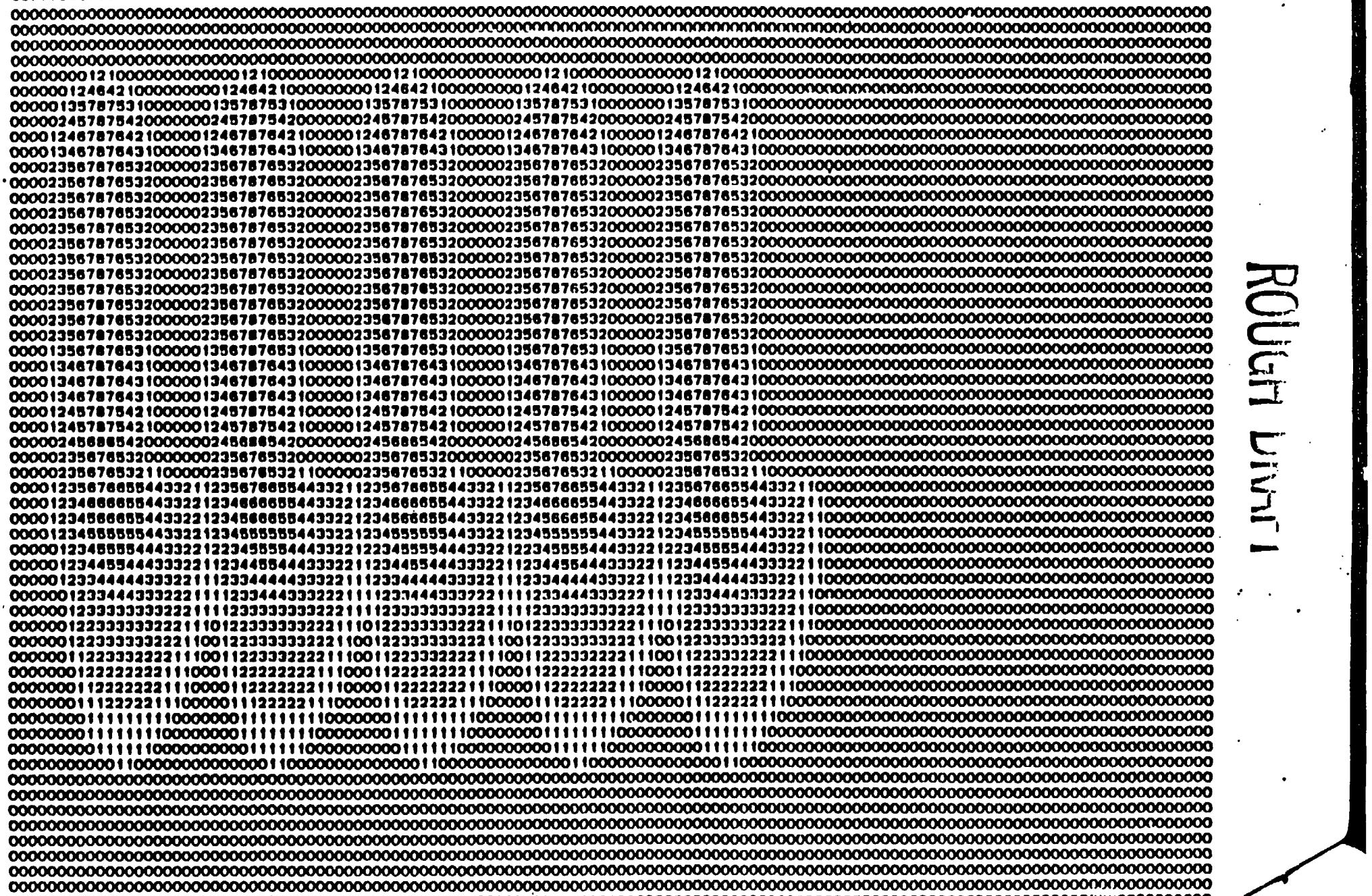

ROUGH DRAFT

888

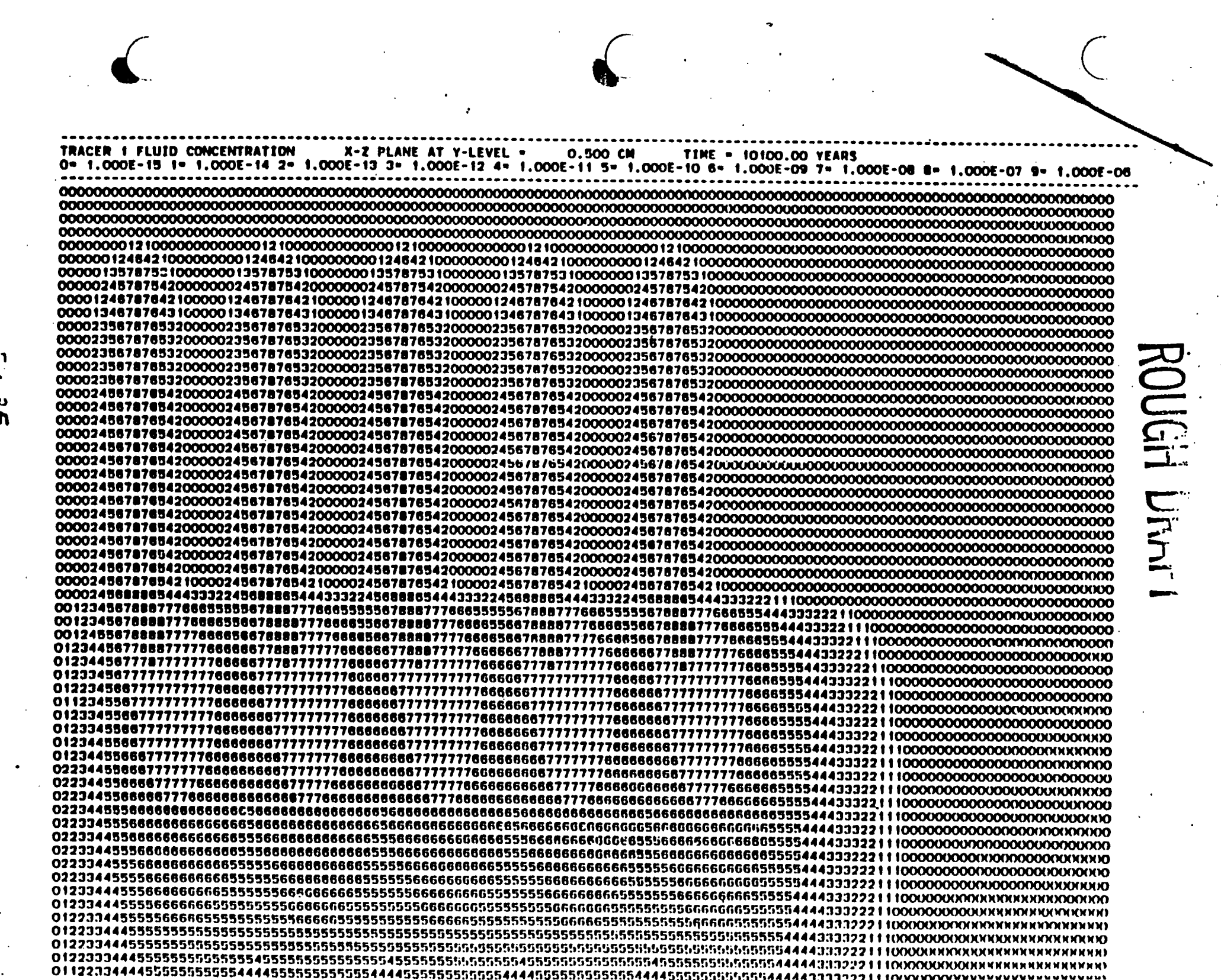
TRACER 1 FLUID CONCENTRATION X-Z PLANE AT Y-LEVEL = 0.500 CM TIME = 10100.00 YEARS
0= 1.000E-15 1= 1.000E-14 2= 1.000E-13 3= 1.000E-12 4= 1.000E-11 5= 1.000E-10 6= 1.000E-09 7= 1.000E-08 8= 1.000E-07 9= 1.000E-06

ROUGH DRAFT

ROUGH DRAFT

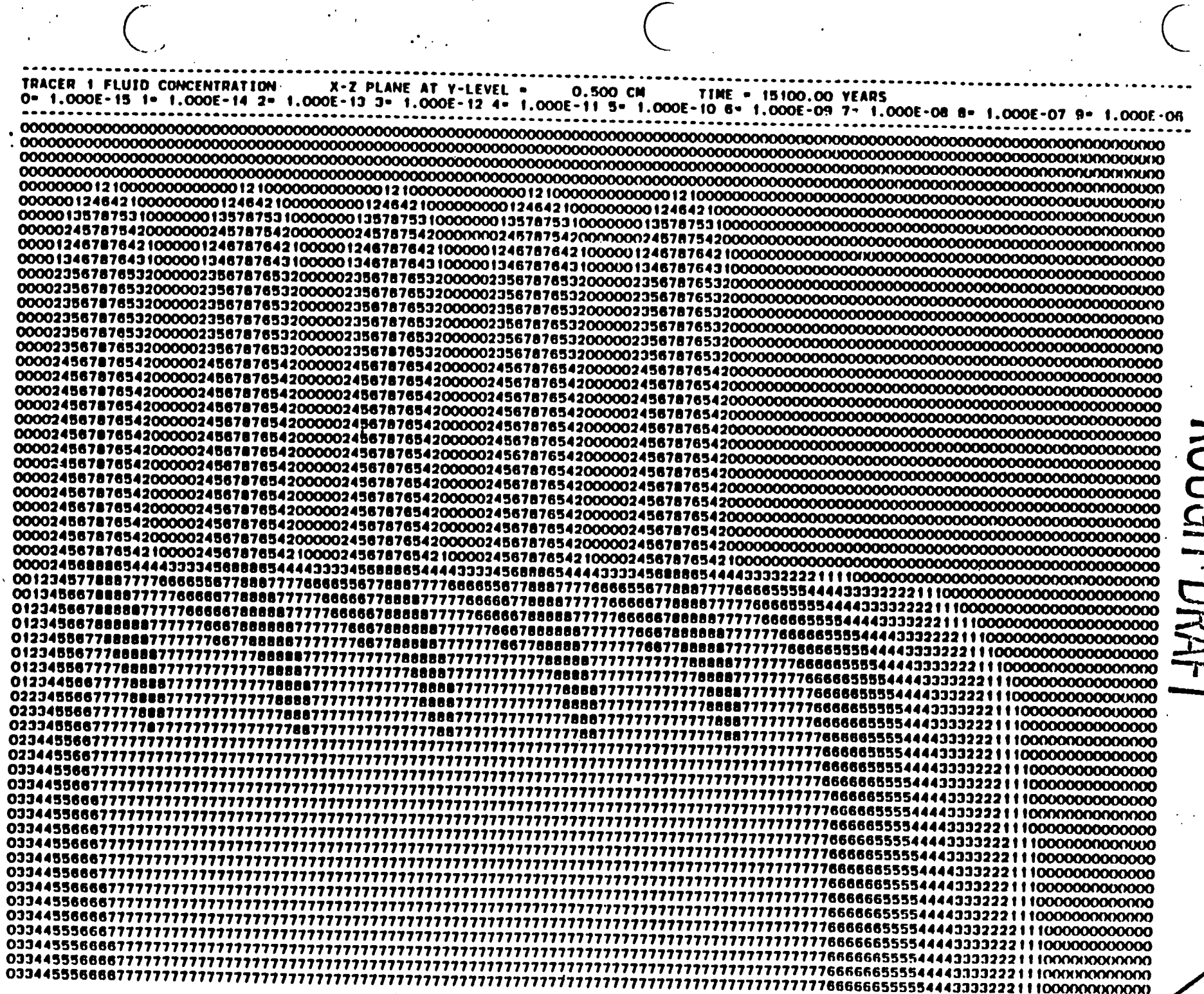
TRACER 1 FLUID CONCENTRATION X-Z PLANE AT Y-LEVEL = 0.500 CM TIME = 15100.00 YEARS
0= 1.000E-15 1= 1.000E-14 2= 1.000E-13 3= 1.000E-12 4= 1.000E-11 5= 1.000E-10 6= 1.000E-09 7= 1.000E-08 8= 1.000E-07 9= 1.000E-06

Fig. 86 cont'd

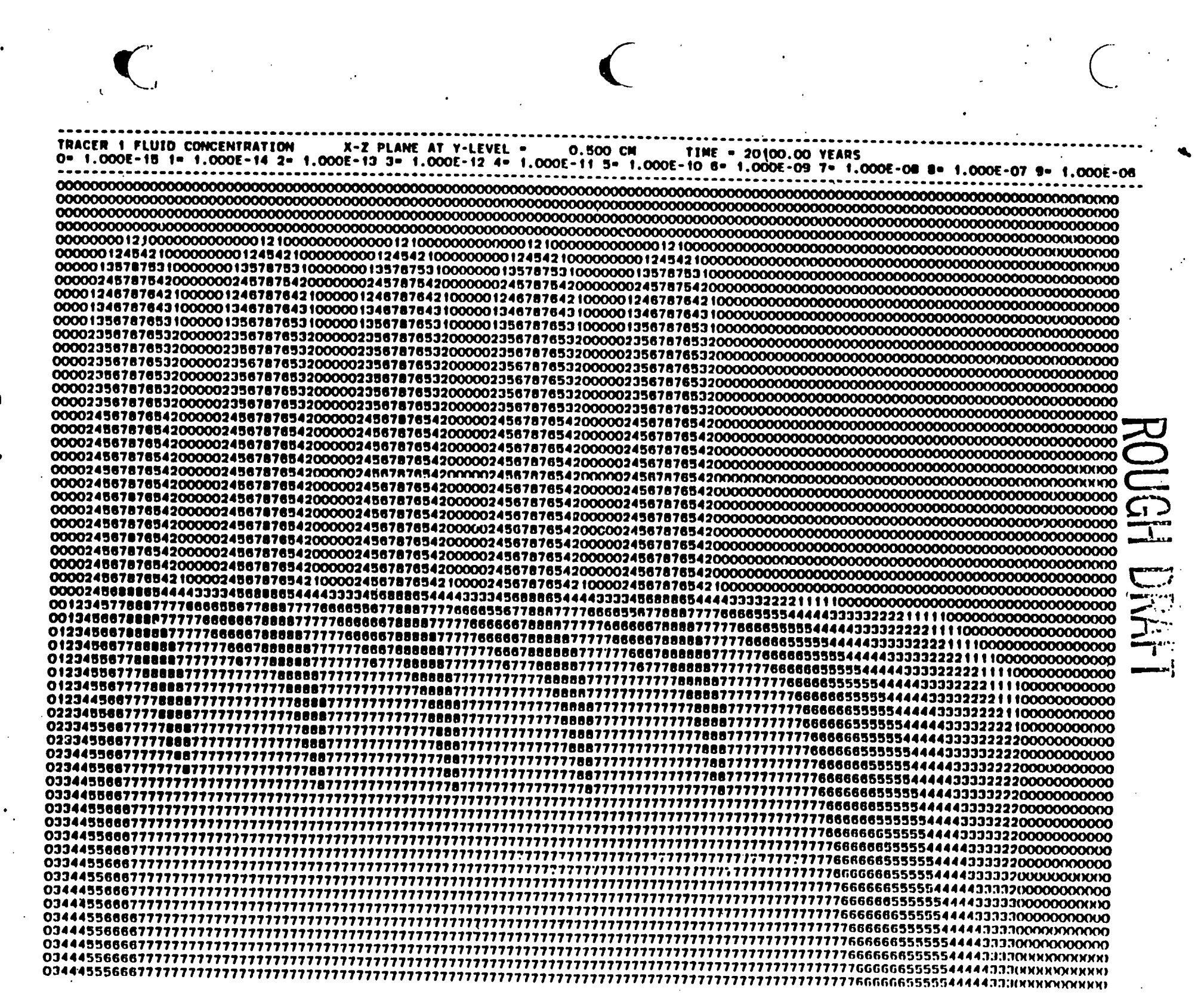
TRACER 1 FLUID CONCENTRATION X-Z PLANE AT Y-LEVEL = 0.500 CM TIME = 20100.00 YEARS
0= 1.000E-15 1= 1.000E-14 2= 1.000E-13 3= 1.000E-12 4= 1.000E-11 5= 1.000E-10 6= 1.000E-09 7= 1.000E-08 8= 1.000E-07 9= 1.000E-06

ROUGH DRAFT

TRACER 1 SOLID CONCENTRATION X-Z PLANE AT Y-LEVEL = 0.500 CM TIME = 5100.00 YEARS

0= 1.000E-15 1= 1.000E-14 2= 1.000E-13 3= 1.000E-12 4= 1.000E-11 5= 1.000E-10 6= 1.000E-09 7= 1.000E-08 8= 1.000E-07 9= 1.000E-06

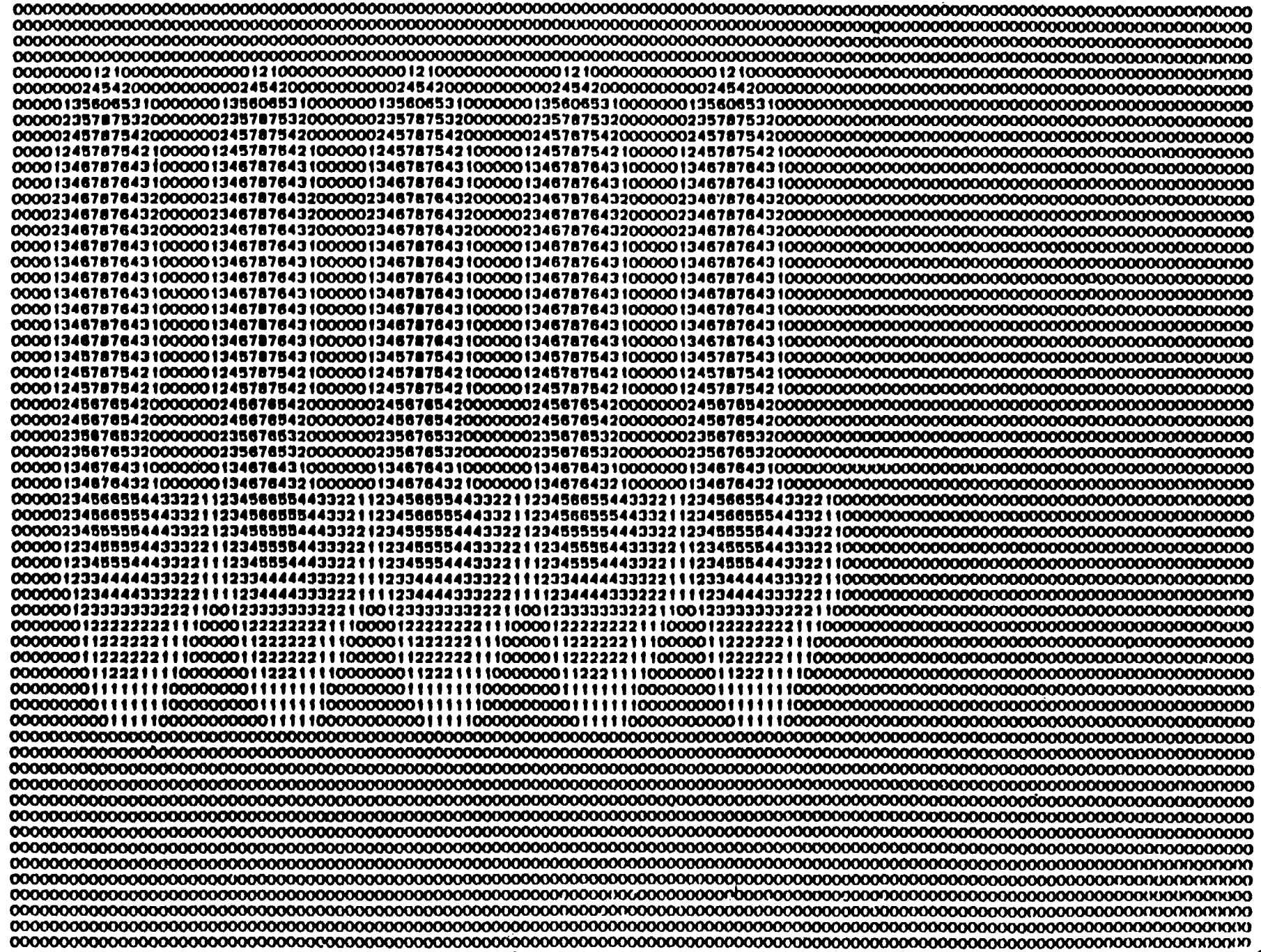

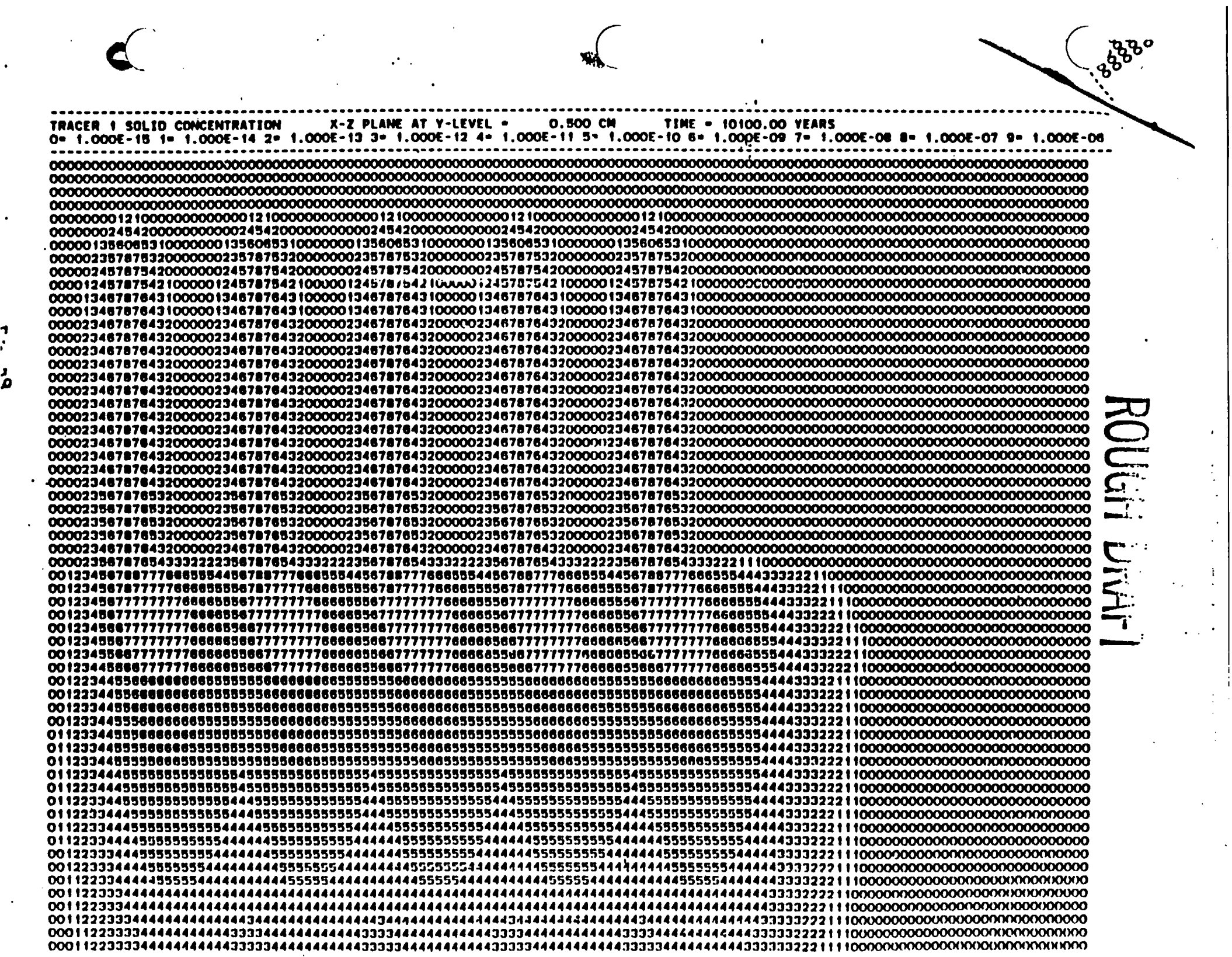
TRACER 1 SOLID CONCENTRATION X-Z PLANE AT Y-LEVEL = 0.500 CM TIME = 10100.00 YEARS
0= 1.000E-15 1= 1.000E-14 2= 1.000E-13 3= 1.000E-12 4= 1.000E-11 5= 1.000E-10 6= 1.000E-09 7= 1.000E-08 8= 1.000E-07 9= 1.000E-06

ROUGH DRAFT

ROUGH DRAFT

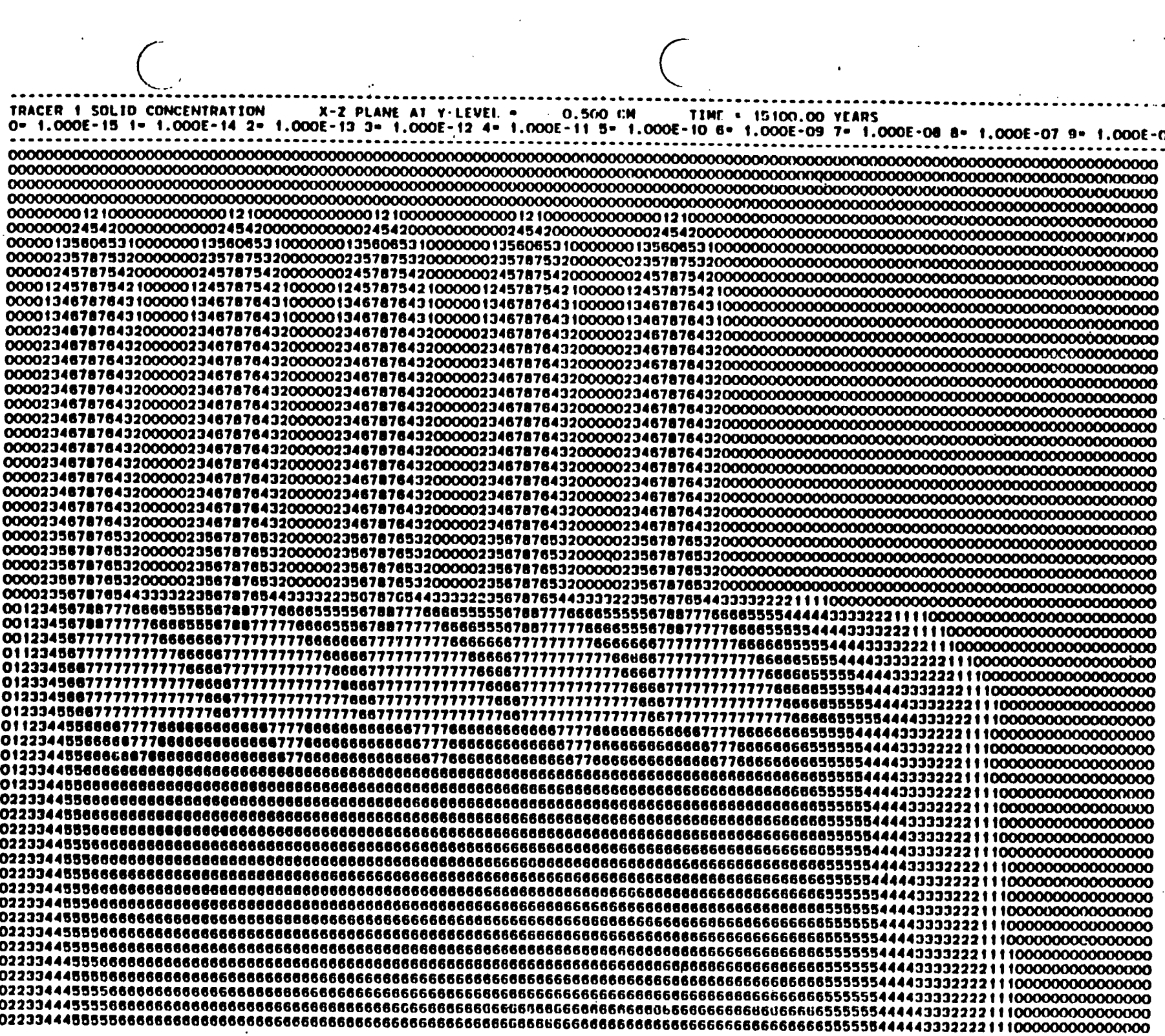
TRACER 1 SOLID CONCENTRATION X-Z PLANE AT Y-LEVEL = 0.500 CM TIME = 15100.00 YEARS
0= 1.000E-15 1= 1.000E-14 2= 1.000E-13 3= 1.000E-12 4= 1.000E-11 5= 1.000E-10 6= 1.000E-09 7= 1.000E-08 8= 1.000E-07 9= 1.000E-06

ROUGH DRAFT

ROUGH DRAFT

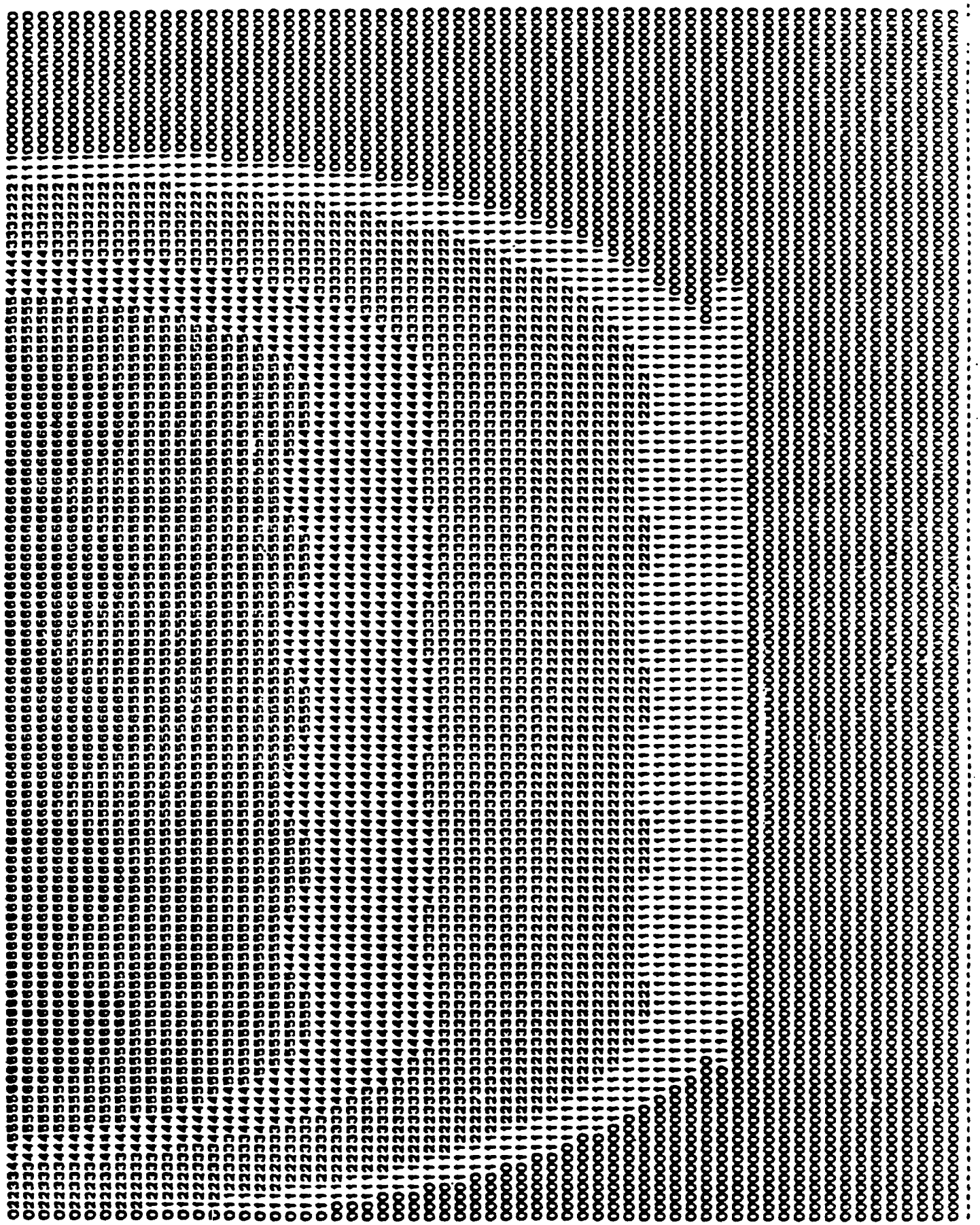

Fig. 3D cont'd

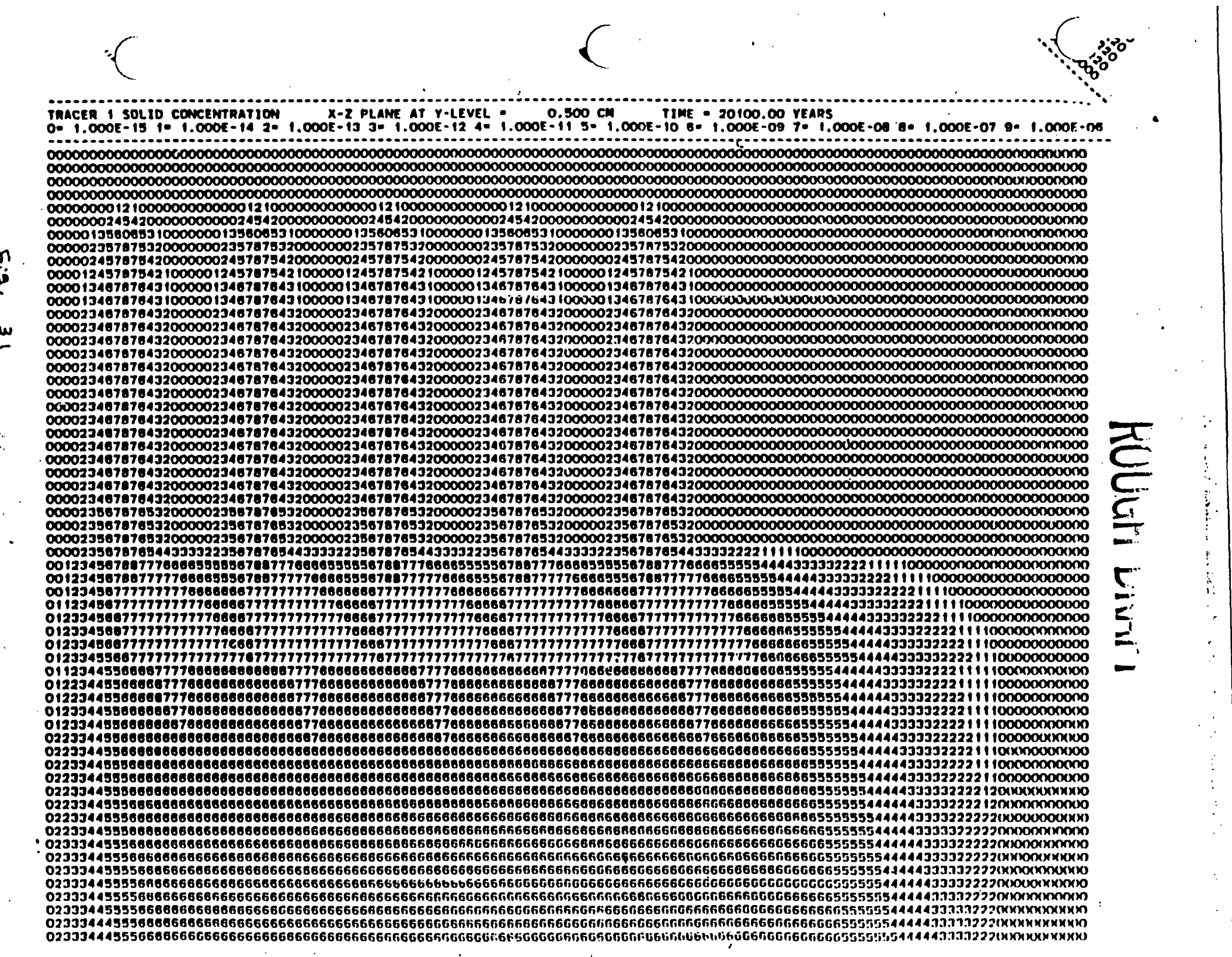
TRACER 1 SOLID CONCENTRATION X-Z PLANE AT Y-LEVEL = 0.500 CM TIME = 20100.00 YEARS
0= 1.000E-15 1= 1.000E-14 2= 1.000E-13 3= 1.000E-12 4= 1.000E-11 5= 1.000E-10 6= 1.000E-09 7= 1.000E-08 8= 1.000E-07 9= 1.000E-06
RUN 1

ROUGH DRAFT

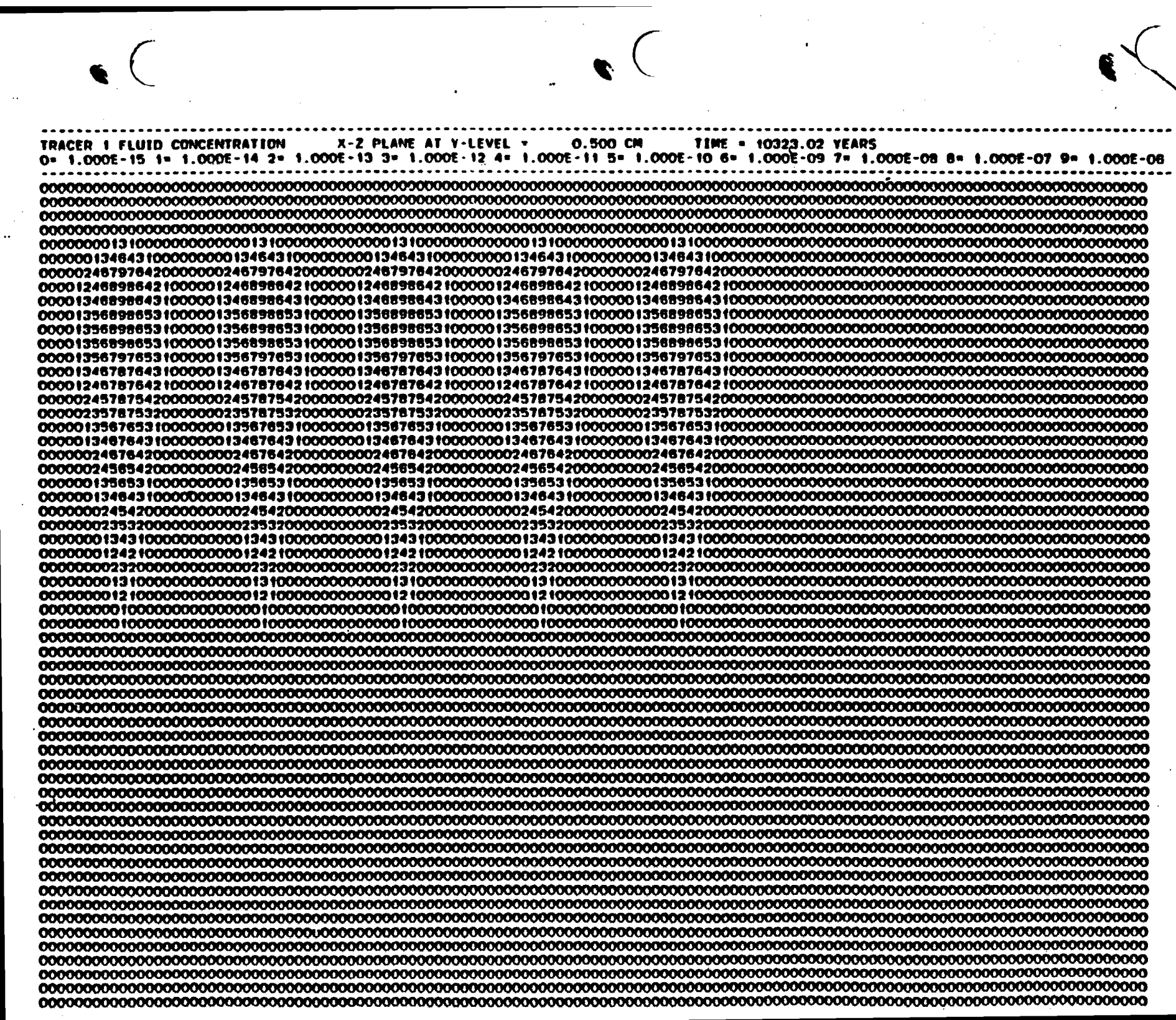
TRACER 1 FLUID CONCENTRATION X-Z PLANE AT Y-LEVEL = 0.500 CM TIME = 10323.02 YEARS
0= 1.000E-15 1= 1.000E-14 2= 1.000E-13 3= 1.000E-12 4= 1.000E-11 5= 1.000E-10 6= 1.000E-09 7= 1.000E-08 8= 1.000E-07 9= 1.000E-06

ROUGH DRAFT

ROUGH DRAFT

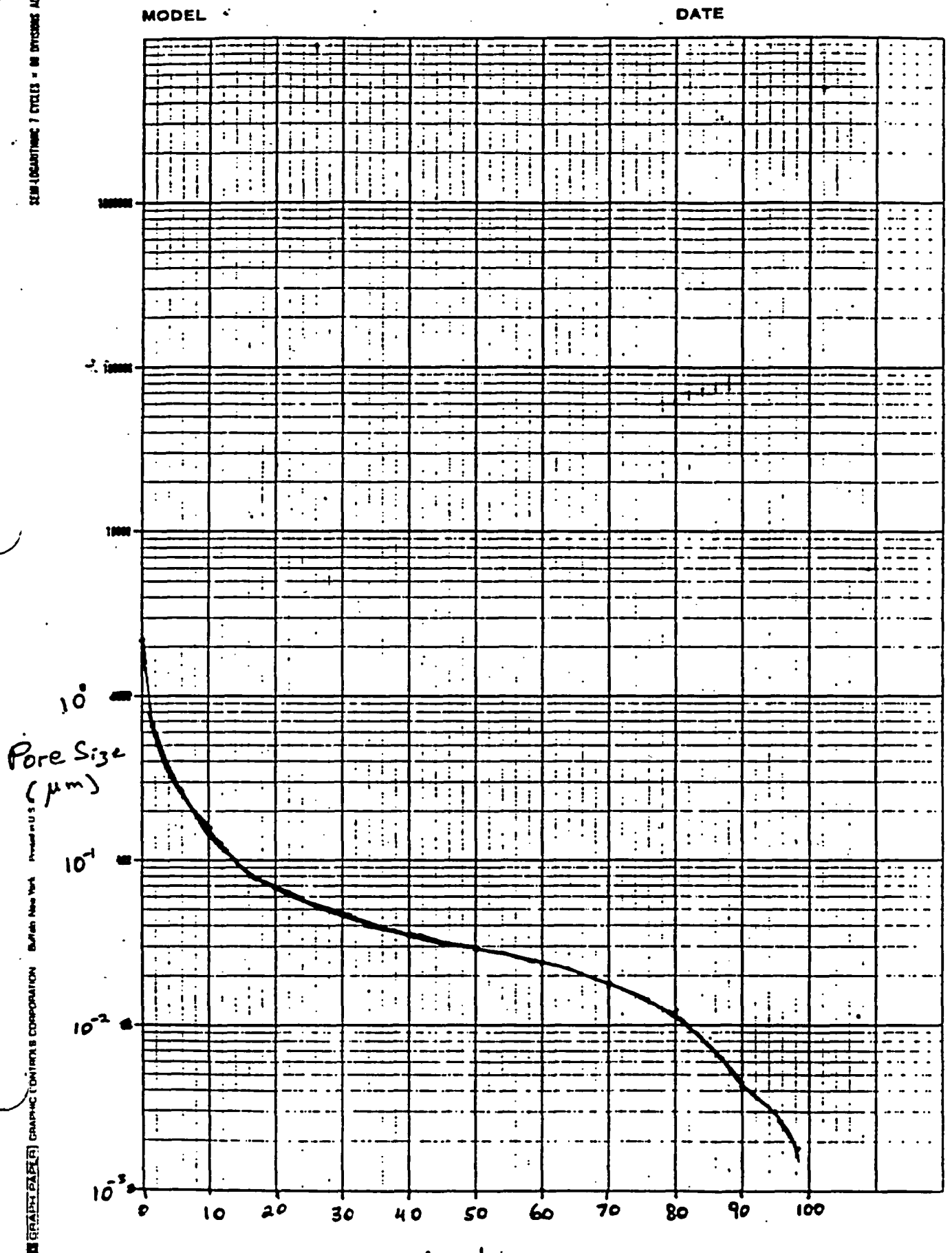
MODEL
DATE
Pore Size (μm)
10°
10⁻¹
10⁻²
10⁻³
0
10
20
30
40
50
60
70
80
90
100

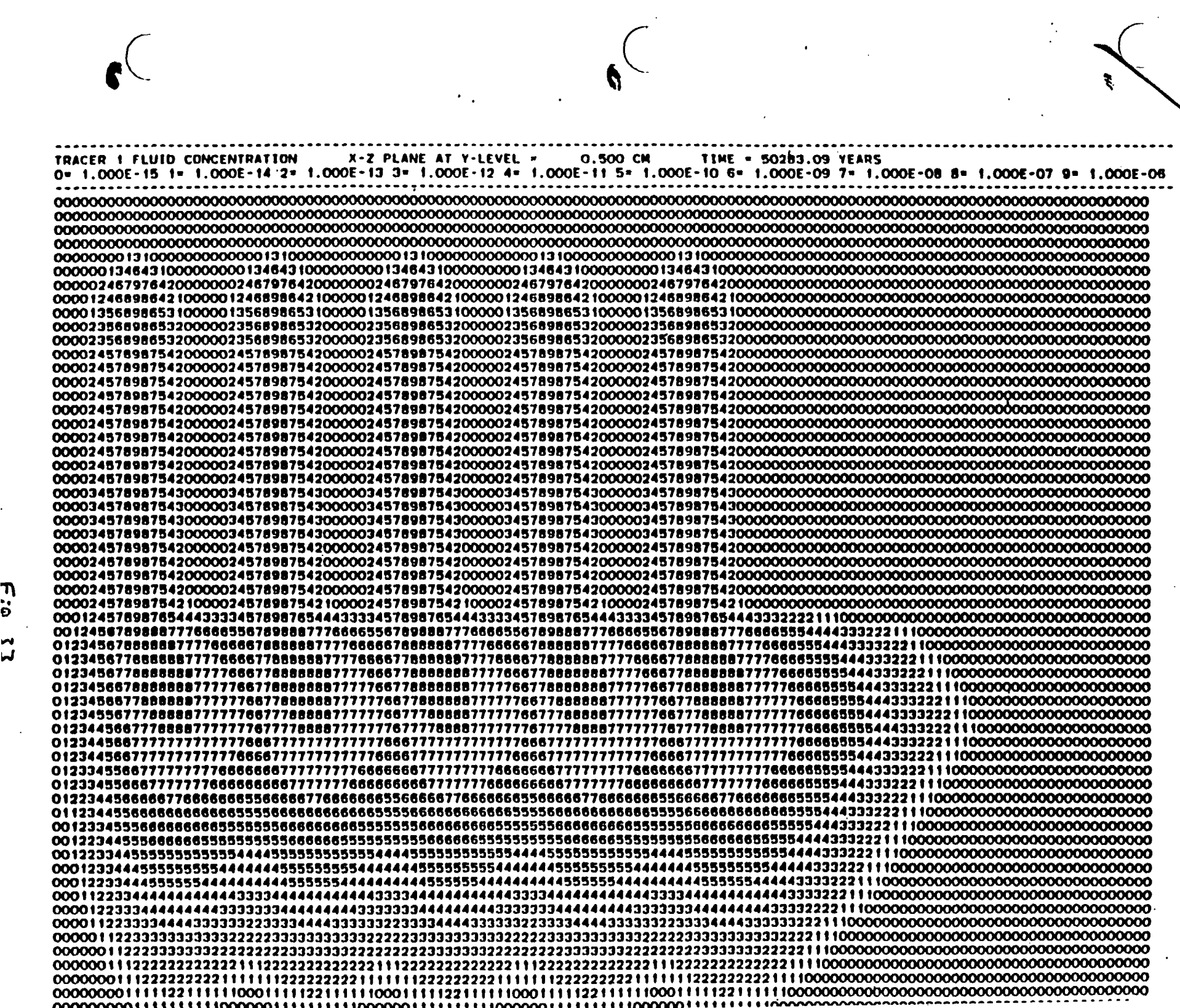

ROUGH DRAFT

F:0 13

ROUGH DRAFT

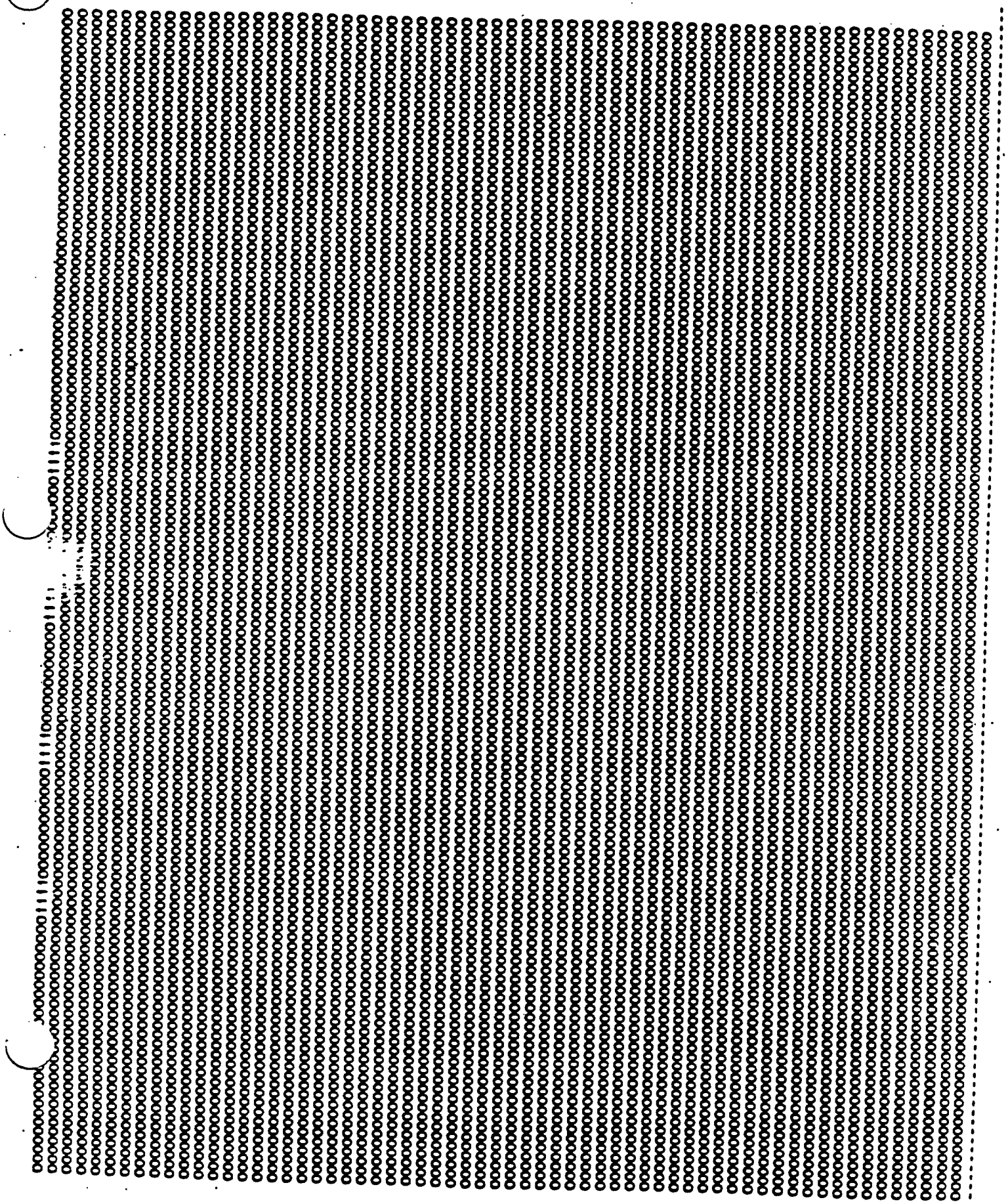

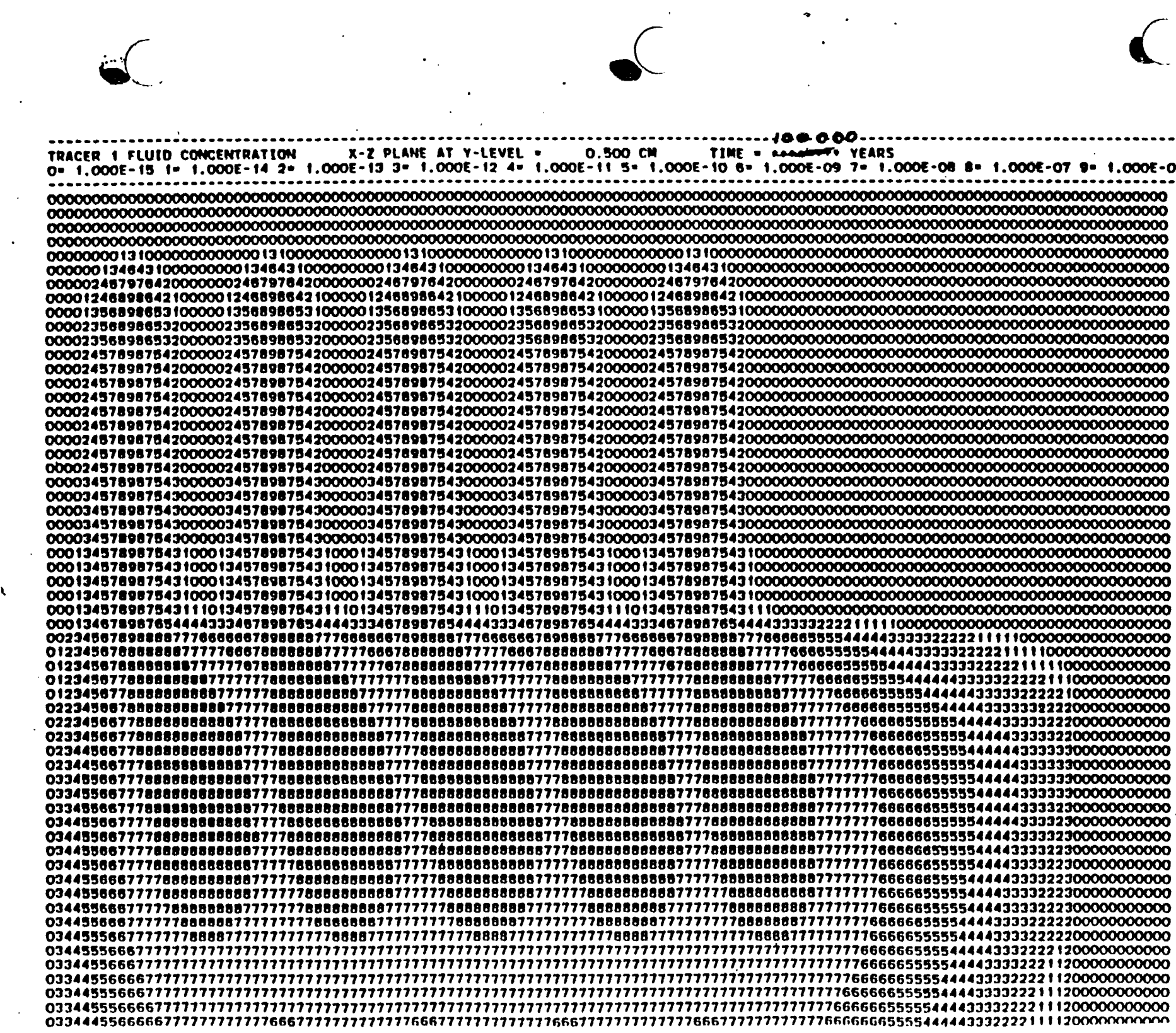
TRACER 1 FLUID CONCENTRATION X-Z PLANE AT Y-LEVEL = 0.500 CM TIME = YEARS
0= 1.000E-15 1= 1.000E-14 2= 1.000E-13 3= 1.000E-12 4= 1.000E-11 5= 1.000E-10 6= 1.000E-09 7= 1.000E-08 8= 1.000E-07 9= 1.000E-06

ROUGH DRAFT

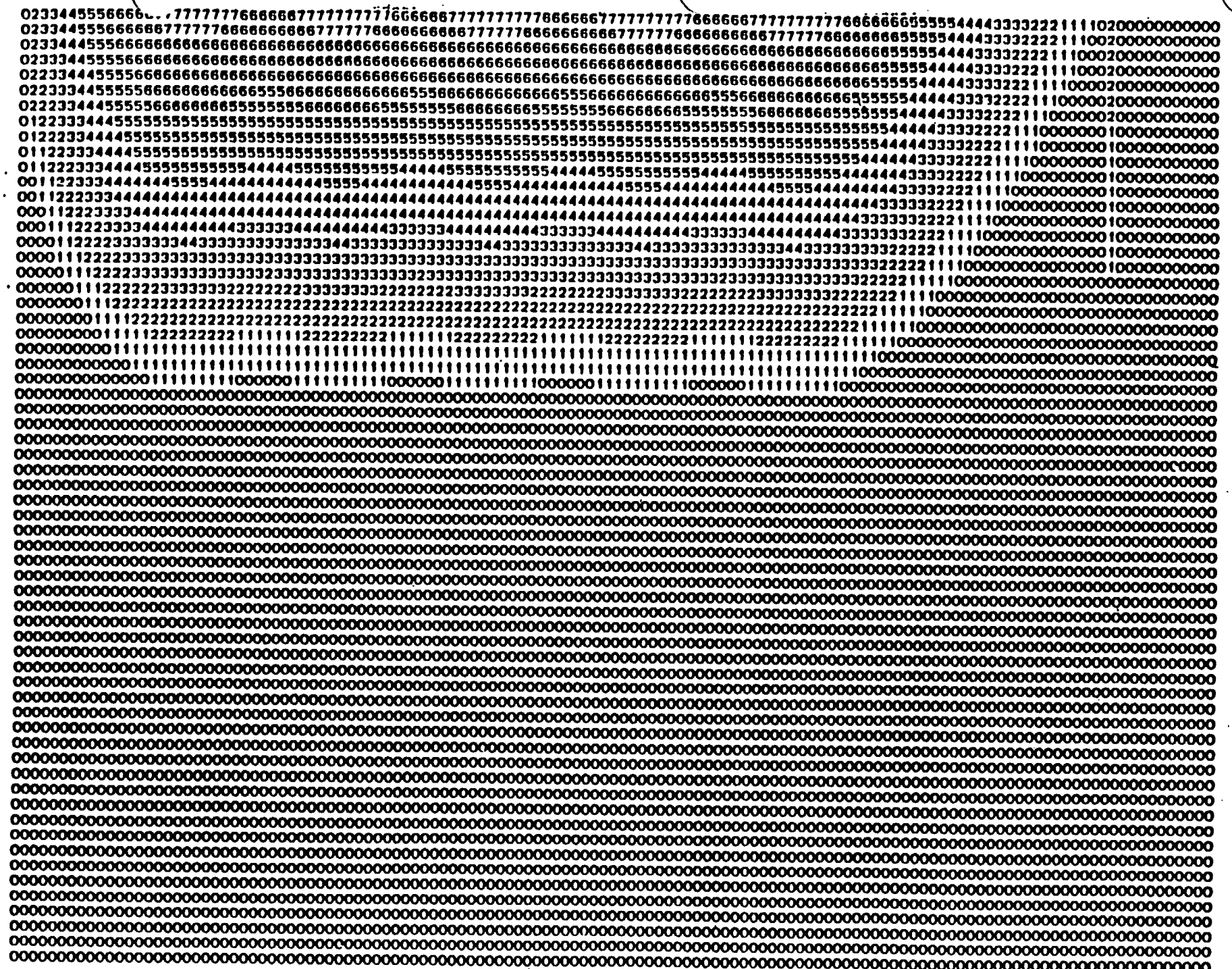

ROUGH DRAFT

TRACER 1 SOLID CONCENTRATION X-Z PLANE AT Y-LEVEL = 0.500 CM TIME = 10323.02 YEARS

0= 1.000E-15 1= 1.000E-14 2= 1.000E-13 3= 1.000E-12 4= 1.000E-11 5= 1.000E-10 6= 1.000E-09 7= 1.000E-08 8= 1.000E-07 9= 1.000E-06

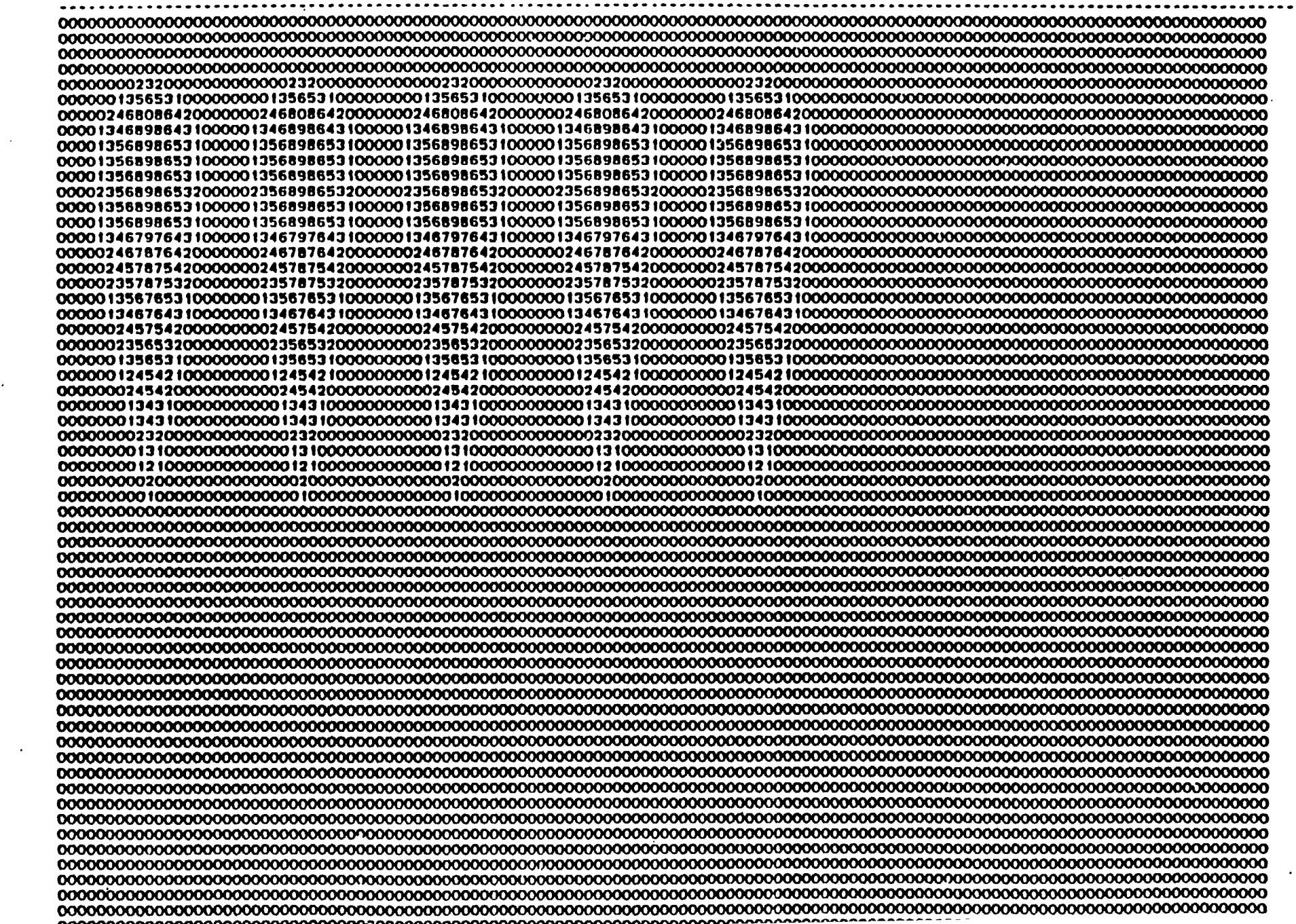

ROUGH DRAFT

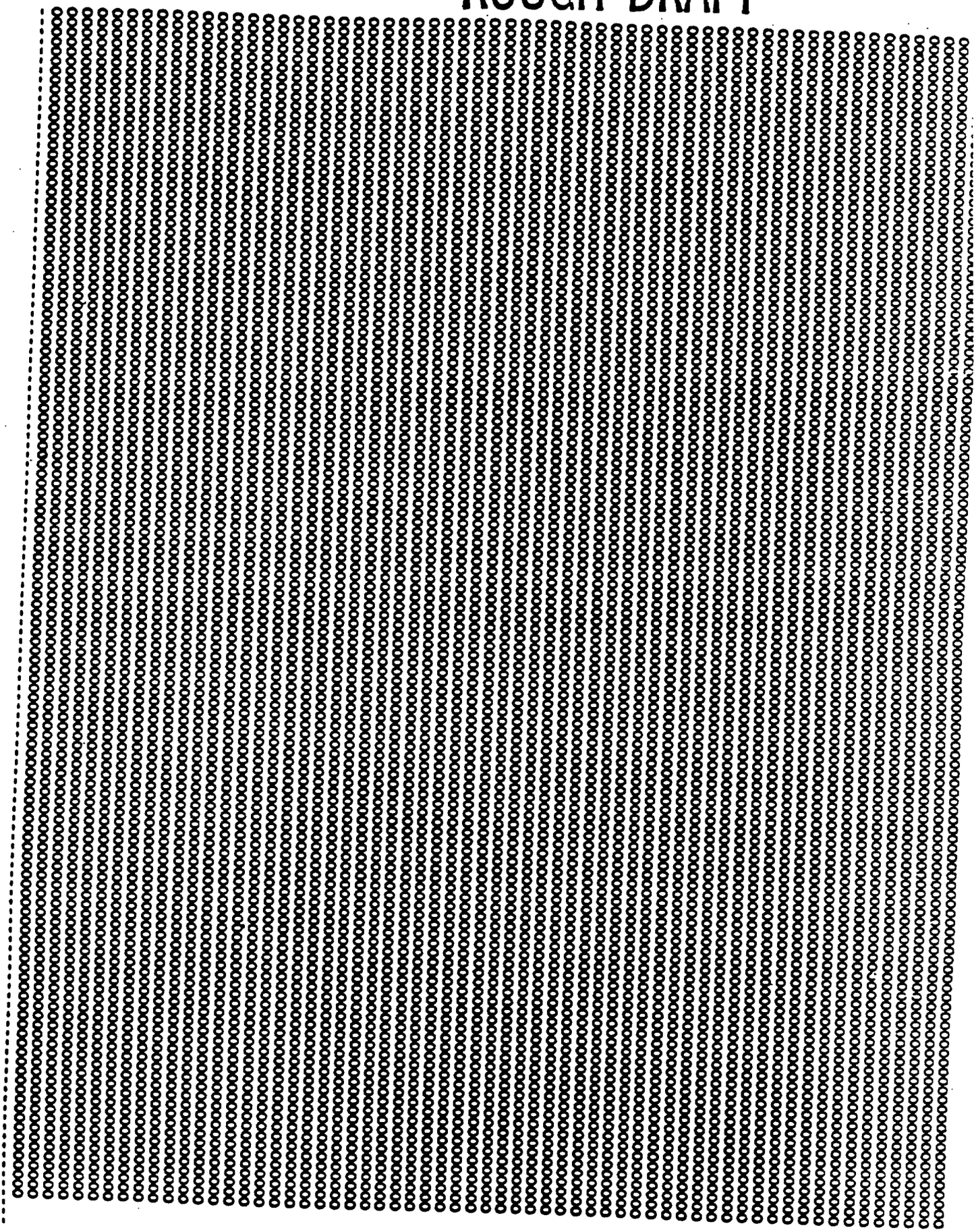

Fig. 35 cont'd

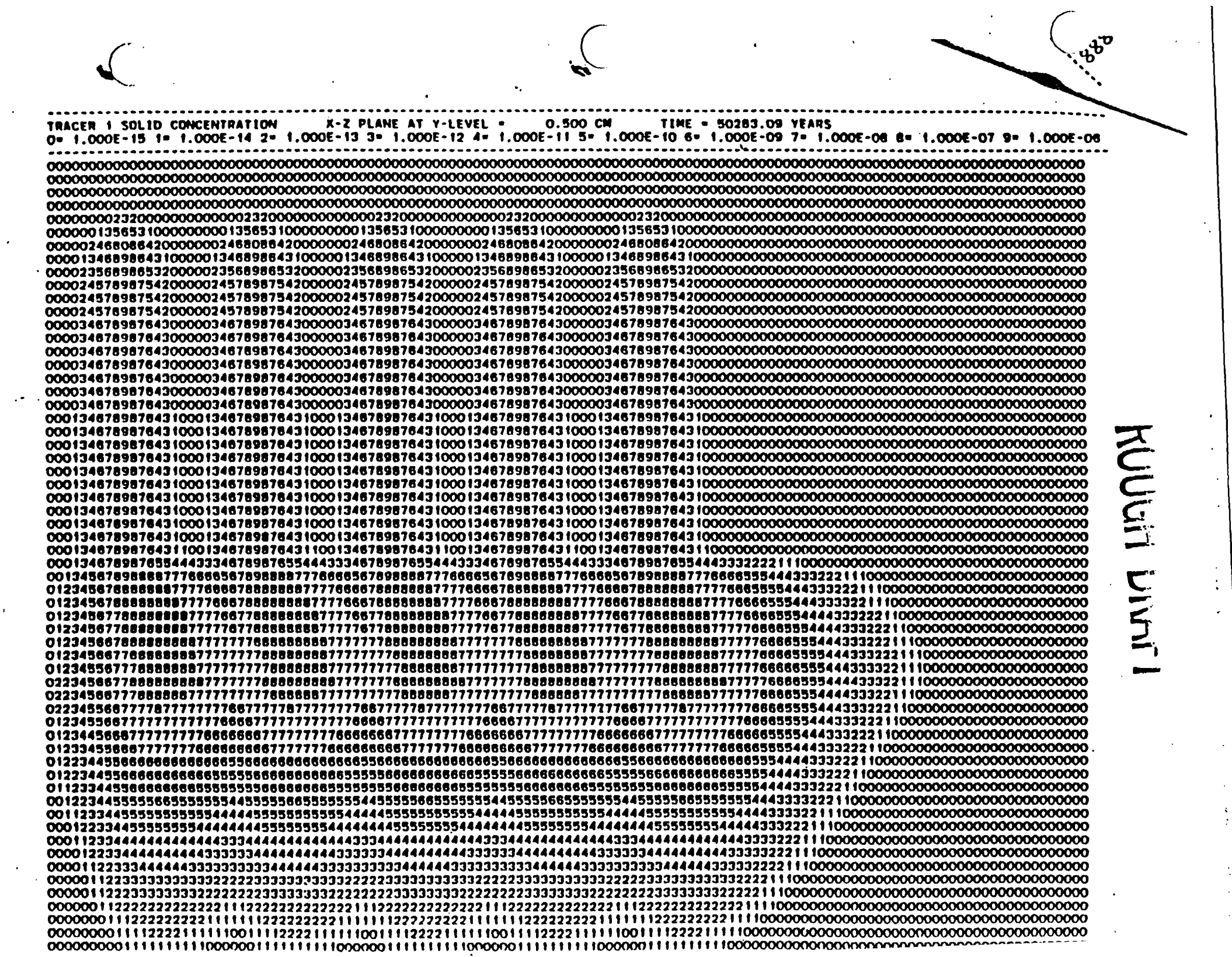
TRACER 1 SOLID CONCENTRATION X-Z PLANE AT Y-LEVEL = 0.500 CM TIME = 50283.09 YEARS
0= 1.000E-15 1= 1.000E-14 2= 1.000E-13 3= 1.000E-12 4= 1.000E-11 5= 1.000E-10 6= 1.000E-09 7= 1.000E-08 8= 1.000E-07 9= 1.000E-06
KUUGH UNIT

ROUGH DRAFT

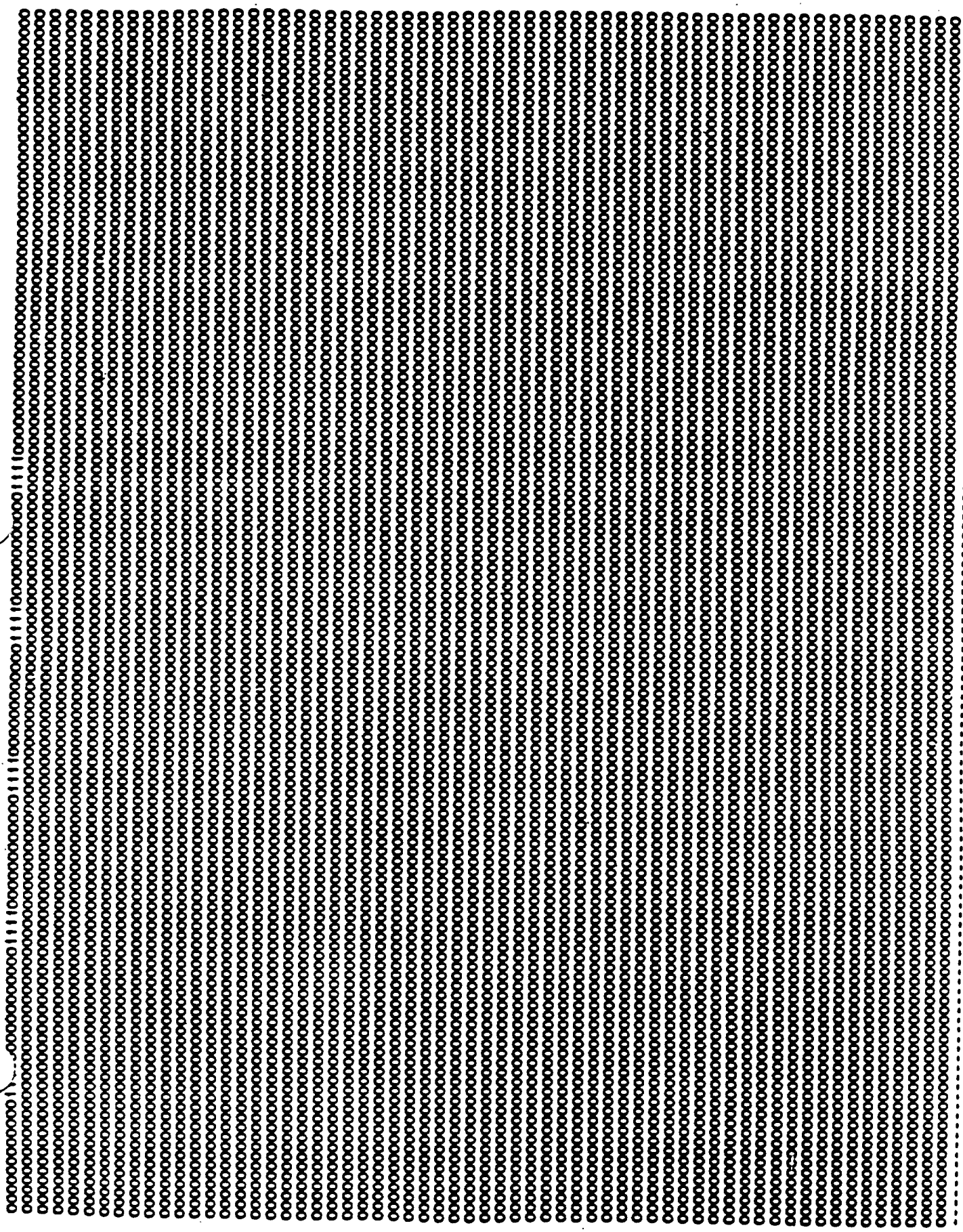

TRACER 1 SOLID CONCENTRATION X-Z PLANE AT Y-LEVEL = 0.500 CM TIME = [illegible] YEARS

0= 1.000E-15 1= 1.000E-14 2= 1.000E-13 3= 1.000E-12 4= 1.000E-11 5= 1.000E-10 6= 1.000E-09 7= 1.000E-08 8= 1.000E-07 9= 1.000E-06

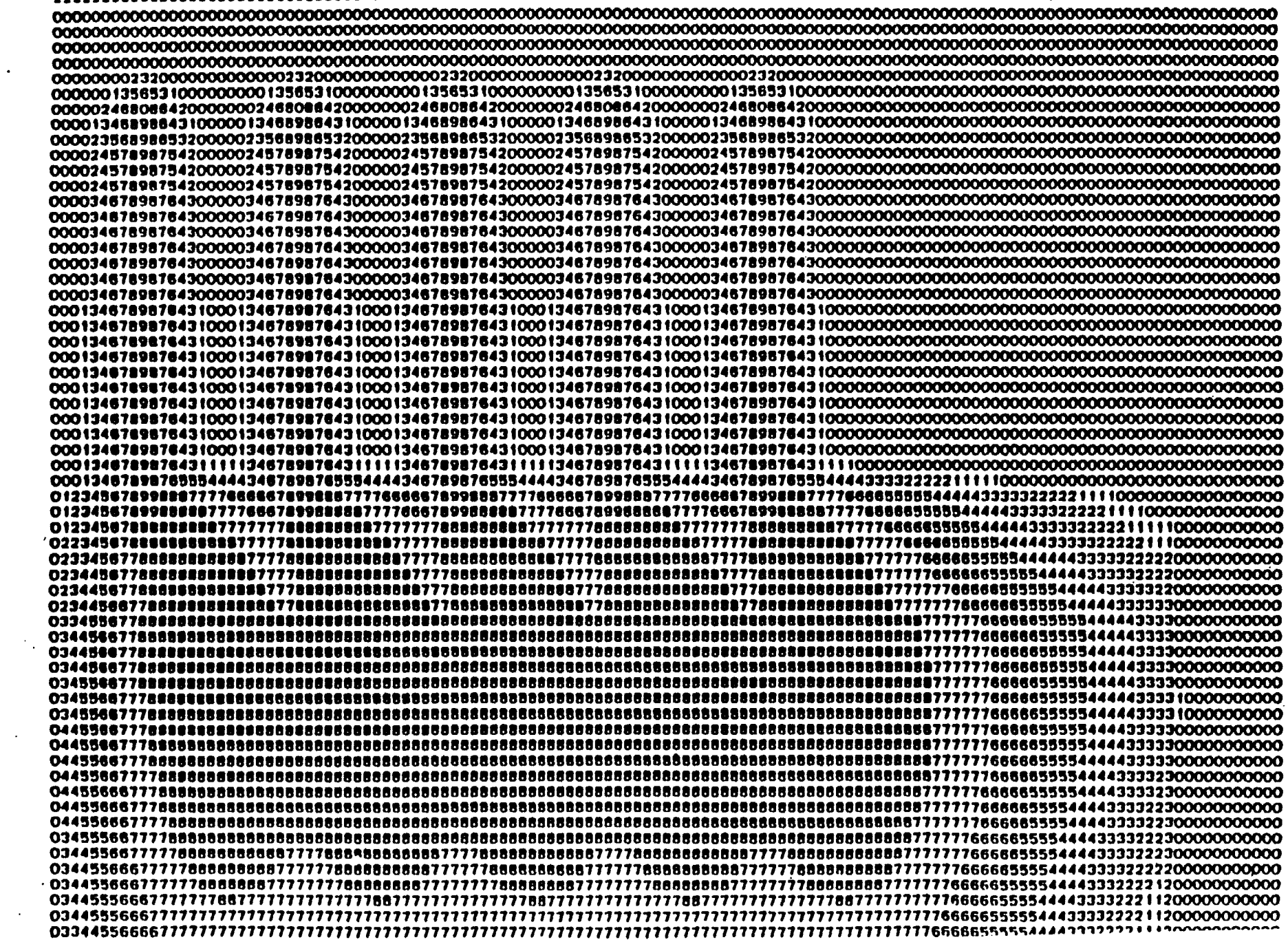

ROUGH DRAFT

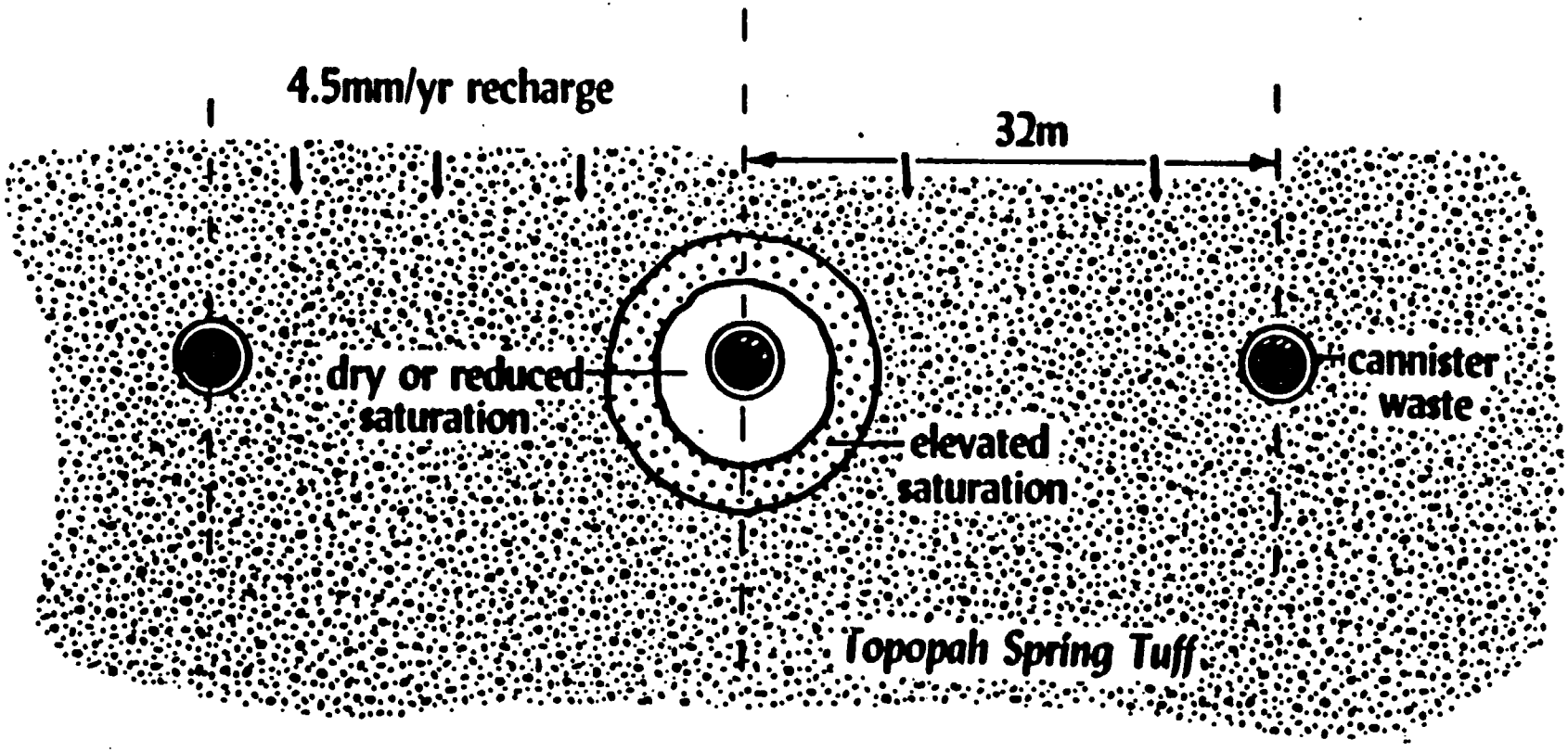
4.5mm/yr recharge
32m
dry or reduced saturation
elevated saturation
cannister waste
Topopah Spring Tuff

ROUGH DRAFT

Fig 39

ROUGH DRAFT

Calculated pressure distribution at selected times.

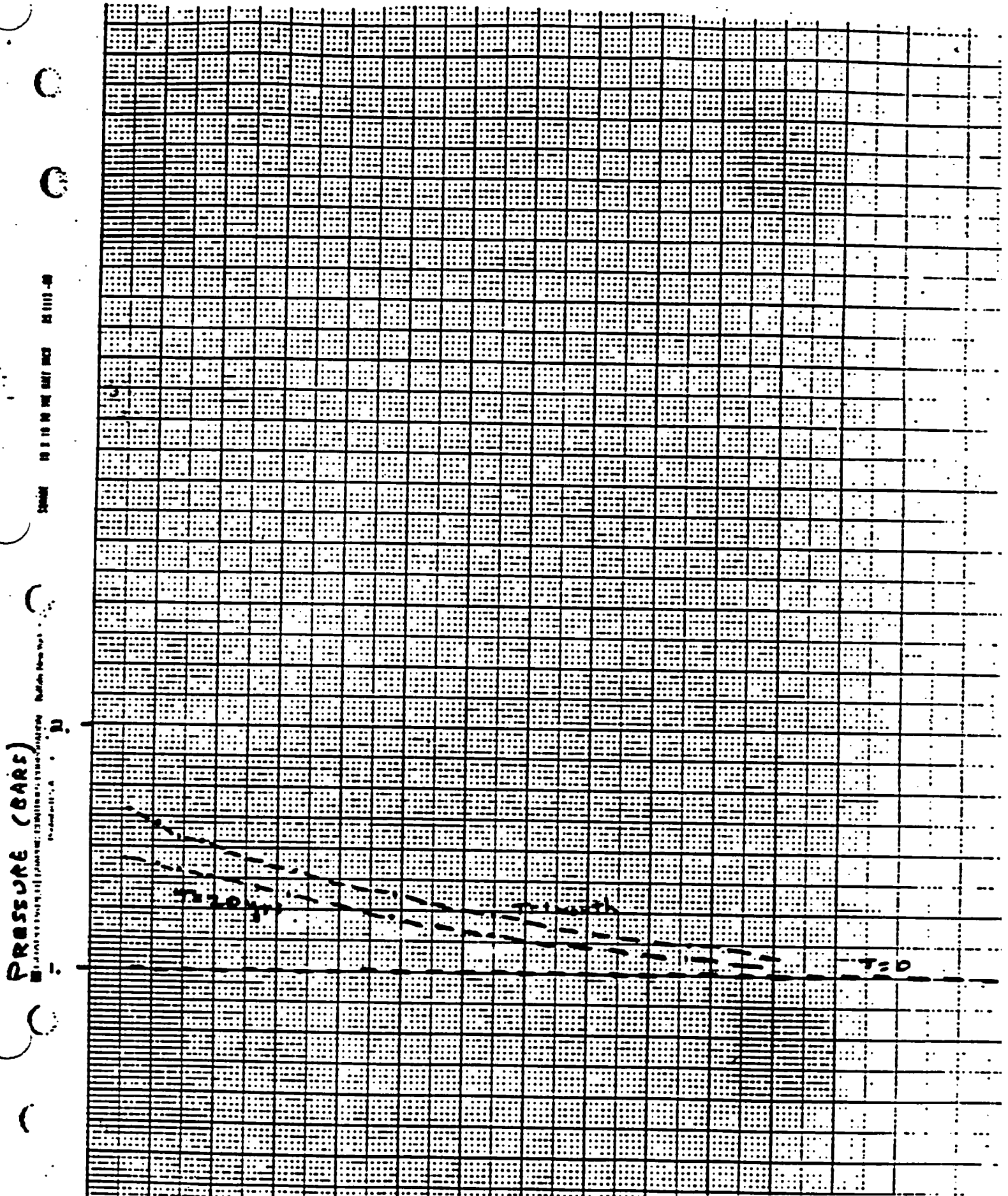

FIG 40

ROUGH DRAFT

Calculated temperature distribution at selected times.

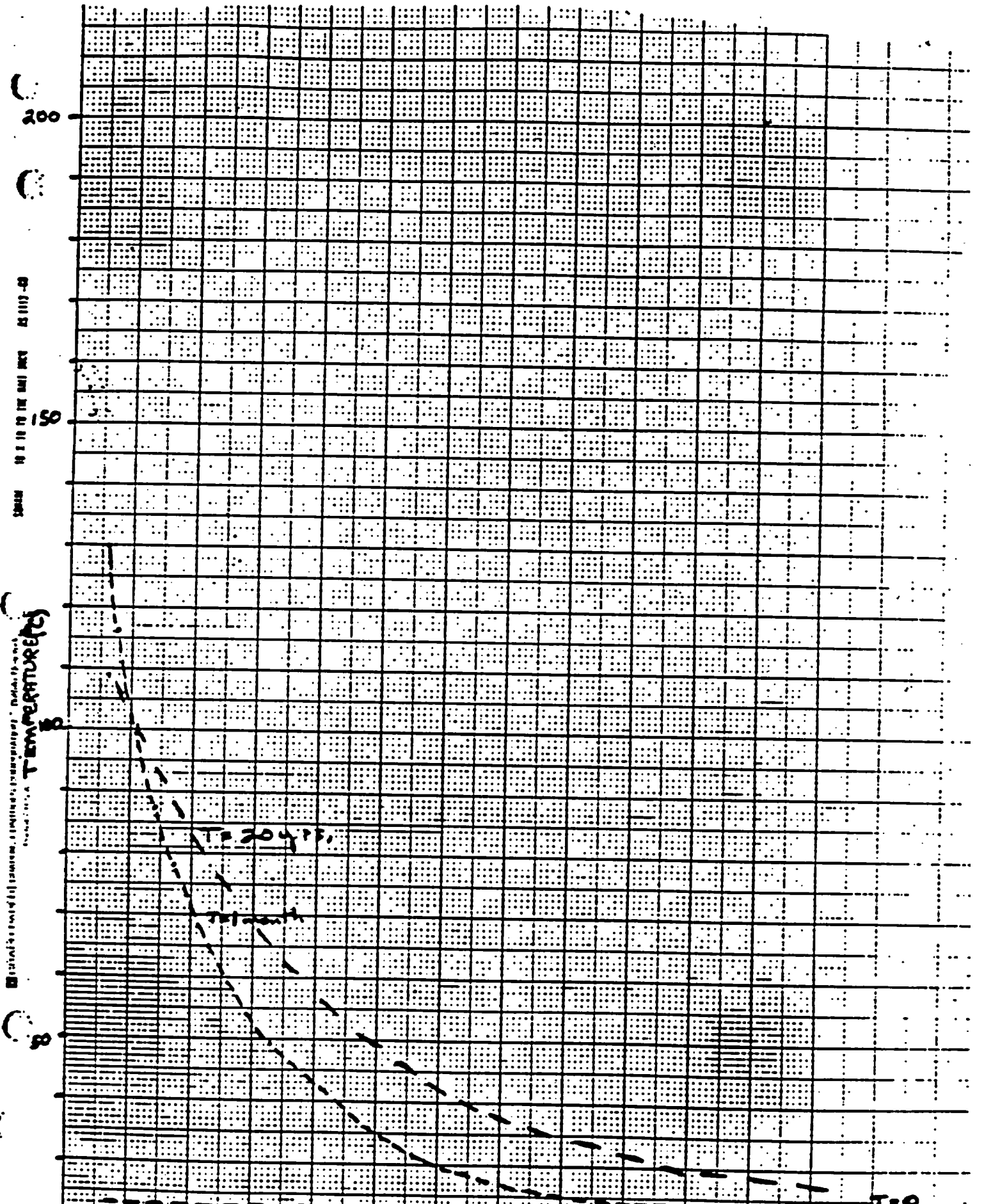

ROUGH DRAFT

Fig 41

Calculated saturation distribution at selected times.

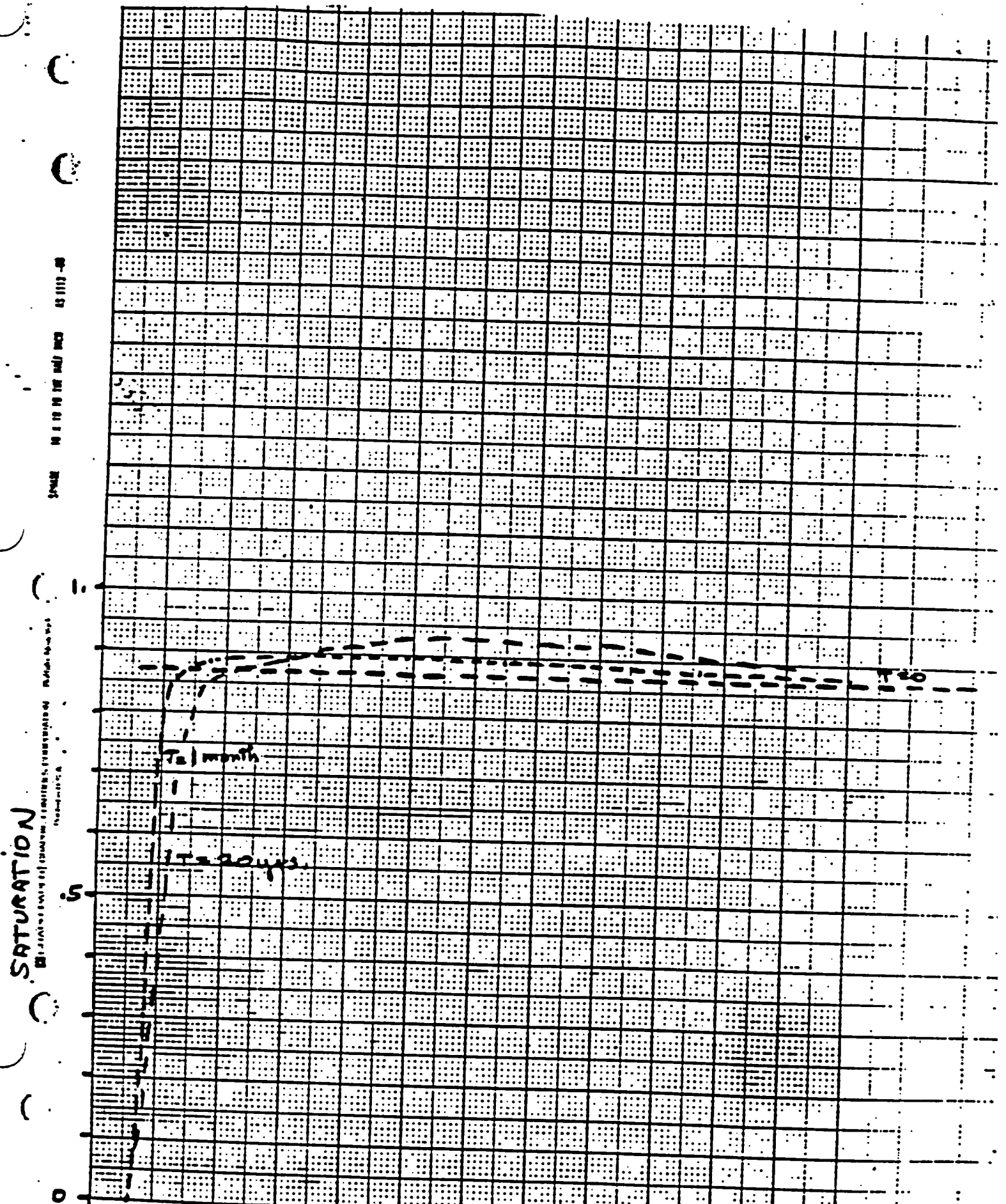

ROUGH DRAFT

Fig 42

Caclulated chloride distribution at selected times.

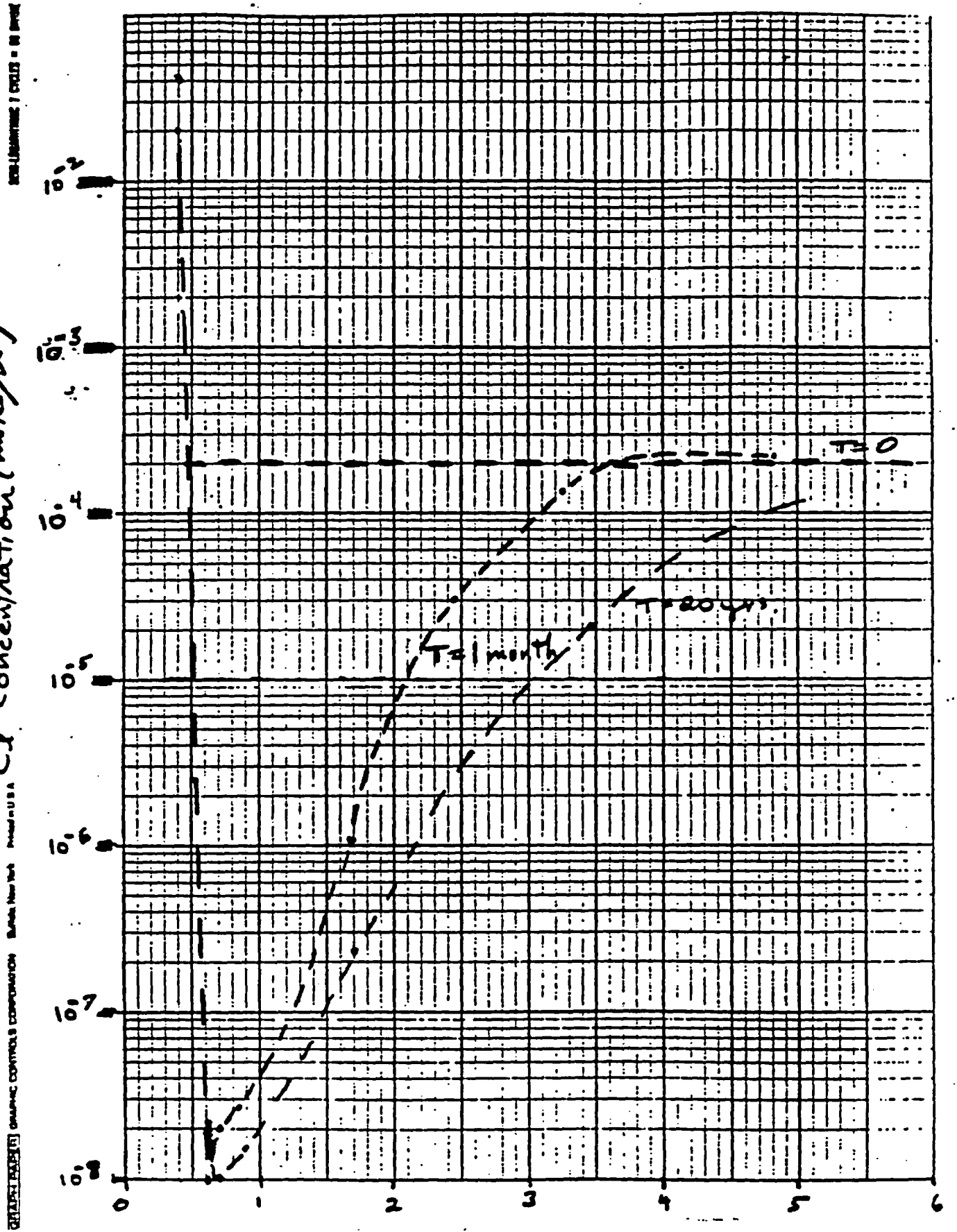

Fig 43

ROUGH DRAFT

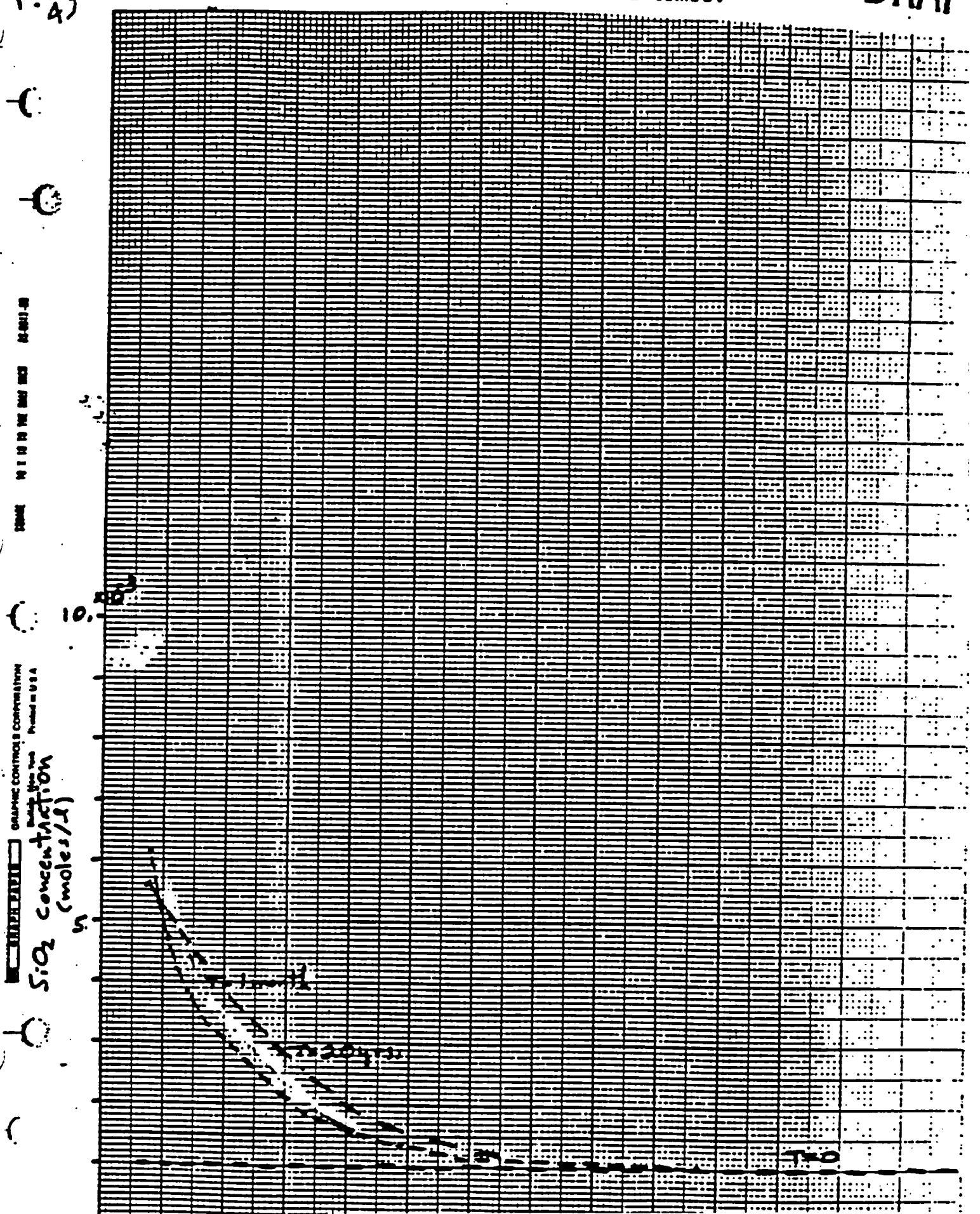

ROUGH DRAFT

Fig 4A

Calculated total SiO2 (dissolved and precipitated) at selected times.

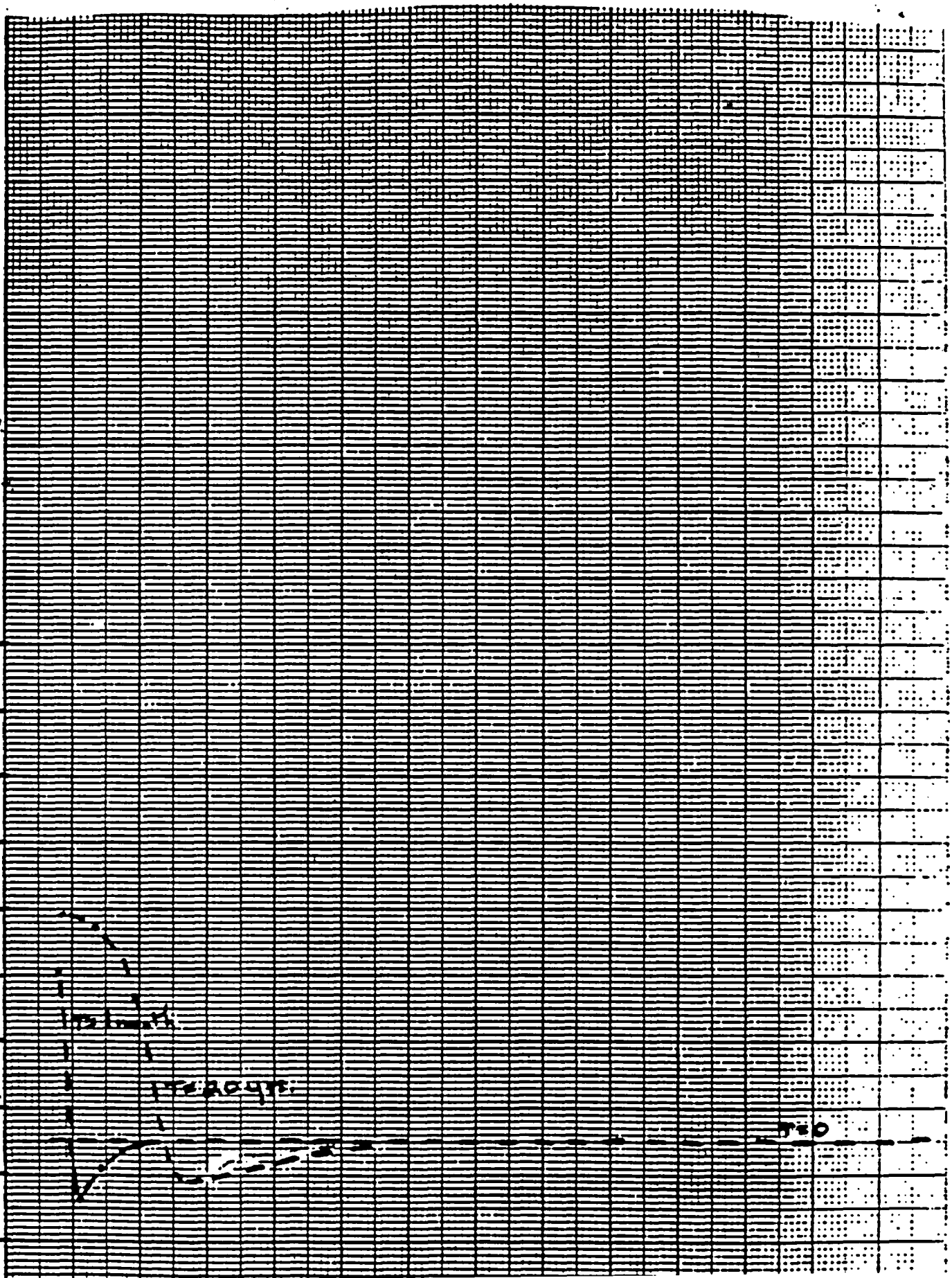

ROUGH DRAFT

Fig 43

Calculated permeability assuming relationships between pore volume and permeability.

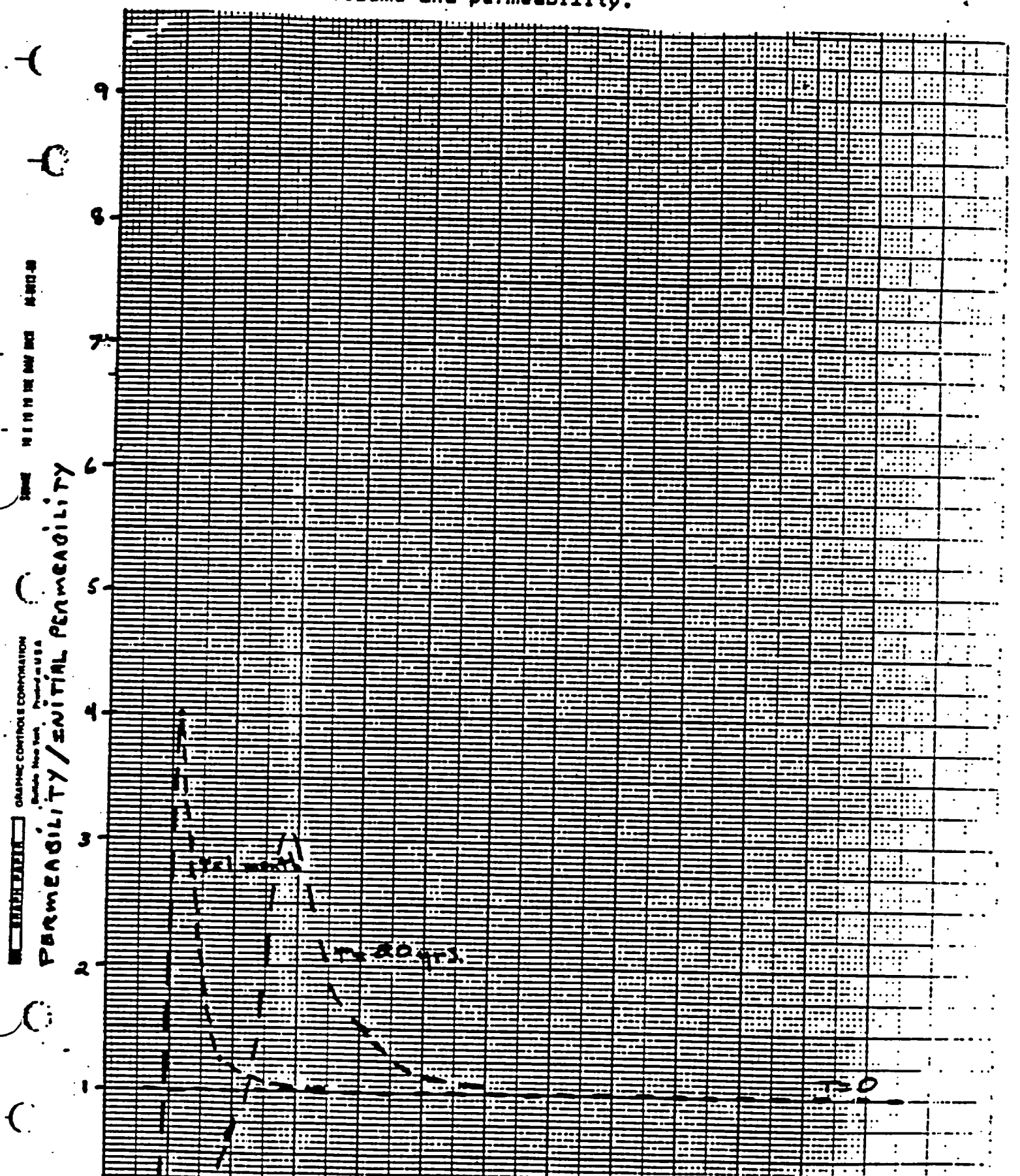

ROUGH DATA 1

MODEL

DATE

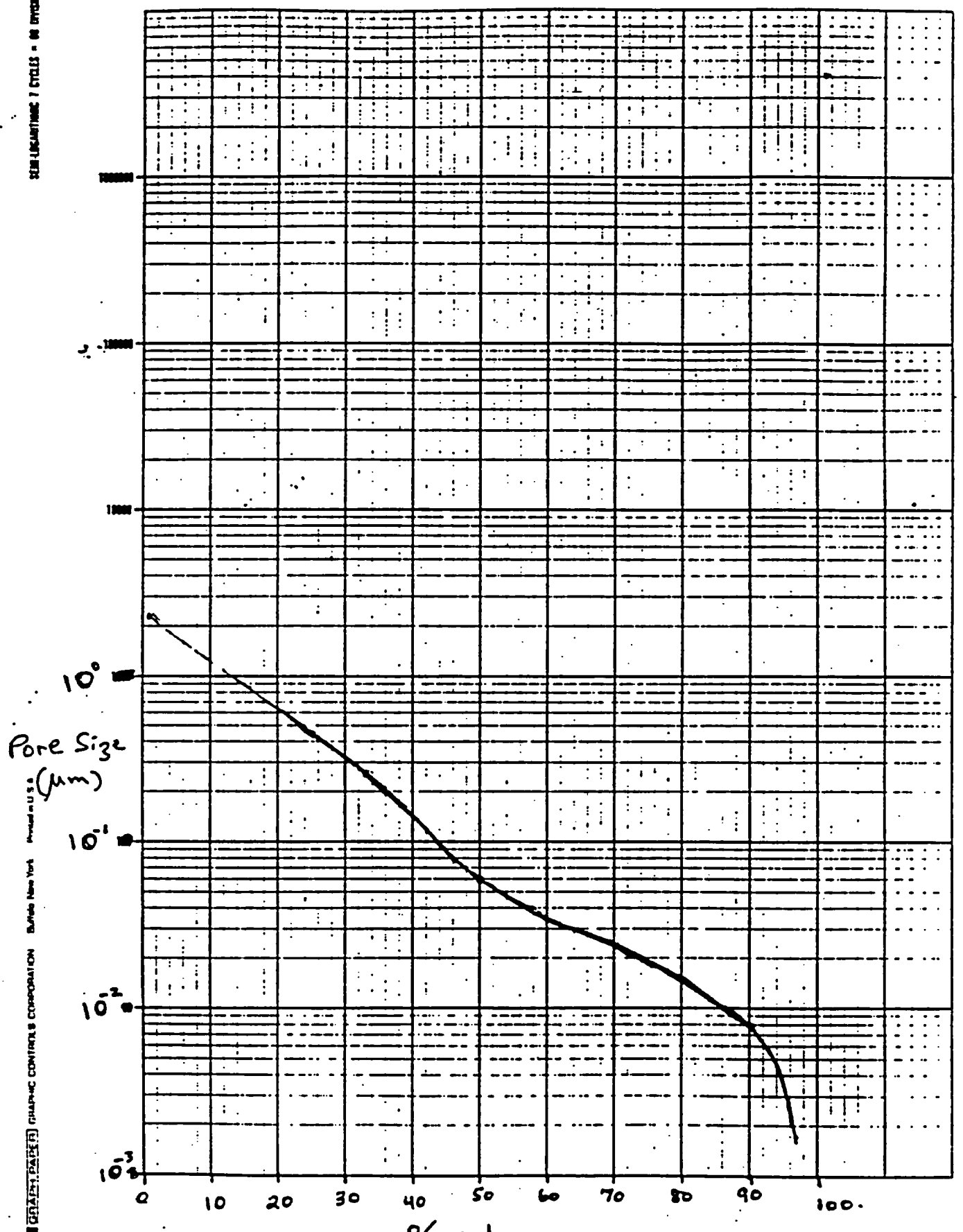

ROUGH DRAFT

MODEL

DATE

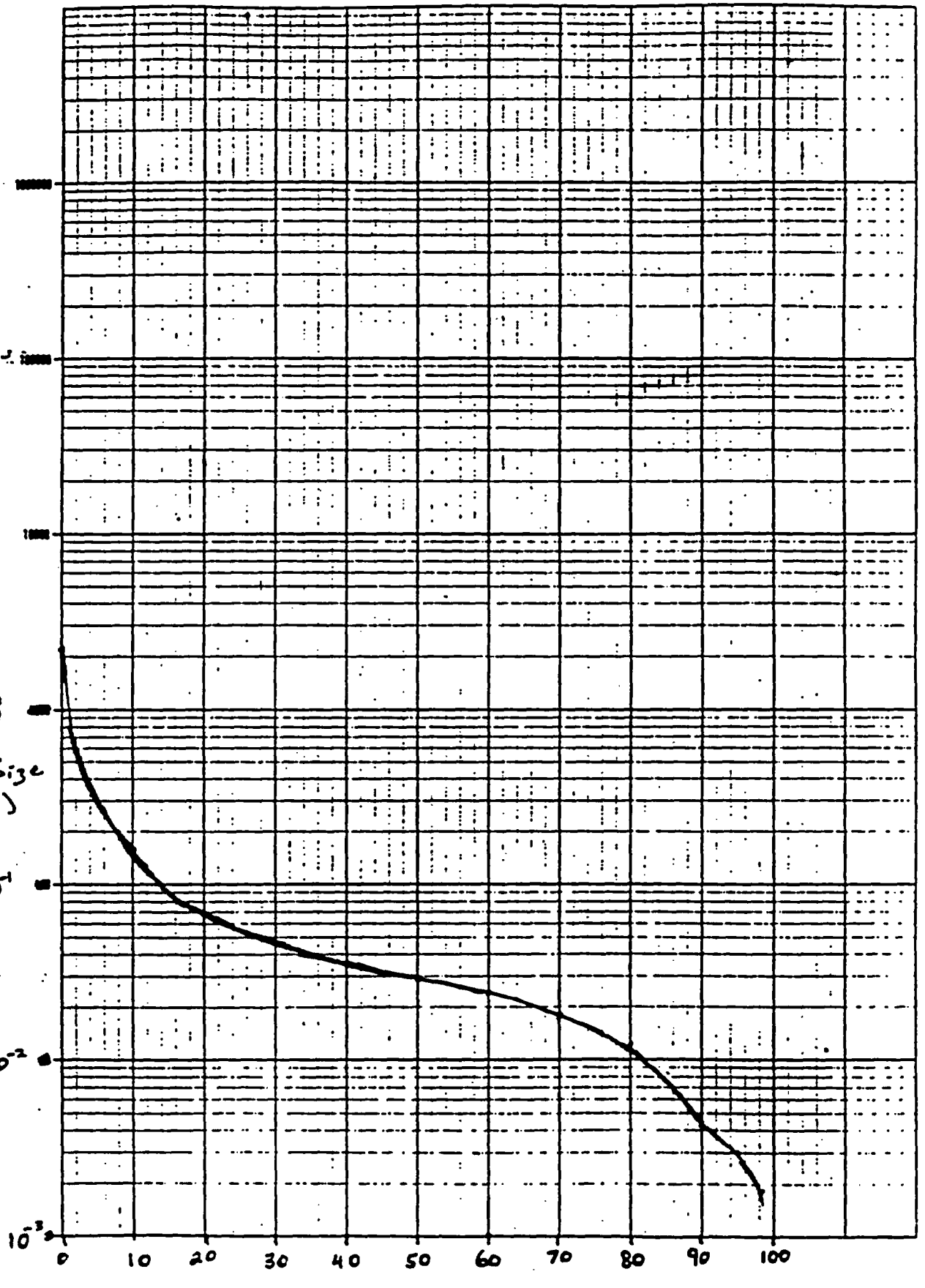

GRAPH PAPER GRAPHIC CONTROLS CORPORATION Buffalo New York Printed in U.S.A.

ROUGH DRAFT

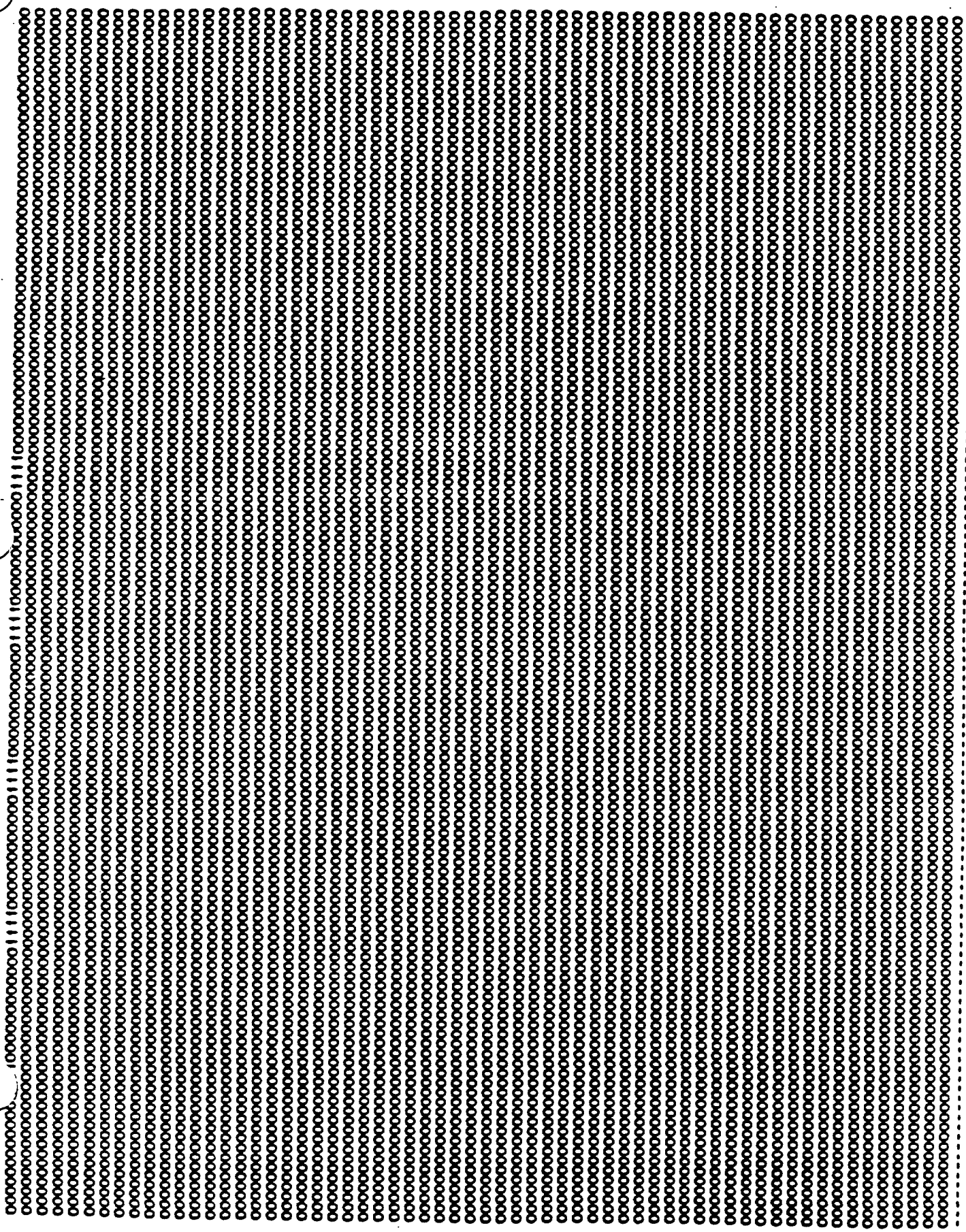

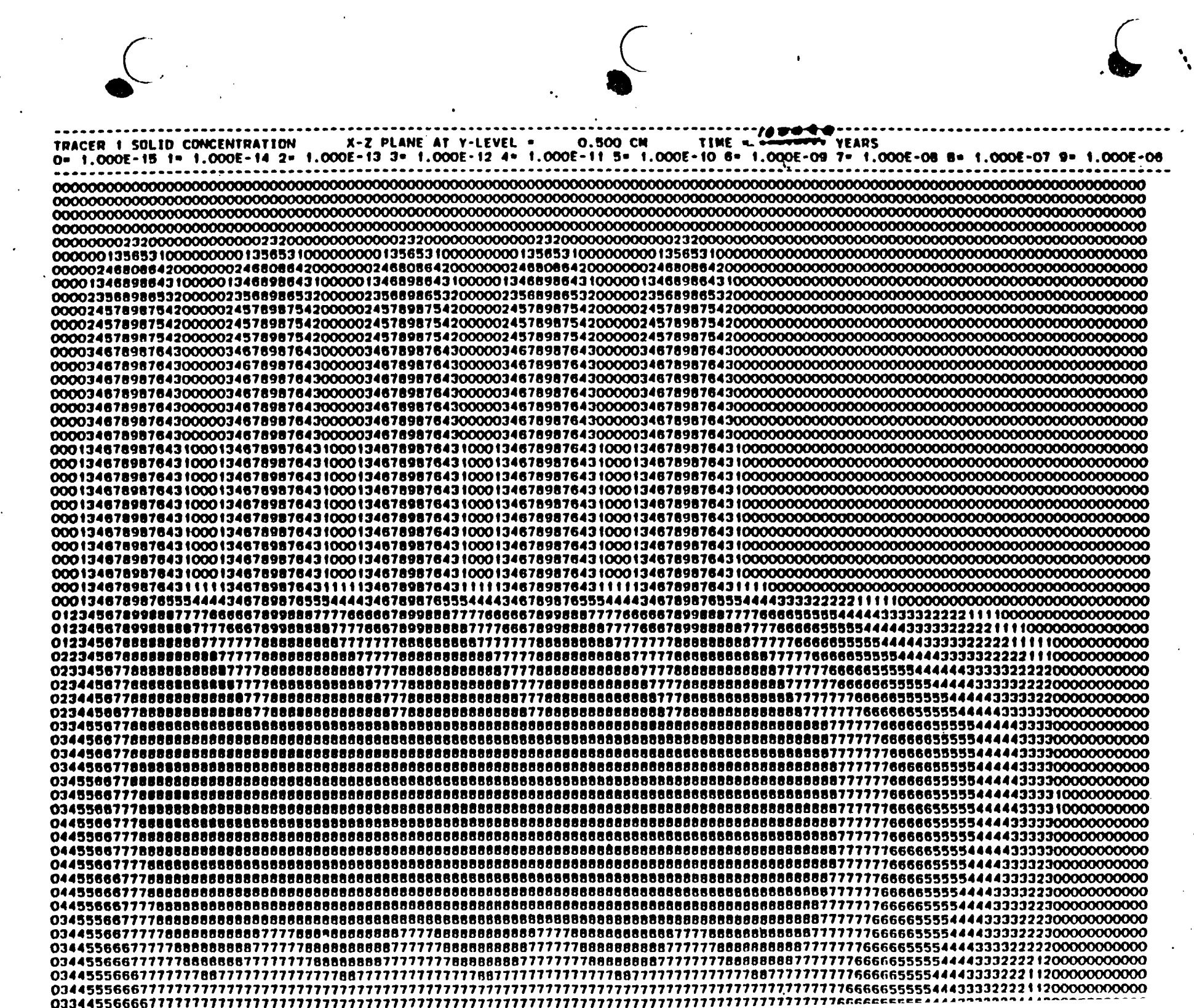
TRACER 1 SOLID CONCENTRATION X-Z PLANE AT Y-LEVEL = 0.500 CM TIME = YEARS
0= 1.000E-15 1= 1.000E-14 2= 1.000E-13 3= 1.000E-12 4= 1.000E-11 5= 1.000E-10 6= 1.000E-09 7= 1.000E-08 8= 1.000E-07 9= 1.000E-06

ROUGH DRAFT

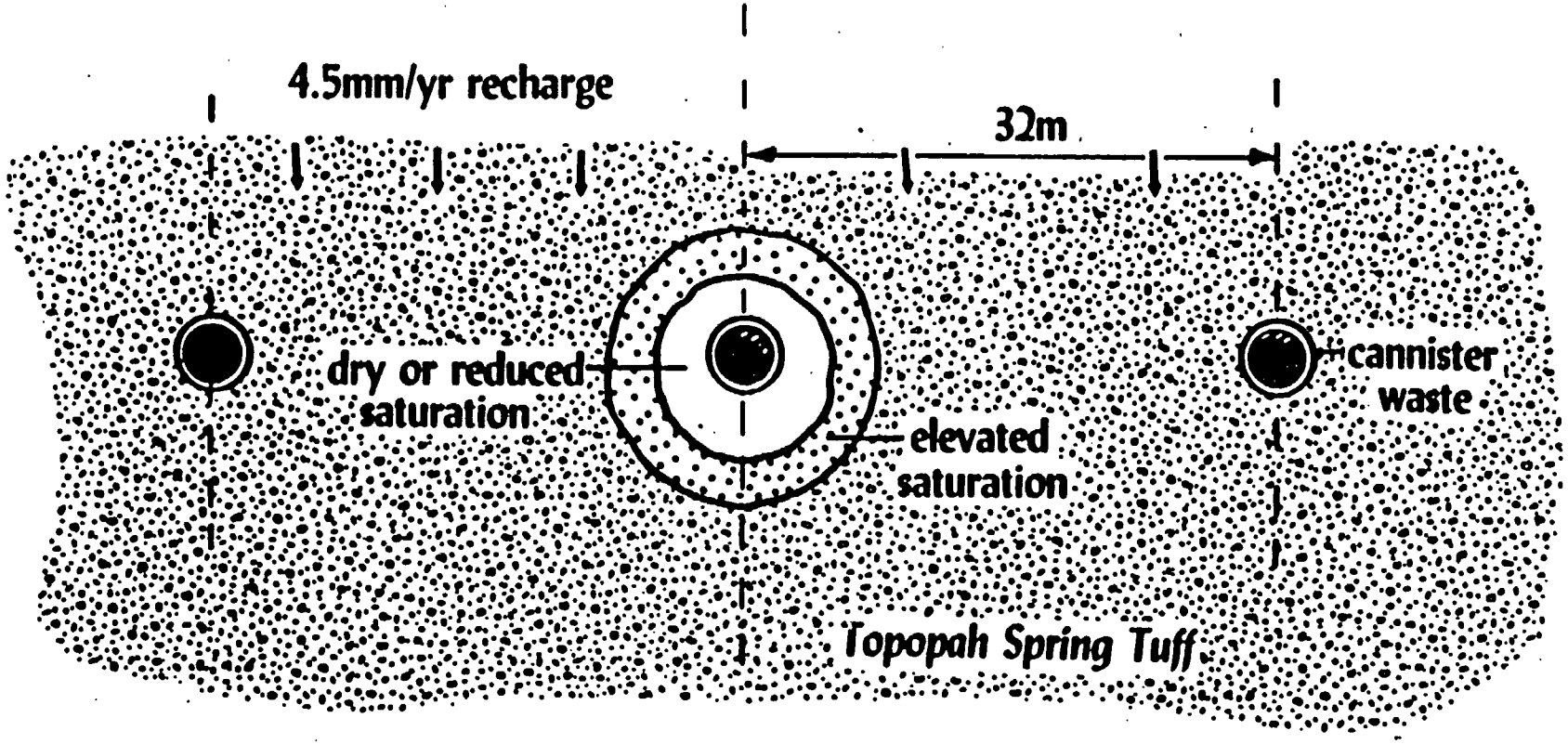
4.5mm/yr recharge
32m
dry or reduced saturation
elevated saturation
cannister waste
Topopah Spring Tuff

ROUGH DRAFT

Fig 39

ROUGH DRAFT

Calculated pressure distribution at selected times.

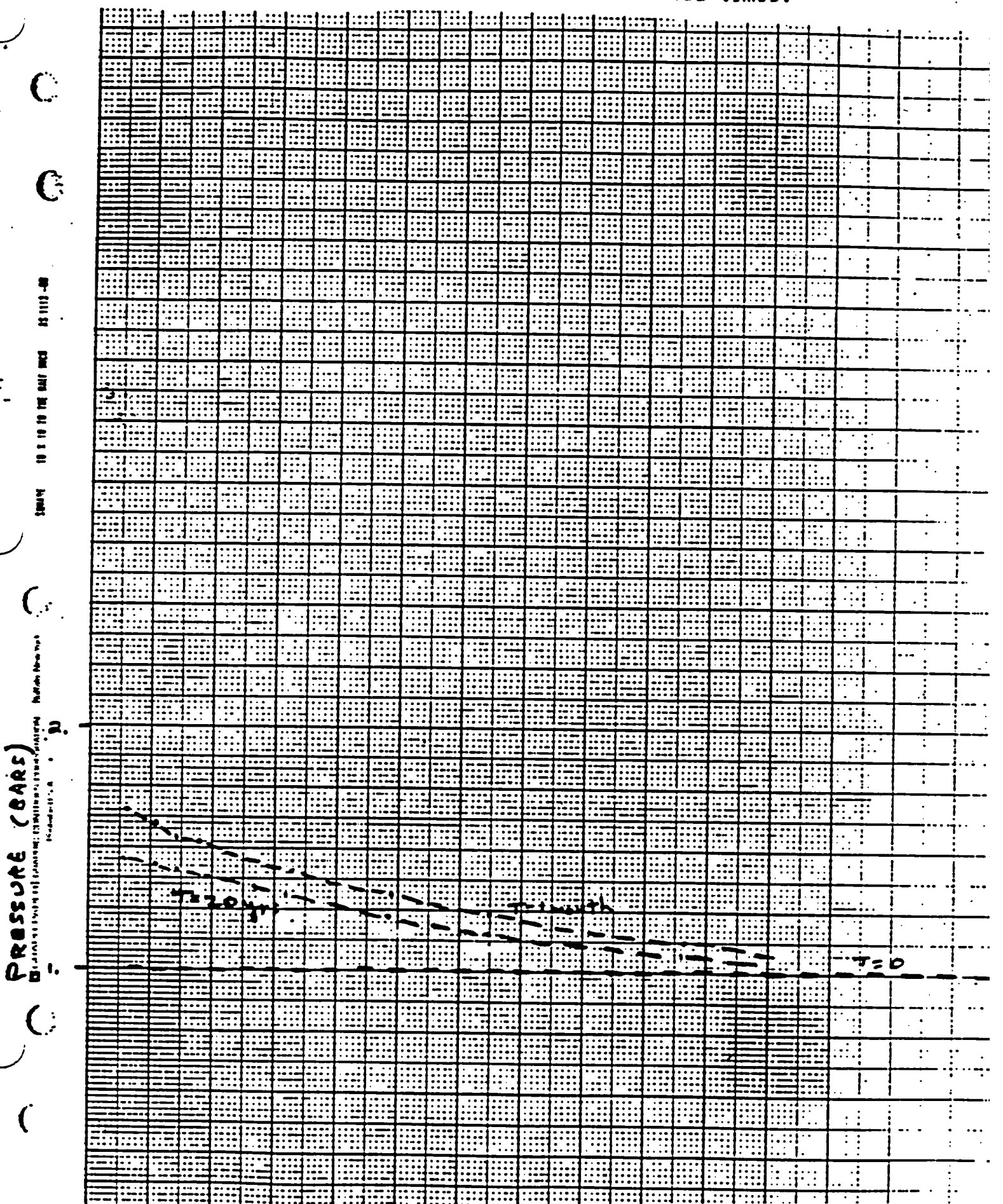

ROUGH DRAFT

Fig 40

Calculated temperature distribution at selected times.

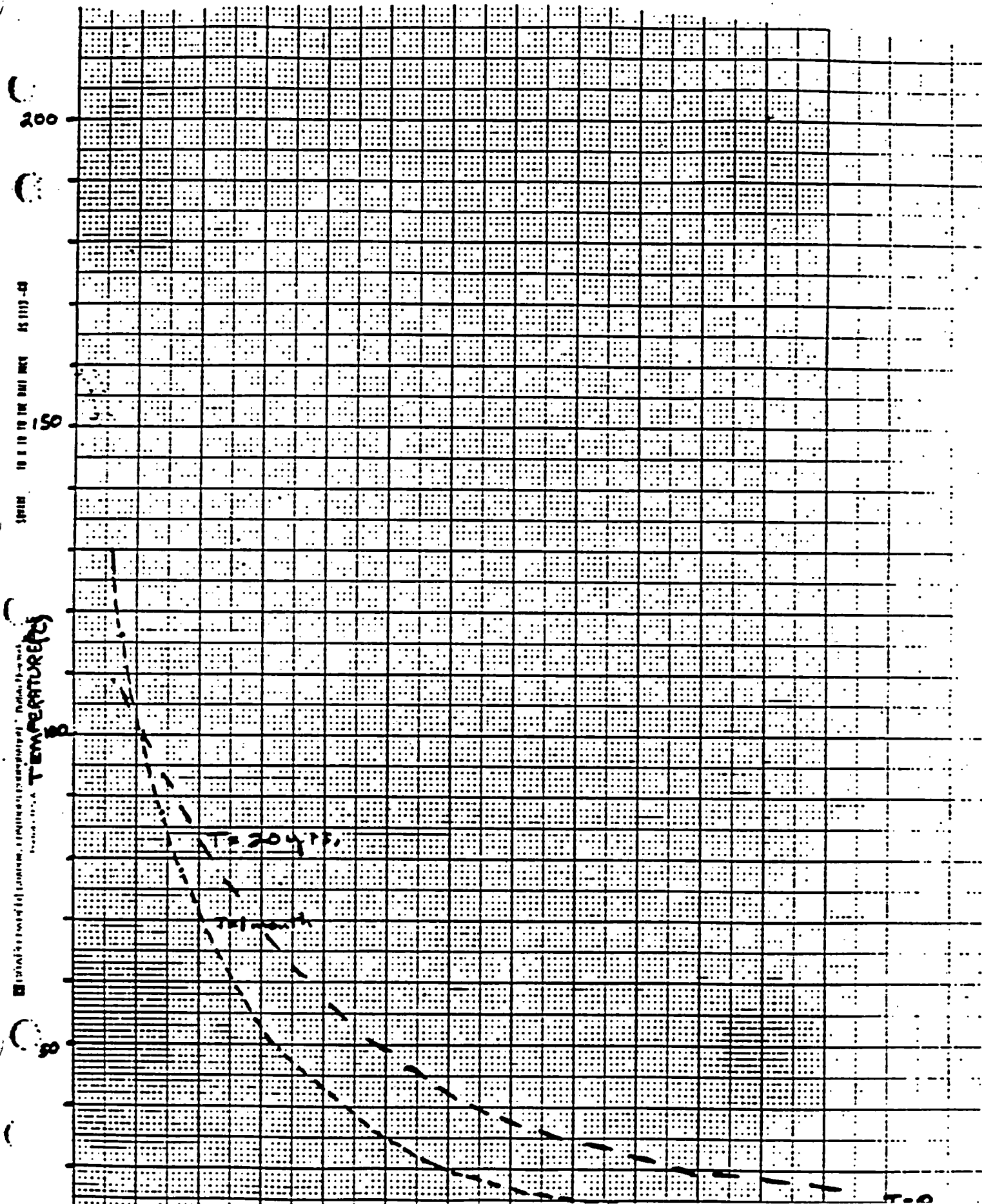

Fig 41

ROUGH DRAFT

Calculated saturation distribution at selected times.

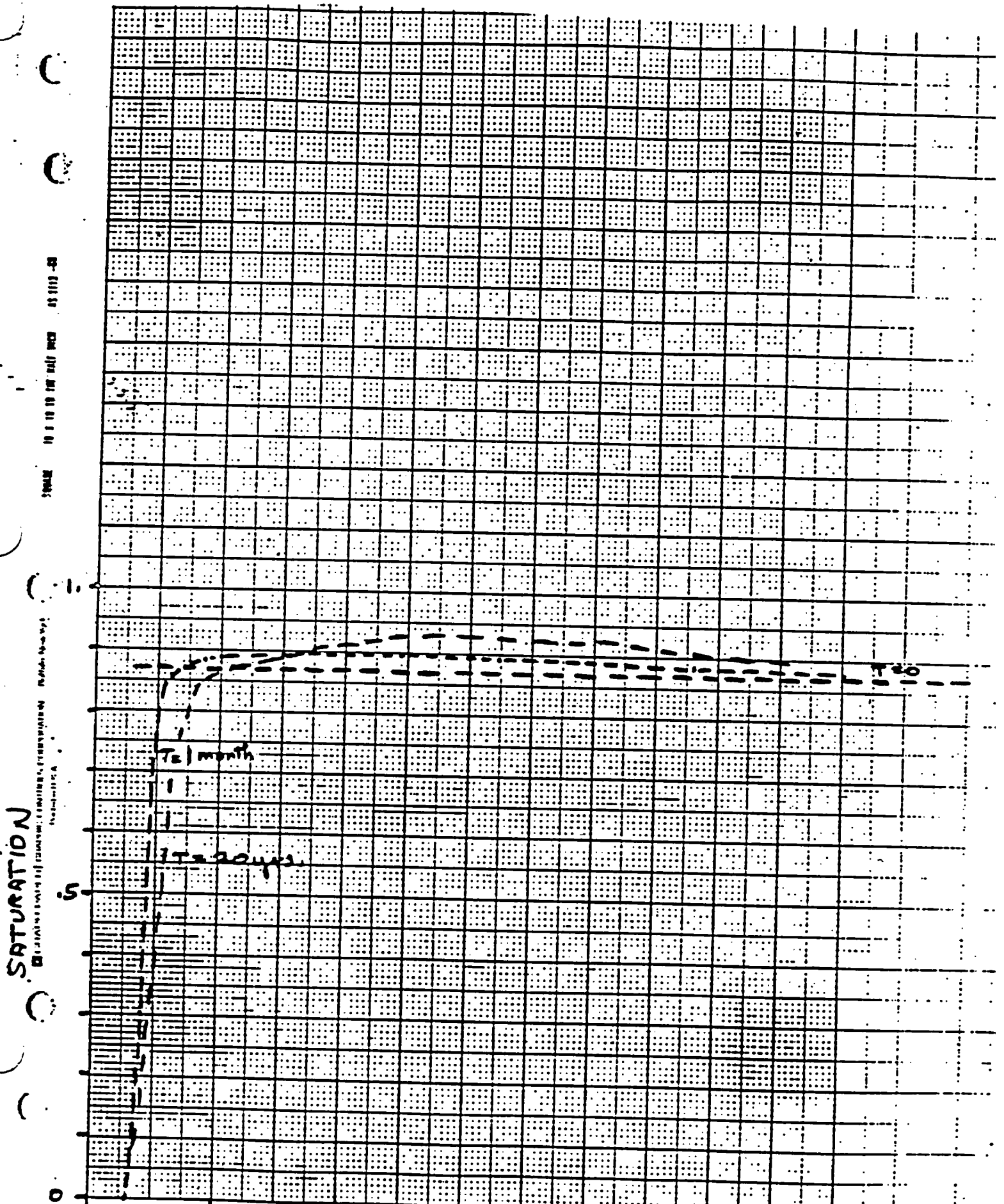

ROUGH DRAFT

Fig 42

Caclulated chloride distribution at selected times.

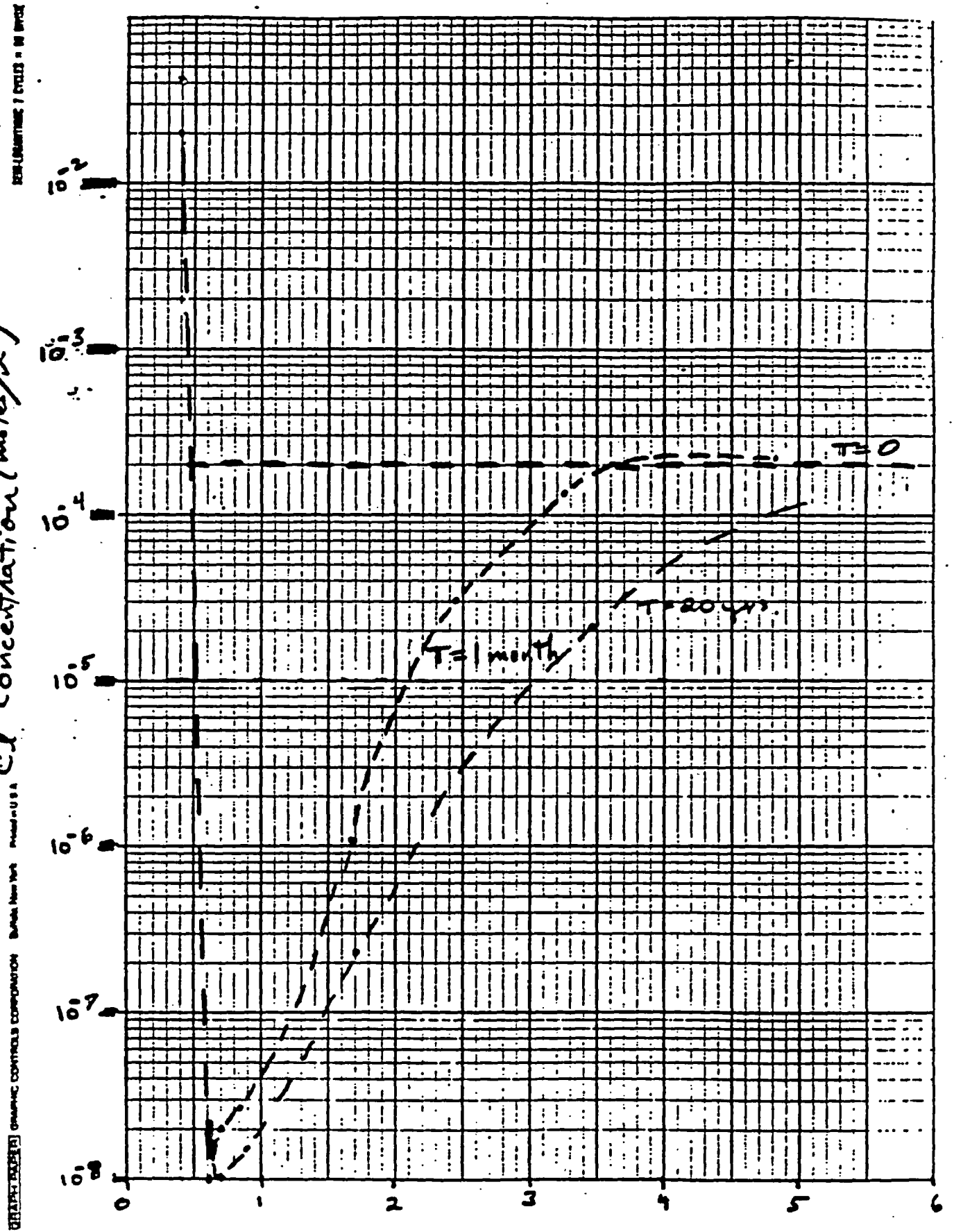

ROUGH DRAFT

Fig 43

Calculated SiO2 distribution at selected times.

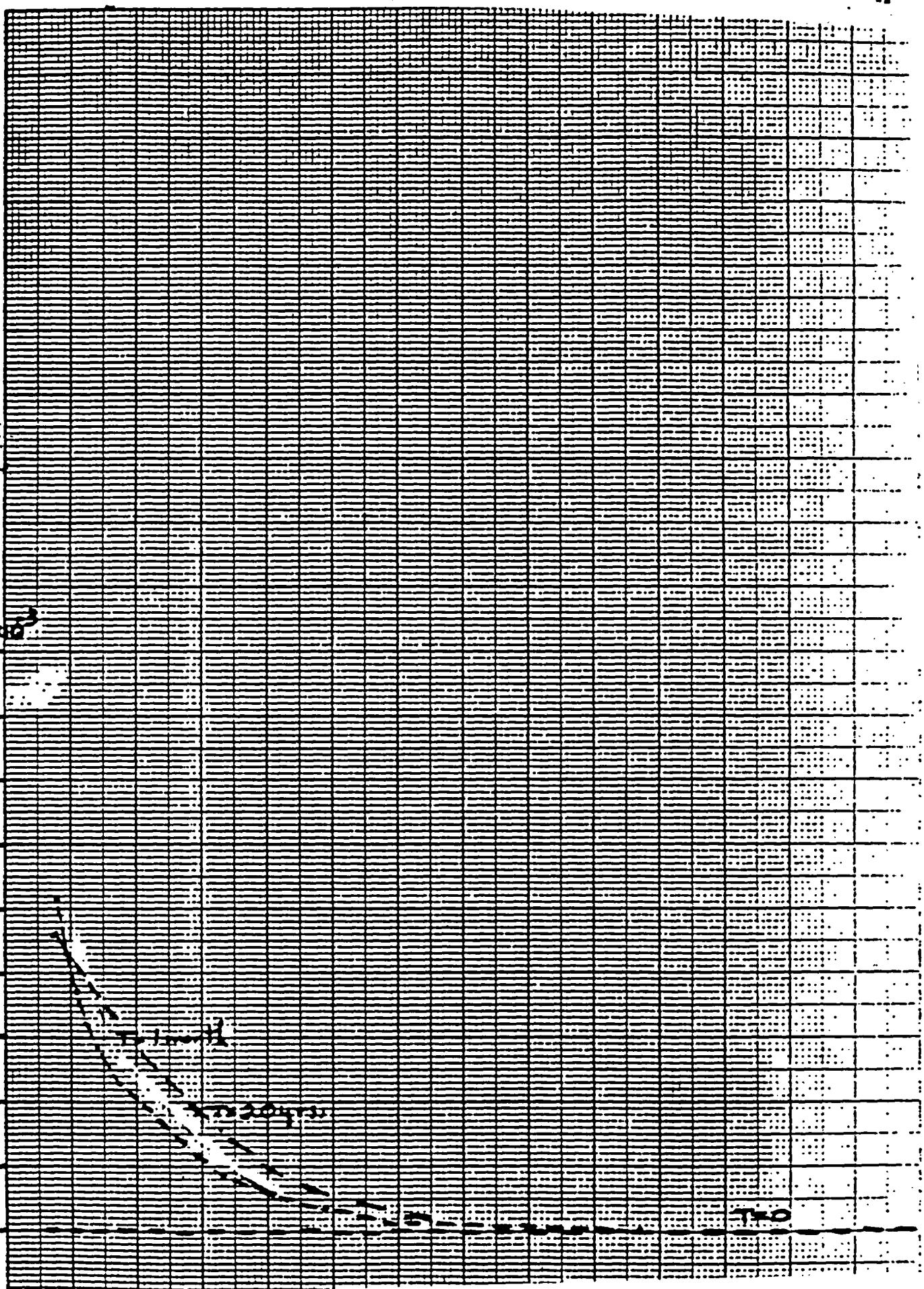

ROUGH DRAFT

Fig 44

Calculated total SiO2 (dissolved and precipitated) at selected times.

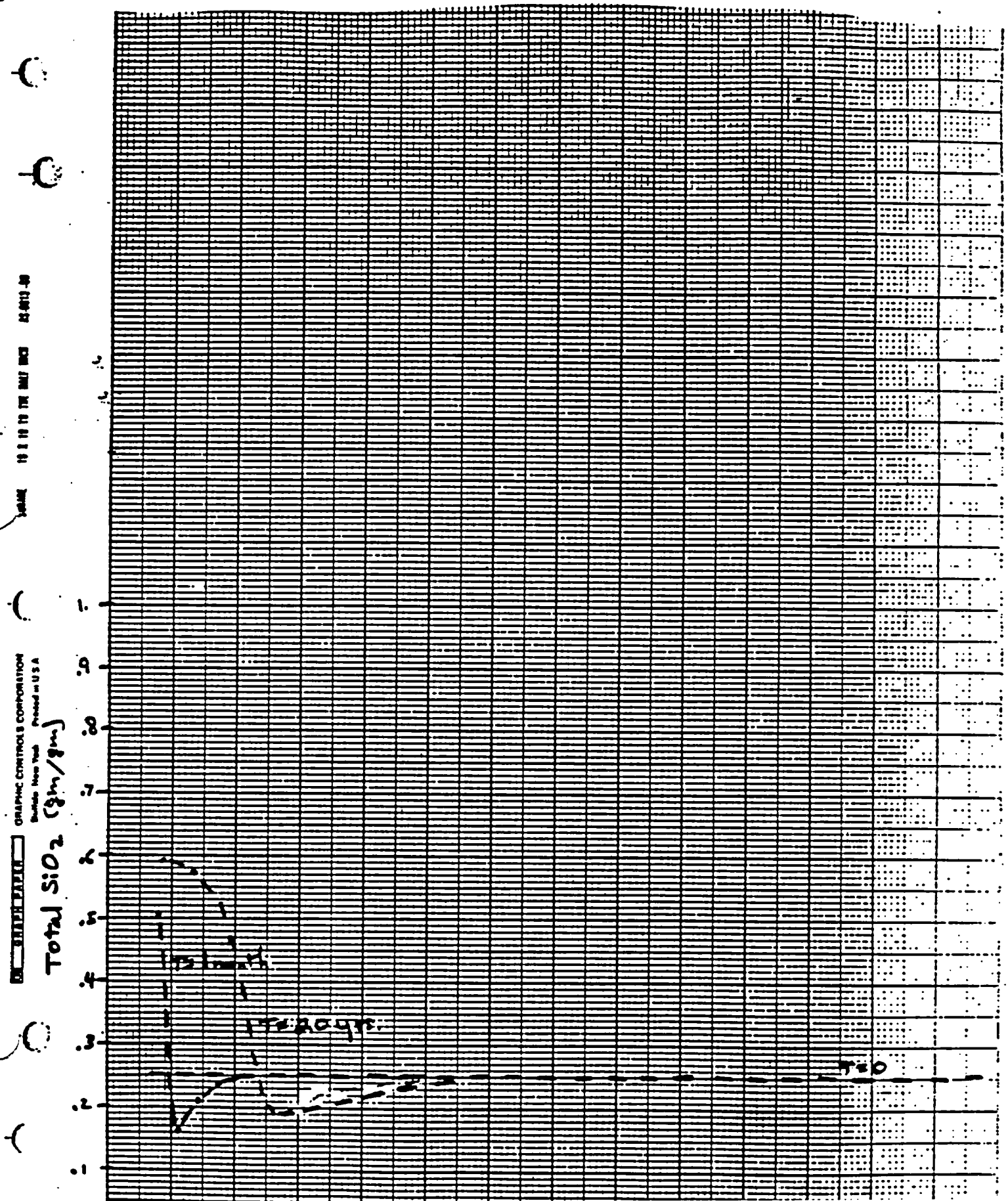

ROUGH DRAFT

Fig 45

Calculated permeability assuming relationships between pore volume and permeability.

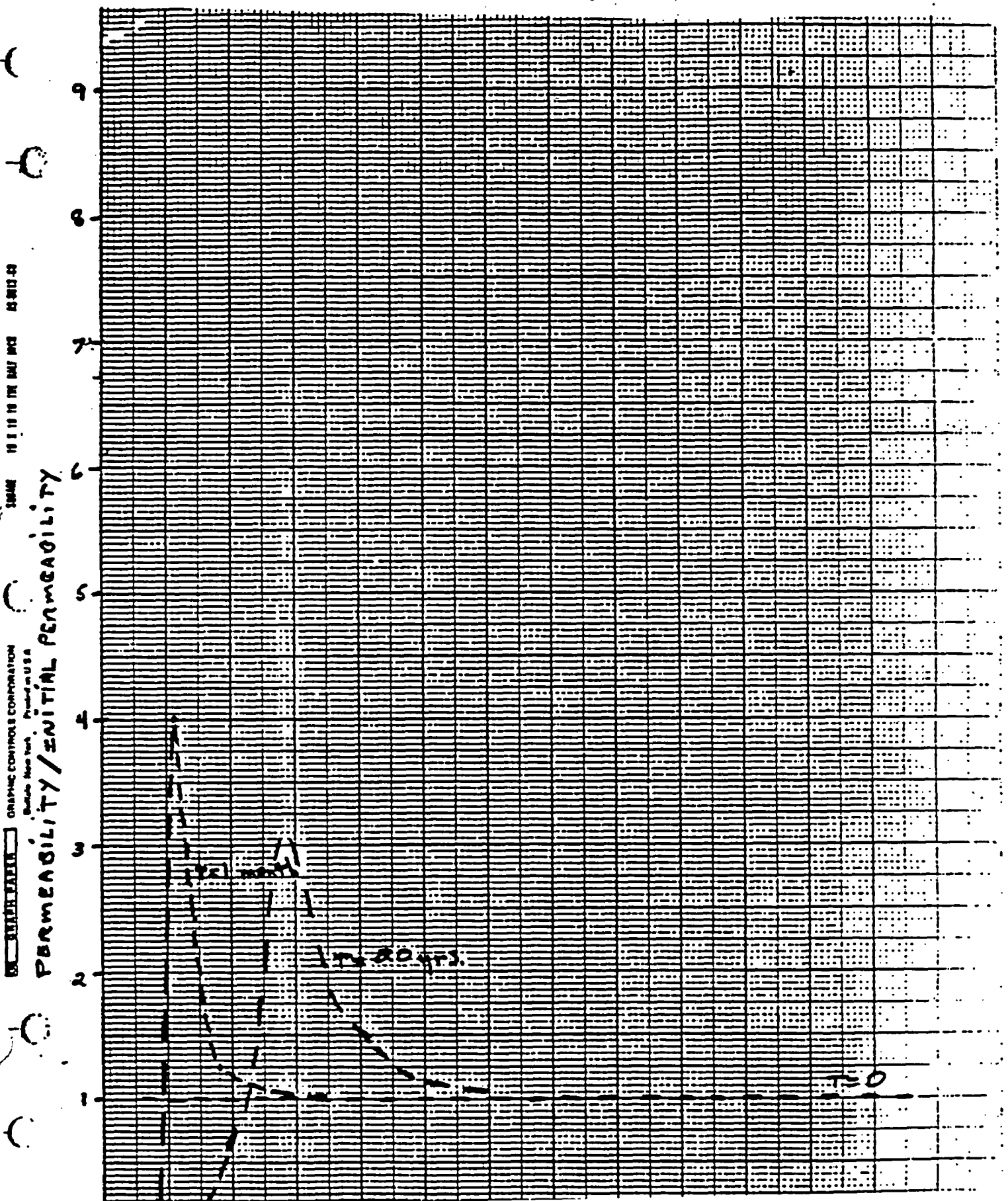

RUDOLPH DIVN I

MODEL

DATE

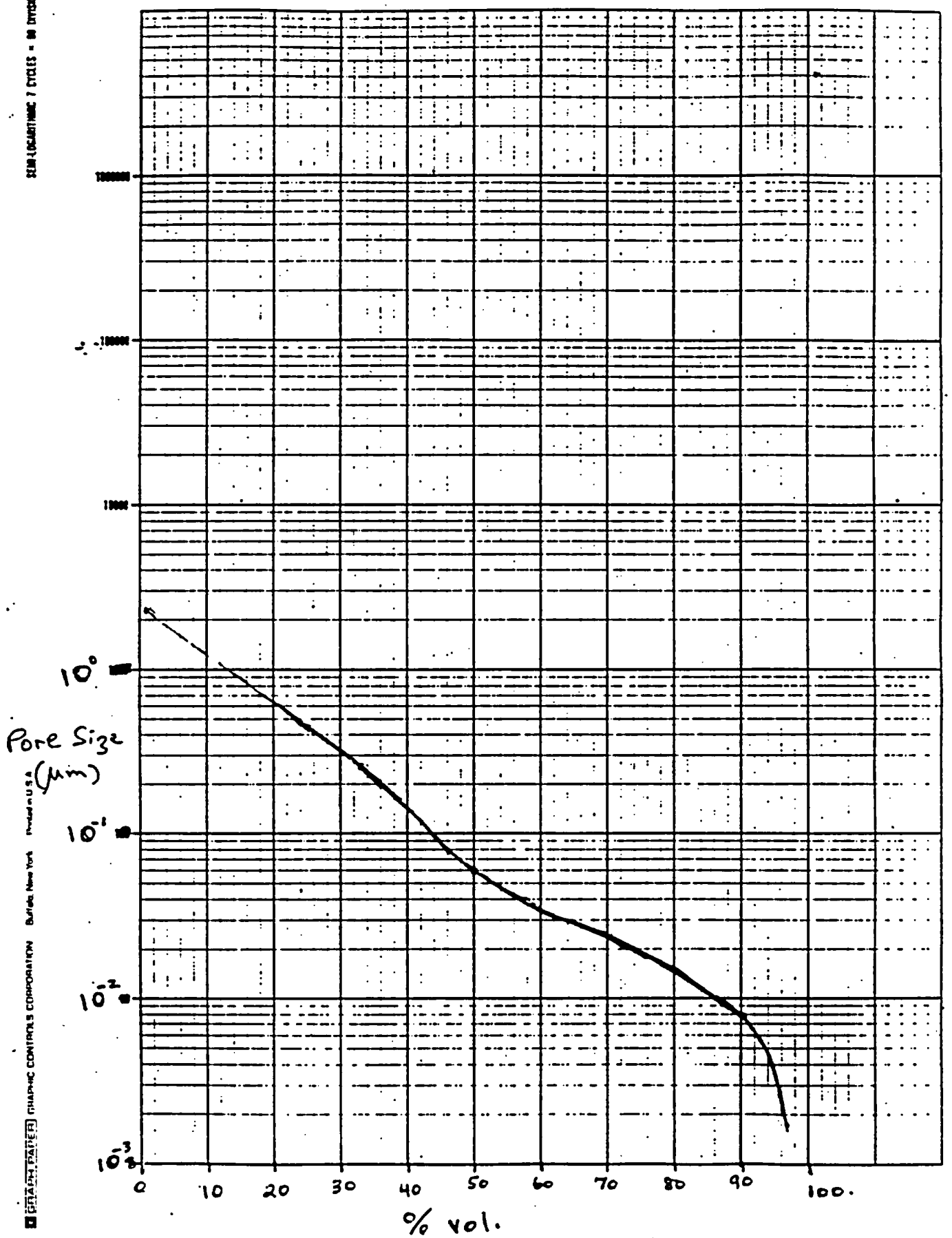

ROUGH DRAFT

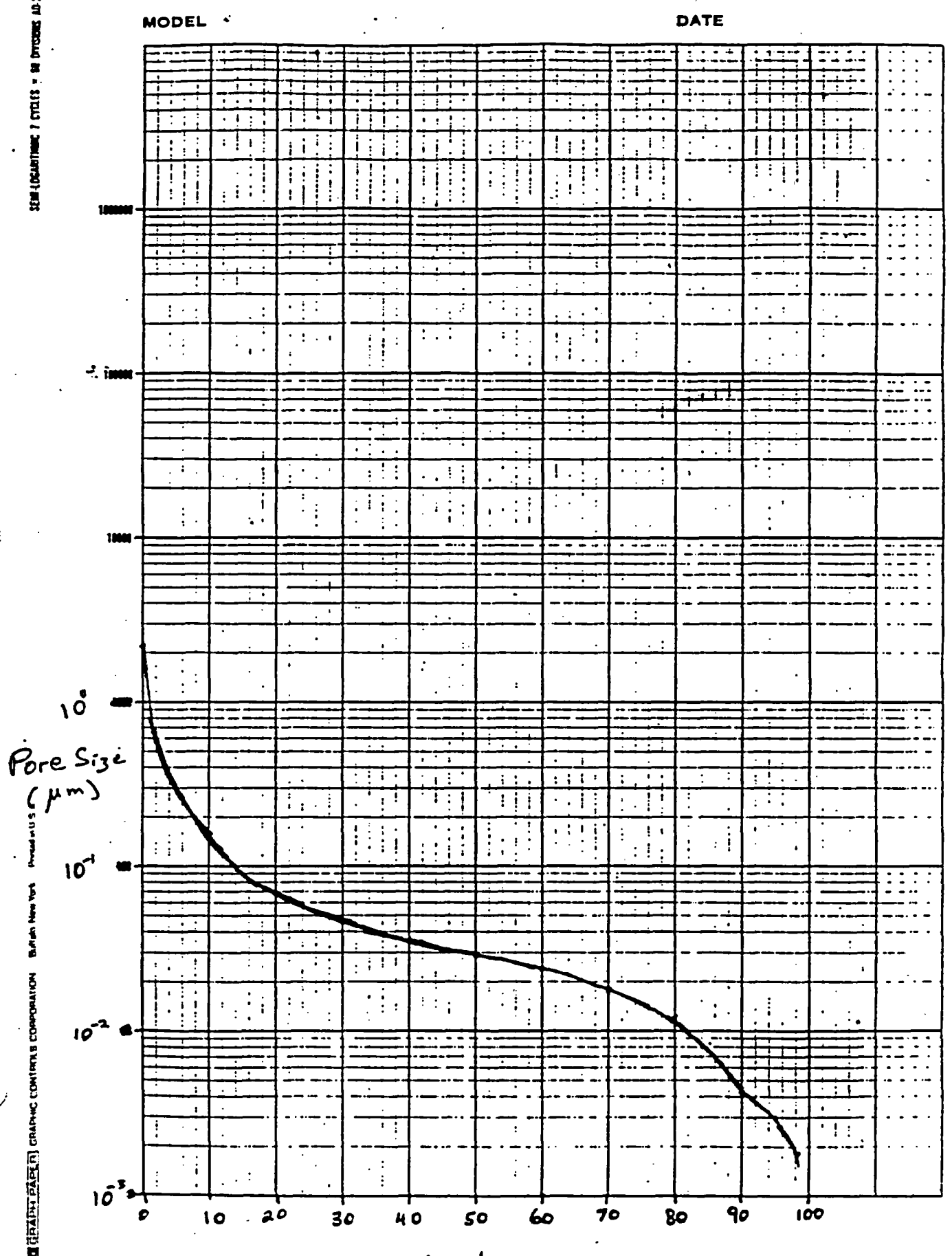
MODEL
DATE
Pore Size (μm)
10⁰
10⁻¹
10⁻²
10⁻³
0
10
20
30
40
50
60
70
80
90
100